Spring 2020

Structural Evolution of La Florida and Guavio Anticlines, Fractures, and Petroleum Systems in a Foreland Fold Belt, Eastern Cordillera Foothills, Colombia

Ziyad Albesher

STRUCTURAL EVOLUTION OF LA FLORIDA AND GUAVIO ANTICLINES, FRACTURES, AND PETROLEUM SYSTEMS IN A FORELAND FOLD BELT, EASTERN CORDILLERA FOOTHILLS, COLOMBIA

by

Ziyad Albesher

Bachelor of Science
King Saud University, 2007

Master of Science
King Saud University, 2012

Submitted in Partial Fulfillment of the Requirements

For the Degree of Doctor of Philosophy in

Geological Sciences

College of Arts and Sciences

University of South Carolina

2020

Accepted by:

James Kellogg, Major Professor

Andrew Leier, Committee Member

David Barbeau, Committee Member

Obi Egbue, Committee Member

Cheryl L. Addy, Vice Provost and Dean of the Graduate School

DEDICATION

This dissertation is dedicated to my wife who encouraged me to pursue my dreams and finish my study. Also, I would like to dedicate my dissertation to my parents for their patience, love, and support through all the years of my studying abroad.

ACKNOWLEDGEMENTS

I would like to express my deepest appreciation to my doctoral advisor, Dr. James Kellogg, for his guidance through each stage of my study journey. I am extremely grateful to him for all the support and help to grow as a professional researcher, where I learned with him the true meaning of success in the face of impossible challenges. I would also like to extend my deepest gratitude to my committee members Drs. Andrew Leier, David Barbeau, and Obi Egbue for their feedback and suggestions that were critical to improving my research.

I would like to send special thanks to Frontera Energy (former Pacific E&P Colombia) for providing the dataset for my research project in the Llanos foothills. In addition, I would like to thank Schlumberger for providing a free license for Petrel and PetroMod software, and Petroleum Experts for the donation of Move structural interpretation software. Finally, I would like to thank King Abdulaziz City for Science and Technology (KACST) in Saudi Arabia, for the full scholarship to complete my doctoral degree in geological sciences.

ABSTRACT

Geological structures and petroleum systems associated with La Florida anticline and the Cusiana fault system in the Llanos foothills and the Guavio anticline and the Guaicaramo fault system in the Medina basin were interpreted based on 3D seismic data from La Florida anticline in the foothills, 2D seismic data in the Medina basin and Guavio anticline, well, and surface geology maps. Unlike previous interpretations of the Guavio anticline and Medina basin area, our interpretation shows that thin-skinned thrusting on the Guaicaramo fault preceded thick-skinned basement thrusting. Late Miocene thin-skinned ramp thrusting was followed by a Pliocene thick-skinned fault-bend fold ramping up from pre-Cretaceous basement to a double-wedge fault. To the east, all the thrusting on the Cusiana fault and La Florida anticline was thin-skinned. At La Florida we propose a previously unrecognized late Miocene-Pliocene fault-bend fold, followed by the Cusiana reverse fault, a forelimb breakthrough fault ramping up from two bedding plane detachments. New 1-D burial models predict that the La Florida anticline has an active petroleum system (source, reservoir, seal, timing of charge, and trap formation) similar to the nearby giant Cusiana field, and source rocks remain in the oil window. In the Llanos foothills high levels of deformation have produced considerable noise in the seismic data and, therefore, seismic attribute analysis has not been used. In this study, techniques to reduce noise and enhance seismic quality make possible the first multi-attribute analysis of a 3D seismic volume in the Foothills using

coherency and ant-tracking techniques for fault and fracture detection. The results could help model reservoir fracture porosity and permeability. Late Miocene NE-SW normal faulting and fractures may have been produced by lithospheric bending as the mountain front advanced. We compared fracture intensity and orientation in folded rocks with non-folded rocks. Our study showed NE-SW, NW-SE, and E-W fracture orientations in the non-folded seismic volume, suggesting that regional stresses could produce these fracture sets, not just folding as previously proposed. Active right-lateral strike-slip displacement on the nearby Algeciras fault system may have generated Riedel-type shear fractures in the Foothills study area.

TABLE OF CONTENTS

LIST OF TABLES

LIST OF FIGURES

LIST OF ABBREVIATIONS

AFT ..... Apatite Fission Track

CA ..... Cabuyarito Anticline

CF ..... Cusiana Fault

EC ..... Eastern Cordillera

GA ..... Guavio Anticline

GF ..... Guaicaramo Fault

LFA ..... La Florida Anticline

ZFT ..... Zircon Fission Track

CHAPTER 1 INTRODUCTION

The Eastern Cordillera of Colombia is an asymmetrical bivergent fan of thrusts toward the Middle Magdalena Valley basins and the Llanos basin, containing a thick Jurassic and lower Cretaceous depocenter (Campbell and Burgl, 1965; Julivert, 1970; Campbell, 1974; Cooper et al., 1995). Numerous structural models have been proposed for the Eastern Cordillera. Based on a retrodeformed cross-section through the Eastern Cordillera, Colletta et al. (1990) proposed that the Cordillera was formed by the inversion of two deep Upper Jurassic-Lower Cretaceous basins during Mio-Pliocene times. In this model, the structure is controlled by low angle thrusts and reactivated normal faults that constitute frontal ramps. They estimated a total shortening of at least 105 km with a decollement at a depth of about 20 km. Dengo and Covey (1993) proposed that basement-detached ("thin-skinned") shortening was followed by uplift on high-angle basement-involved reverse faults ("thick-skinned") deformation and estimated approximately 150 km of shortening (40%) from a regional retrodeformable cross-section. Cooper et al. (1995) proposed that deformation in the Llanos foothills was predominantly inversion of pre-existing extensional faults by basement involved "thick-skinned" listric reverse faults. They estimated only 68 km of shortening.

The eastern flank of the Eastern Cordillera EC (Figure 1.1) is an active foreland fold belt formed by both thin-skinned and thick-skinned deformation (e.g.,Dengo and Covey, 1993; Egbue and Kellogg, 2012). The basement block, "germanotype," or thick-

skinned tectonic style of the Laramide orogeny in the central and southern Rocky Mountains of the United States was characterized by broad zones of uniform strike and dip separated by narrow zones of steeper dips or high-angle faults. Examples of thick-skinned basement tectonics are found throughout the Laramide US Rocky Mountains (e.g., Smithson et al., 1978; Miller and Mitra, 2011) and the Sierras Pampeanas in Argentina (Jordan and Allmendinger, 1986; Ramos et al., 2002; Fan and Carrapa, 2014), as well as in the northern Andes (e.g., Kellogg and Bonini, 1982; De Toni and Kellogg, 1993). Thin-skinned thrust belts often involve greater folding and shortening and less uplift than thick-skinned deformation. The shortening is confined to the sedimentary cover rocks and involves low-angle thrust faults (e.g., Chapple, 1978; Baby et al., 1992).

The discovery of giant petroleum fields in the eastern foothills in the 90's led to numerous research studies of the area, e.g., (Cazier et al., 1995; Cooper et al., 1995; Mora et al., 2006; Parra et al., 2009a; Parra et al., 2009b; Mora et al., 2010b; Garcia et al., 2015; Sánchez et al., 2015; Carrillo et al., 2016). These studies focused on the lithology, structural styles, and petroleum system of the foothills. Previous studies have faced various challenges, such as complex geology, poor-quality seismic images, and lack of well data. With new seismic and well data, this research addresses the structural style and relative importance and timing of thin-skinned and basement involved deformation in the evolution of the Eastern Cordillera Foothills. This research also relates the structural evolution of the Foothills to the petroleum system, including the timing of generation, migration pathways, and hydrocarbon trap synchronicity. In addition, this study relates the orientation and intensity of fracture systems in the Llanos foothills zone to changing regional stress fields. The research presented in subsequent chapters integrates a

varietylenty of datasets (Figure 1.2) including 2D seismic reflection profiles, a 3D seismic volume, wells, and surface geology to provide the structural framework, fracture systems, and petroleum system analysis of the Llanos foothills.

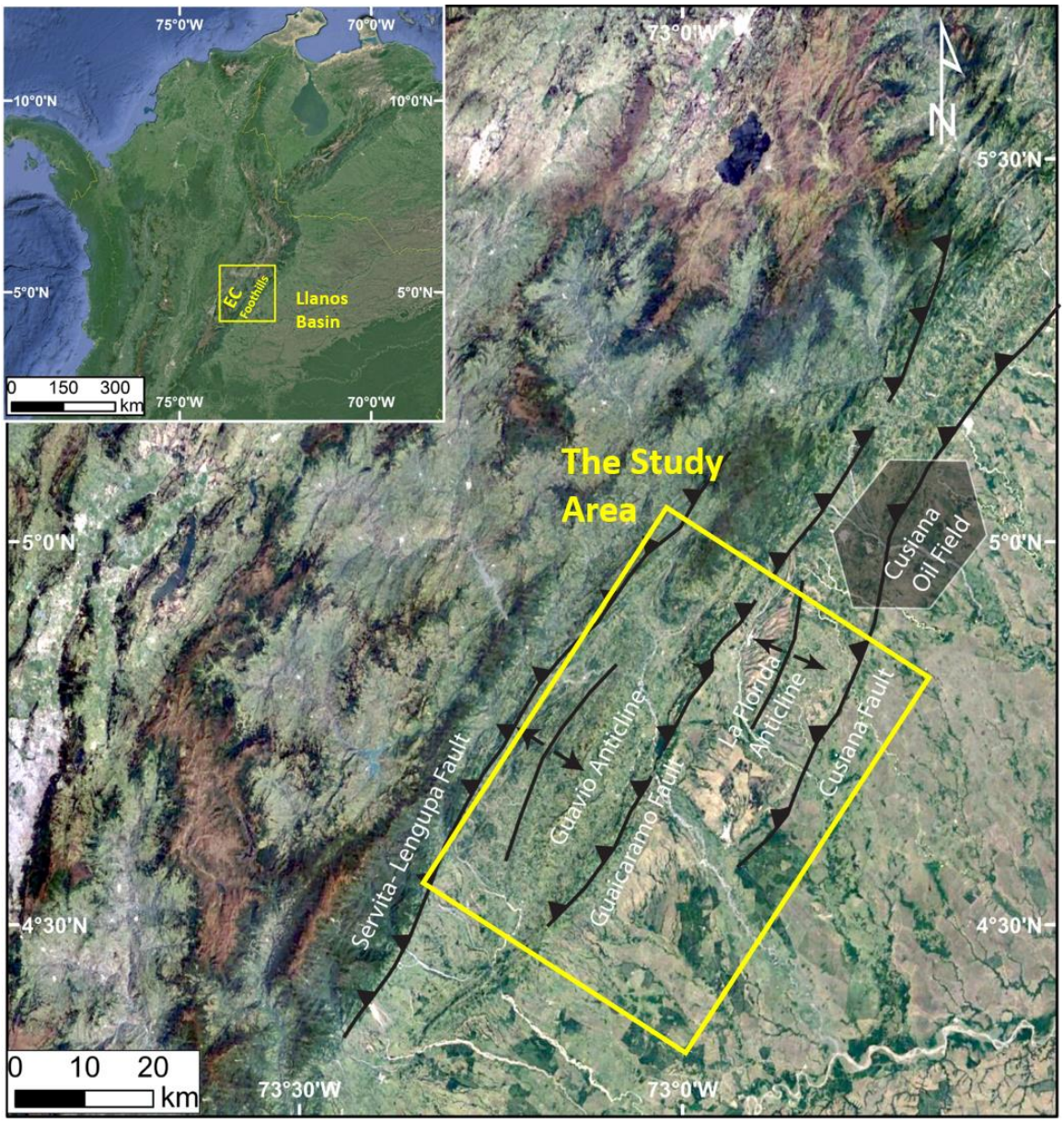

Figure 1.1: Satellite image from Google Earth showing major faults and anticlines in the study area (yellow box) as well as the location of the Cusiana oil field. Inset Shows regional location. EC: Eastern Cordillera Colombia.

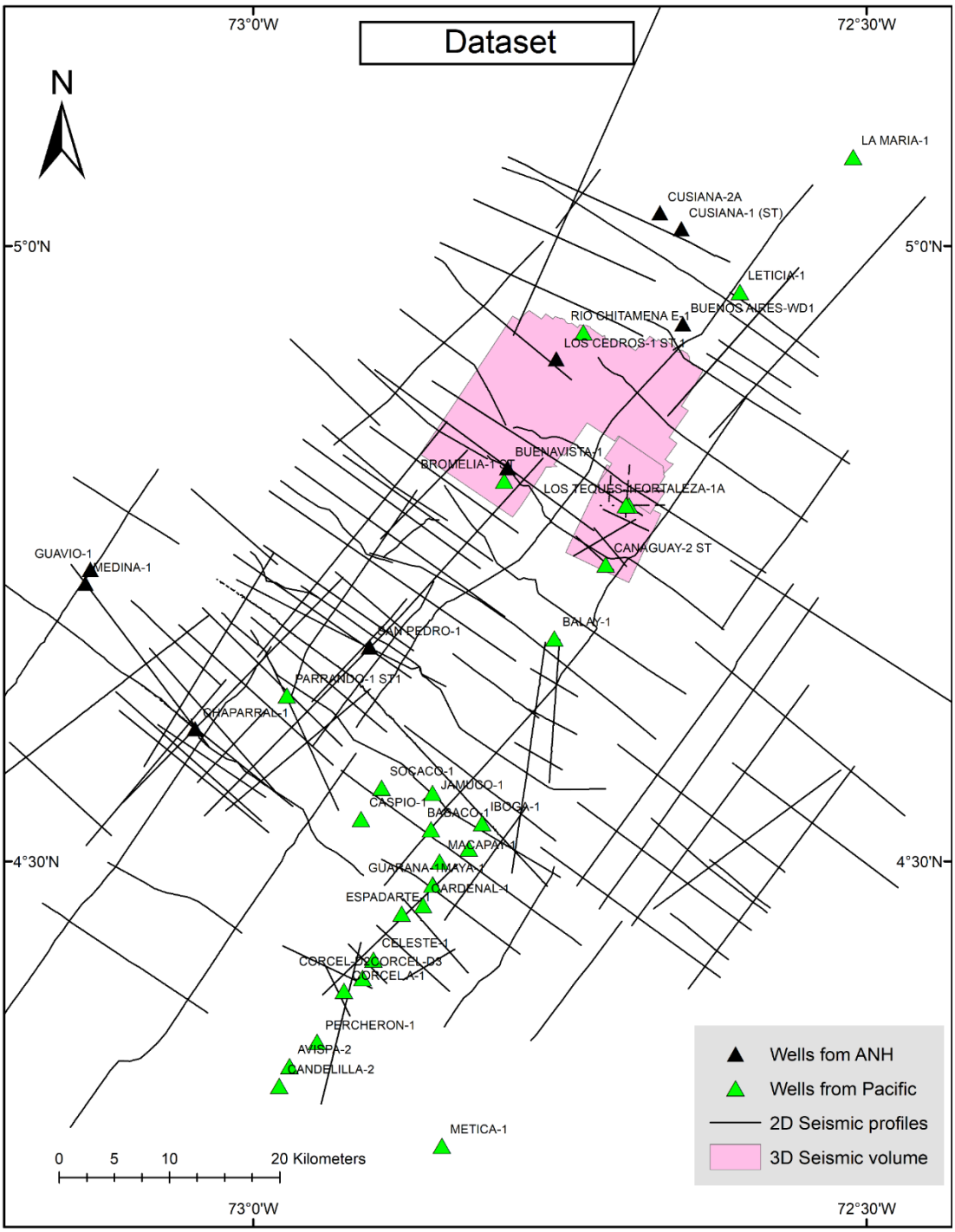

Figure 1.2: The project dataset was provided by Pacific Energy (now Frontera Energy) including 2D seismic profiles (dated from 70's to 2005), 3D seismic volume, and well logs. In addition, old-wells data (black tringles) was provided by National Hydrocarbon Agency of Colombia.

This dissertation is organized in four chapters, including an introductory chapter, two core research chapters, and a concluding chapter. The core chapters were written as manuscripts for peer-reviewed journals. Chapter 2 was submitted to *Journal of South American Earth Sciences*; Chapter 3 has been submitted to and published by *Journal of Geosciences*.

Chapter 2 focuses on the structural evolution and petroleum systems of La Florida and Guavio anticlines, southwest of the giant Cusiana oilfield in the Llanos foothills (Figure 1.1). 2D seismic profiles, a 3D seismic volume, well logs, and surface geology were used to construct balanced cross-sections for La Florida anticline (A-A') associated with the Cusiana fault system, and to the southwest in the adjacent Medina basin, the northern termination of the Guavio anticline (B-B'), where the Guaicaramo thrust transitions from thick-skinned thrust in the south to thin-skinned thrust in the north (Jimenez et al., 2013). This study presented the first retro-deformed model for the La Florida anticline as well as a new interpretation as thin-skinned thrusting on the Cusiana fault as opposed to previous interpretations as an inverted normal fault. The interpretation also includes a previously unrecognized Miocene fault-bend fold origin for the La Florida anticline. The new interpretation for the northern Guavio anticline shows that thin-skinned thrusting preceded the thick-skinned basement uplift on the Guaicaramo fault. It also documents a new interpretation of wedge faulting on the Guaicaramo fault.

A new compilation of thermochronometric data (Apatite and zircon fission track) reveals three cycles of late Cenozoic tectonic events: first, late Oligocene ages coincide with uplift and thrusting on the Tesalia fault west of Medina basin. Second, late Miocene ages mark thrusting on the Guaicaramo fault separating the Medina and Llanos foothills

basins. Third, dominant Pliocene-Pleistocene ages coincide with Andean uplift, thrusting on the Cusiana fault, and basement involved inversion of the Guaicaramo fault.

The Guavio anticline was explored in the 60's and discovered to be a noncommercial hydrocarbon trap (Cazier et al., 1995). Later the Medina basin source rock was found to have no organic matter to produce oil from late Miocene to present (Sánchez et al., 2015. Although the Medina basin has no active kitchens, the source rocks in the foothills have been generating hydrocarbons from local restricted kitchens from late Miocene to present (Sánchez et al., 2015). This study confirmed the time of generation in the foothills with new 1-D burial models for Rio-Chitamena E-1 and Bromelia-1 wells. The 1-D models predict that oil generation began in La Florida in the late Miocene ~ 9 Ma in the hanging-wall and 6 Ma in the footwall, respectively.

The La Florida anticline, therefore, has successful petroleum system elements (source, reservoir, seal, timing of charge, and trap formation) similar to the nearby giant Cusiana field, and source rocks locally remain in the oil window. However,the Medina basin to the west of La Florida is isolated from the active Foothills source pods by the major sealing Guaicaramo thrust fault.

Chapter 3 describes research to identify fracture systems in the Llanos foothills and their distribution and orientations with multi-attribute analysis of a 3D seismic data volume. This study is the first use of seismic attribute analysis and ant-tracking techniques to map fracture sets in the Eastern Cordillera of Colombia. In fact, very few studies applying this technique have been published worldwide. The identified fracture systems were then related to folding mechanisms and regional stress fields. Since the

Llanos foothills rocks are highly deformed producing significant noise levels, the application of seismic attribute analysis is difficult and uncommon. However, this chapter presents new techniques to reduce noise and enhance seismic image, making attribute analysis feasible in the La Florida 3D seismic volume. This method can help to reduce production risks by predicting fracture orientations and possible migration pathways at the locations of potential wells. The ant-tracking attribute volume, including the Cusiana fault hangingwall and footwall, reveals the primary northeast-southwest orientation of fractures parallel to the structural strike of the adjacent Eastern Cordillera Foothills. The orientation and greater intensity in folded rocks suggest that this fracture set is related to the folding process. The secondary WNW-ESE orientation is particularly prominent in the Guayabo Formation in the Cusiana footwall, suggesting a correlation with late Miocene-Pliocene regional stress fields. The ENE-WSW minimum principal stress direction could have been produced by with the WNW-ESE principal stress direction of the mountain building compression or by Riedel shears associated with the recent (last 2 m.y.) northeastward “escape” of the North Andes and right-lateral shear on the Algeciras fault system (Egbue and Kellogg, 2010). Also, ant-tracking shows that fracture intensity was relatively low in the Late Cretaceous - Eocene reservoir rocks.

CHAPTER 2 STRUCTURAL EVOLUTION OF LA FLORIDA AND GUAVIO ANTICLINES AND PETROLEUM SYSTEMS IN A FORELAND FOLD BELT, EASTERN CORDILLERA FOOTHILLS, COLOMBIA[1]

2.0 OVERVIEW

We interpret the geological structures and petroleum systems associated with La Florida anticline and the Cusiana fault system in the Llanos foothills and the Guavio anticline and the Guaicaramo fault system in the Medina basin. Our interpretation is based on 3D seismic data from La Florida anticline in the foothills, 2D seismic data in the Medina basin and Guavio anticline, well, and surface geology maps. A new compilation of AFT and ZFT age data shows three periods of Neogene tectonic activity, late Oligocene (25-22 Ma) uplift and thrusting on the Tesalia fault to the west, late Miocene (12-8 Ma) thrusting on the Guaicaramo fault, and Pliocene-Pleistocene (4-1 Ma) thrusting on the Cusiana fault and basement involved inversion of the Guaicaramo fault. Unlike previous interpretations of the Guavio anticline and Medina basin area, our interpretation shows that thin-skinned thrusting on the Guaicaramo fault preceded thick-skinned basement thrusting. Late Miocene thin-skinned ramp thrusting was followed by a

[1] Albesher, Z., J. Kellogg, I. Hafiz, E. Saeid, Structural evolution of La Florida and Guavio anticlines and petroleum systems in a foreland fold belt, Eastern Cordillera foothills, Colombia, Submitted to Journal of South American Earth Sciences

Pliocene thick-skinned fault-bend fold ramping up from pre-Cretaceous basement to a double-wedge fault. To the east, all the thrusting on the Cusiana fault and La Florida anticline was thin-skinned. At La Florida we propose a previously unrecognized late Miocene-Pliocene fault-bend fold, followed by the Cusiana reverse fault, a forelimb breakthrough fault ramping up from two bedding plane detachments. In the late Miocene to present (9 – 0 Ma), no active kitchens existed in the Medina basin, but source rocks in the foothills to the east generated hydrocarbons throughout the Neogene. New 1-D burial models for Rio-Chitamena E-1 and Bromelia-1 wells in this paper predict that oil generation began in the La Florida Cusiana foothills in the late Miocene (~ 9 to 6 Ma). The La Florida anticline, therefore, has an active petroleum system (source, reservoir, seal, timing of charge, and trap formation) similar to the nearby Cusiana giant field, and source rocks remain in the oil window. The Medina anticline to the southwest of La Florida is isolated from the active Foothills source pods by the major sealing Guaicaramo thrust fault.

2.1 INTRODUCTION

Mountains are built by both viscous/plastic deformation and fault-related deformation. Compressive mountain belts, such as the Eastern Cordillera of Colombia, are primarily built by slip on reverse faults. Earthquake focal mechanisms for the Eastern Cordillera are characterized by WNW-ESE compression on reverse faults (e.g., Taboada et al., 2000; Corredor, 2003; Cortés et al., 2006). Both seismic and aseismic slip on the reverse faults produces horizontal shortening and vertical thickening (permanent deformation). The rate of mountain growth depends on the rate of shortening, the erosion rate, the dip of the thrust faults, and isostatic adjustments of the crust to the mountain

load. The contractional deformation style may be either thick-skinned basement faulting or thin-skinned thrusting involving only sedimentary rocks.

The basement block, "germanotype," or thick-skinned tectonic style of the Laramide orogeny in the central and southern Rocky Mountains of the United States was characterized by broad zones of uniform strike and dip separated by narrow zones of steeper dips or high-angle faults. Examples of thick-skinned basement tectonics are found throughout the Laramide US Rocky Mountains (e.g., Smithson et al., 1978; Miller and Mitra, 2011) and the Sierras Pampeanas in Argentina (Jordan and Allmendinger, 1986; Ramos et al., 2002; Fan and Carrapa, 2014), as well as in the northern Andes (e.g., Kellogg and Bonini, 1982; De Toni and Kellogg, 1993). Thin-skinned thrust belts often involve greater folding and shortening and less uplift than thick-skinned deformation. The shortening is confined to the sedimentary cover rocks and involves low-angle thrust faults (e.g., Chapple, 1978; Baby et al., 1992).

The Eastern Cordillera of Colombia was formed by both thick-skinned and thin-skinned deformation. Dengo and Covey (1993) proposed that the Eastern Cordillera is an east-verging structure formed in two tectonic phases. The first phase was a thin-skinned basement detached style that created large, east-verging thrust faults with the greatest shortening in the middle Miocene to Pliocene (Cortés et al., 2006). During the Pliocene, deformation changed to basement involved as Jurassic and Early Cretaceous normal faults were inverted (Dengo and Covey, 1993). Many recent reconstructions of the Eastern Cordillera attribute most of the deformation to inversion of mid-crustal normal faults or thick-skinned deformation with minimal thin-skinned thrusting (e.g., Cooper et al., 1995; Mora et al., 2015). The style of compressive deformation is often linked to the

dip of the subducting slab at a convergent plate boundary. Thin-skinned fold and thrust belts are associated with steeply dipping slabs, and thick-skinned basement uplifts are associated with flat or shallow slab subduction (e.g., Wagner et al., 2017; Kellogg et al., 2019; Mora-Páez et al., 2019).

In this study, we examine Neogene deformation (25 – 0 Ma) on the southeastern margin of the Eastern Cordillera west of the Guaicaramo fault in the Medina basin(Guavio anticline) and east of the Guaicaramo fault in La Florida anticline and Cusiana reverse fault (Figure 2.1 and Figure 2.2). Both thick-skinned and thin-skinned deformation styles have been proposed for the evolution of these folded foothills. The

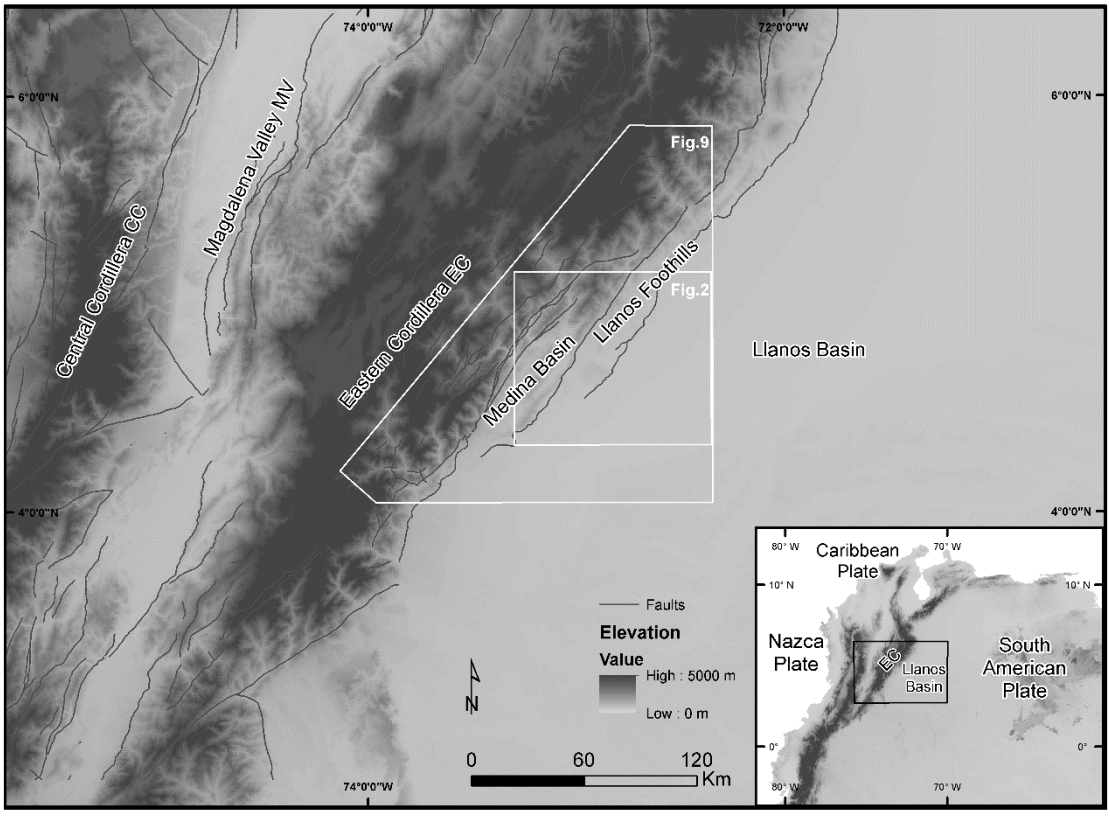

Figure 2.1: Shaded relief map of the digital elevation model (DEM) showing the major tectonomorphic provinces. Dark lines are reverse faults that delimit topographic breaks. Inset shows the major plates surrounding the area of study.

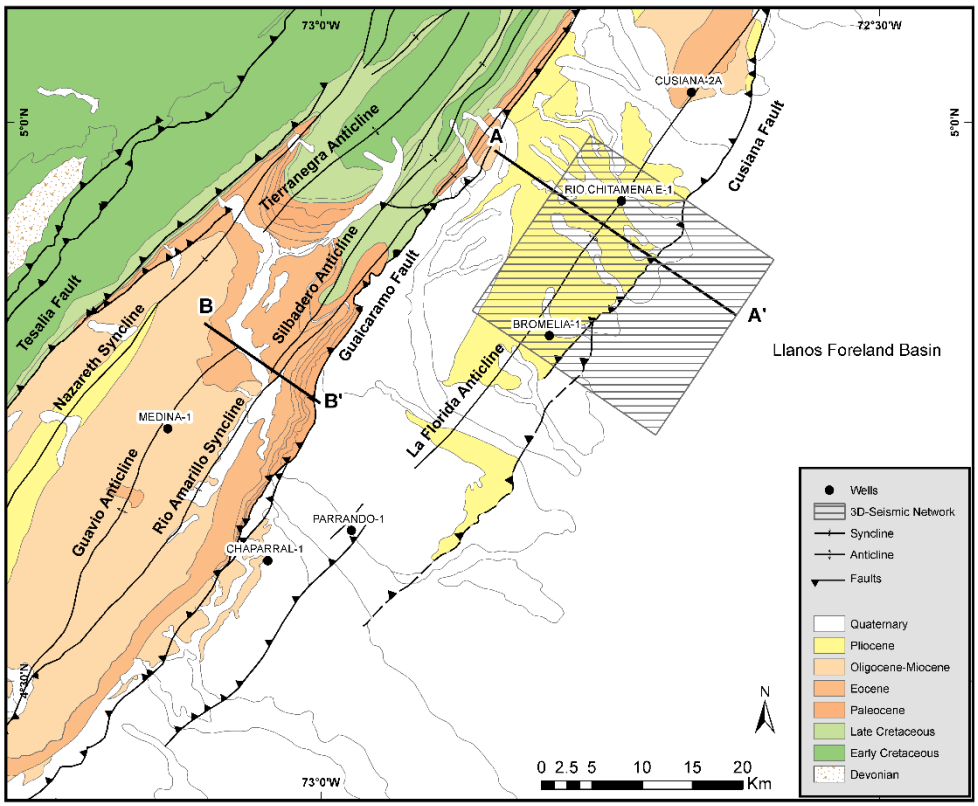

Figure 2.2: Geologic map of the Eastern Cordillera and Llanos basin (location shown in Figure 2.1) showing major structural features, locations of cross-sections, wells, and the 3D seismic volume used for this study. Geological data was provided by the Colombian Geological Survey (Montoya et al., 2013).

large Guavio anticline west of the Guaicaramo fault lacks commercial hydrocarbons, while just 55 km to the northeast across the Guaicaramo fault is the giant Cusiana oil field (Cazier et al., 1995; Cooper et al., 1995), Our study relates the structural and petroleum system evolution in the foothills west of the Guaicaramo fault to the structural and petroleum system evolution in the foreland east of the fault.

In the Medina basin foothills, we interpreted a previously unpublished seismic profile across the northern Guavio anticline. Unlike other interpretations, our retrodeformed model requires thin-skinned thrusting on the Guaicaramo fault before the

present Guavio ramp anticline formed. We estimate the timing of the Guavio anticline trap formation, a critical element in the evolution of the petroleum system and the lack of economic hydrocarbons presently in the anticline. Toward the foreland, we present the first retrodeformed model for La Florida anticline and the Cusiana fault to test the timing of folding and whether basement was involved or the deformation was entirely thin-skinned. Our results call into question previous models that predicted pre-Cretaceous basement involvement. Our La Florida model also predicts a previously unrecognized late Miocene-Pliocene ramp anticline. With 1D burial models for two wells, Rio Chitamena E-1 and Bromelia-1, we estimate the timing of oil expulsion and relate it to the timing of trap formation.

2.2 GEOLOGIC SETTING

2.2.1 Regional tectonics.

During the Jurassic and Early Cretaceous, two rift basins developed in the area of the present Eastern Cordillera (Maze, 1984; Jaillard et al., 1990). Tectonic subsidence from extension and crustal thinning was followed by Cretaceous thermal subsidence as the lithosphere thermally equilibrated (Ojeda, 1996). The thickness of Cretaceous basin fill was estimated to be from 5 km (Restrepo-Pace, 1989) to 8km (Cardozo Puentes, 1988). At ~75 Ma, the Caribbean Large Igneous Province (CLIP) collided with South America, resulting in the accretion of the oceanic terrane of the Western Cordillera (Spikings et al., 2015). Subsequently buoyant Caribbean crust began amagmatically subducting under the North Andes, resulting in flat slab subduction and basement block uplifts in the overriding plate (Kellogg et al., 2019). 50 million years ago, the Caribbean-South American relative plate motion changed dramatically (Boschman et al., 2014), and

since then, the Caribbean has moved 1000 km eastward relative to the South American plate. Uplift of the Central Cordillera during middle Eocene to middle Miocene times induced flexural subsidence and deposition in a foreland basin to the east, the future Magdalena Valley and Eastern Cordillera (Gómez et al., 2005; Horton et al., 2010). The Miocene collision of the Panama-Choco arc with the North Andes (Duque-Caro, 1990; Kellogg and Vega, 1995; Taboada et al., 2000; Cediel et al., 2003) produced the principal phase of tectonic inversion and shortening in the Eastern Cordillera (Van der Hammen, 1958; Cooper et al., 1995) and separated the Llanos basin from the middle Magdalena Valley (Moreno et al., 2011; Horton et al., 2015). The collision and subduction related shortening and uplift of the Eastern Cordillera took place on inverted normal faults and low angle thrust faults (Colletta et al., 1990; Dengo and Covey, 1993; Toro et al., 2004; Cortés et al., 2006; Mora et al., 2006; Bayona et al., 2008; Parra et al., 2009a; Horton et al., 2010; Delgado et al., 2012; Bayona et al., 2013; Mora et al., 2013; Tesón et al., 2013).

2.2.2 Stratigraphic setting and petroleum system of Llanos foothills and Medina basin.

The sedimentary sequence in the Medina and Llanos foothills basins study area (Figure 2.1 and Figure 2.2) is up to 12 km thick, including at least 6 km of Cenozoic synorogenic sediments (Parra et al., 2009a; Teixell et al., 2015). The stratigraphy column (Figure 2.3) contains three major depositional cycles (Toro et al., 2004). The first cycle of deposition includes up to 5 km of Early Cretaceous syn-rift units deposited over Late Paleozoic rocks (Ramon and Fajardo, 2006). This shallow-marine sedimentary sequence included hydrocarbon source rocks in the Macanal and Fómeque formations that expelled their oils prior to the deposition of the main Eocene reservoir rocks in the Medina and Llanos basins (Sánchez et al., 2015). The second cycle was deposited during Late

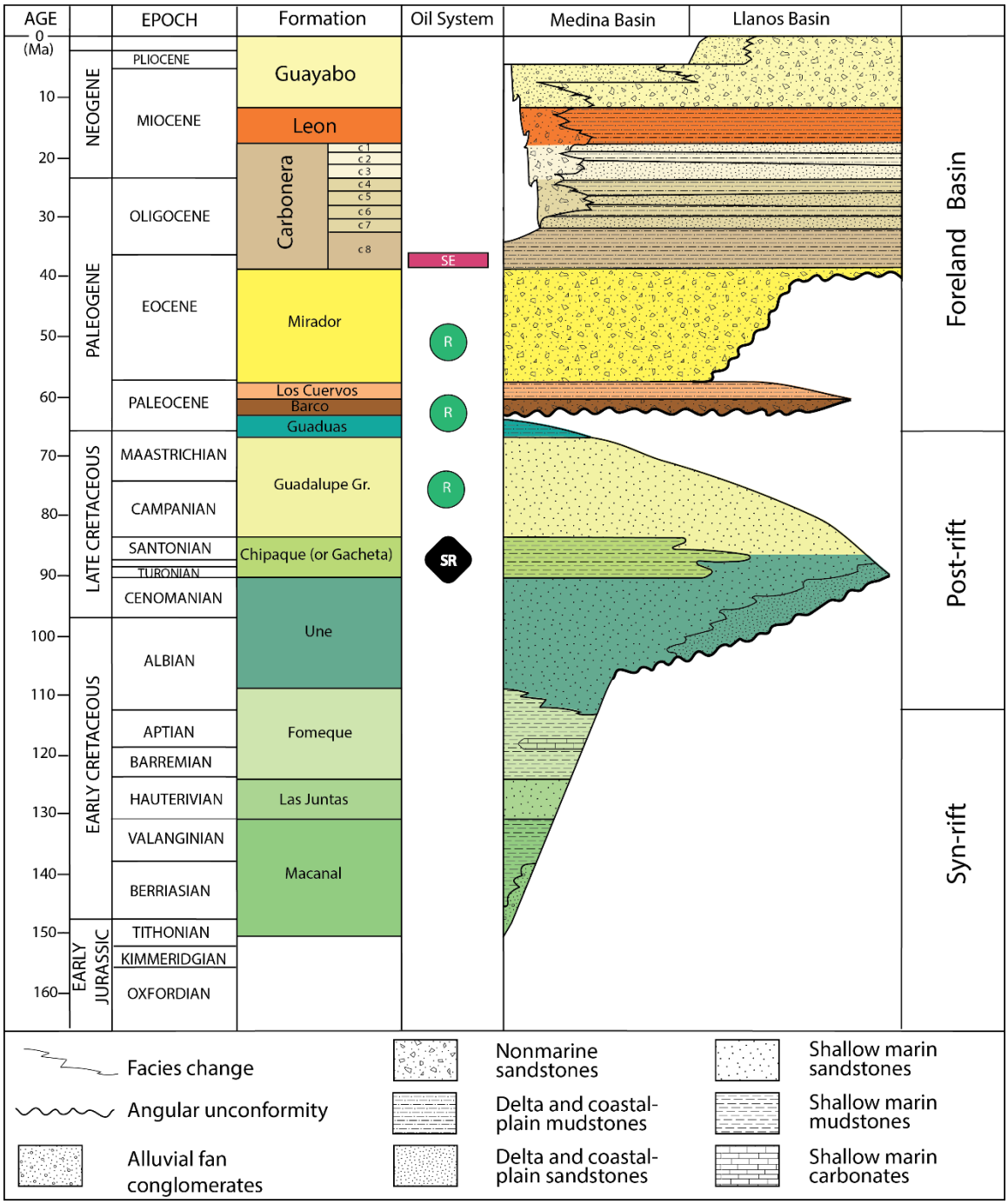

Figure 2.3: Stratigraphic column of the Medina and Llanos basins showing petroleum system elements. Modified after Ramon and Fajardo, 2006; Parra et al., 2009a.

Cretaceous post-rift thermal subsidence (Horton et al., 2010), beginning with the deposition of the Une Formation (Garcia et al., 2015). An angular unconformity near the end of the Early Cretaceous marks the transition from rifting to post-rift thermal

subsidence (Parra et al., 2009a). During the post-rift cycle the source rocks of the marine Late Cretaceous Chipaque Formation were deposited in the Medina basin. The Chipaque Formation is the lateral equivalent of the Gacheta Formation in the eastern foothills (Mora et al., 2019a). These source rocks were overlain by shallow-marine Santonian–Campanian upper Guadalupe sandstone reservoir rocks (Cazier et al., 1995). The final cycle extends from Maastrichtian to the present, marginal marine to non-marine foreland basin sediments up to 7 km thick (Cooper et al., 1995; Gómez et al., 2005; Parra et al., 2009a). The estuarine sandstone of the Paleocene Barco Formation is deposited as a lower reservoir and is sealed by the late Paleocene Los Cuervos Formation. The overlying Eocene sandstone of the Mirador Formation is the main reservoir in the Llanos basin, and is widely covered by the regional seal of the lower muddy interval (C8) of the Carbonera Formation (Cooper et al., 1995; Reyes-Harker et al., 2015). The overlying Oligocene shales of the Carbonera Formation may be potential source rocks charging the foothills (Mora et al., 2019a). The uplift of the Eastern Cordillera from the middle Miocene to the Pleistocene is recorded in the deposition of Leon Formation mudstones, followed by coarse to fine fluvial gravels of the Miocene–Holocene Guayabo Formation (Ramon and Fajardo, 2006; Parra et al., 2009a).

2.2.3 Structural geology previous work

The structural geology of the eastern foothills and Medina basin has been described by Cazier et al. (1995); Branquet et al. (2002); Toro et al. (2004); Parra et al. (2009a); Mora et al. (2010b); Jimenez et al. (2013); Mora et al. (2013); Teixell et al. (2015); and Carrillo et al. (2016). To date, no interpretations have been published for the

northernmost Guavio anticline, and no retrodeformed models have been proposed for La Florida anticline and the Cusiana fault.

2.2.3.1 La Florida anticline

Using 2D seismic line CO-95-22, Mora et al. (2010b) interpreted La Florida anticline (Figure 2.2) as produced by slip on the Cusiana fault, a listric high angle reverse fault involving pre-Late Cretaceous basement rocks. La Florida anticline is located on the trend of anticlinal traps associated with the Yopal-Cusiana fault system, including Rio Chitamena 3 km to the northeast and the giant Cusiana oilfield 16 km to the northeast (Cazier et al., 1995). Both Cooper et al. (1995) and Cazier et al. (1995) interpreted the Cusiana fault as a listric reverse fault involving Early Cretaceous and older basement. Cooper et al. (1995) modeled the Cusiana fault as an inverted normal fault. None of the published interpretations attempted to explain the Cusiana hanging wall anticline. Total slip on the Yopal-Cusiana high angle reverse faults is over 4 km. Based on thermochronometric data and kinematic restorations, Bande et al. (2012) and Carrillo et al. (2016) suggest that the folds associated with the Cusiana fault originated in the last 3 Myr. Mora et al. (2010b) also noted that Pliocene-Pleistocene units on the back-limb of the Florida anticline are folded conformably with no significant growth strata.

2.2.3.2 Guavio Anticline

The Medina Basin contains the broad Guavio-Nazareth anticline–syncline pair between the Tesalia thrust to the west and the Rio Amarillo syncline and Guaicaramo fault to the east (Figure 2.2). To the west of the Guavio anticline, the Nazareth syncline is an asymmetric, east-verging fold that formed as a result of fault-propagation folding along the Servita/Tesalia fault system (Parra et al., 2009a). Branquet et al. (2002)

interpreted the Guavio anticline as a basement pop-up related to dextral strike-slip faulting. Most researchers, however, have characterized the Guavio anticline as a broad fault-bend fold formed in the hanging wall of the Guaicaramo reverse fault (Rowan and Linares, 2000; Mora et al., 2006; Parra et al., 2009a; Mora et al., 2010b; Tamara et al., 2015). Rowan and Linares (2000) used 2D seismic profiles to produce a 3-dimensional model for the Guavio anticline as a fault-bend fold with lateral variations in ramp height, ramp dip, and intermediate flat length. Using improved seismic data, Parra et al. (2009a) interpreted the Guavio anticline as a broad Guaicaramo thrust fault-bend fold piggybacked on a deeper fault-bend fold. All the interpretations involved Early Cretaceous and pre-Cretaceous basement and inversion of a Cretaceous Guaicaramo rift fault. None of the models proposed an early bedding plane thin-skinned thrust fault in the Guavio anticline, although south of the Guavio anticline, Teixell et al. (2015) and Mora et al. (2010b) observed a bedding plane unconformity in the lower Carbonera Formation that was used as a slip surface. Hafiz et al. (2019) interpreted the Guavio basement fold as formed by a ramp from pre-Cretaceous basement to a double wedge fault folding the Guaicaramo thrust footwall rocks. Hafiz et al. (2019) did not rule out the possibility that a thin-skinned bedding plane thrust fault ramping to the surface along the Guaicaramo fault may have preceded the formation of the Guavio anticline. No interpretations have been published previously for the transition zone between the Guavio anticline and the Tierranegra anticline to the northeast.

2.3 DATA AND METHODOLOGY

2.3.1 Seismic interpretation

Data for this study included 480 km2 of 3D seismic reflection data collected in 2012 covering La Florida anticline and the Cusiana fault (Figure 2.2), 540 2D seismic profiles, and 28 wells. The surface geology (Figure 2.2) was from the Colombian Geological Survey for Plate 229 (Montoya et al., 2013) and the geologic map of Colombia (Gómez et al., 2015), and maps by Branquet et al. (2002) and Parra et al. (2009a). The direct field measurements of bedding strikes and dips in the Montoya et al. (2013) and Branquet et al. (2002) maps were particularly useful for our structural interpretations. This study is based on the integration of geophysical and geological interpretations. Seismic reflection profiles provided the main structural control for the subsurface geological interpretation constrained with available exploration wells. The research included seismic interpretation, structural modelling, 1D basin modeling, and data analyses. Seismic interpretation used Petrel software, including regional seismic stratigraphy, structural maps, surface attributes and time-depth conversion. PetroMod software was used to generate 1D basin models, including burial history curves and source rock maturity.

La Florida anticline was covered by the 3D seismic volume as shown in Figure 2.2, and we have well-data for Rio Chitamena E-1 well in the Cusiana hanging wall and Bromelia-1 in the Cusiana footwall. Well ties were based on well check shot surveys, sonic logs, and synthetic seismograms using Petrel software. The Guavio profile B – B' (Figure 2.2) was tied by a seismic strike line to Medina-1 well (Hafiz et al., 2019). La Florida profile A – A' (Figure 2.2) was extended by combining a 2D profile with a 3D

seismic inline. The 2D survey parameters (Automatic Gain Control and datum) were adjusted to merge with the 3D survey.

2.3.2 Cross-section construction and kinematic restoration

Structural models were created with Move software and were constrained by seismic and well data and surface geology. The 3D seismic volume was converted from time to depth using well check shot surveys and synthetic seismograms. Digital elevation models (DEMs) were uploaded with the geologic maps to construct cross sections using volume-balancing techniques (Suppe, 1983). Surface geology, topography, and well data were displayed on the seismic sections as close to 1:1 vertical exaggeration as possible. Regions of homogeneous dip (dip domains) and major discontinuities were identified. Spectral analysis was used to identify fundamental step-up angles (Suppe, 1983). Stratigraphic thicknesses were determined from surface geology, seismic, and well data, and depths to basal detachments were estimated from the seismic profiles. The Guavio and La Florida profiles were then retrodeformed to test the interpretations and predict the timing of potential migration pathways and trap formation. We used the 2D kinematic modeling tool to establish the retro-deformation models and the fault-parallel-flow (FPF) algorithm (Egan et al., 1999) to restore fault displacements. We applied the Wedge algorithm on fault-bend fold (FBF) (Medwedeff, 1992) for the Guaicaramo fault restoration. Petroleum systems analysis utilized PetroMod software to generate 1D basin models including burial history curves and source rock maturity assuming heat flow values of Bachu et al. (1995), Cazier et al. (1995), and Toro et al. (2004).

2.4 RESULTS

2.4.1 La Florida anticline

The most prolific oil fields in the north Andes of Colombia are located in the Llanos foothills of the Eastern Cordillera. To understand the thin-skinned thrusting that characterizes the foothills belt and the nearby giant Cusiana oil field, we interpreted a profile across La Florida anticline located 16 km southwest and along structural strike for the Cusiana structure (Figure 2.2).

2.4.1.1 La Florida anticline structural interpretation

The La Florida anticline profile shown in Figure 2.4 was selected for interpretation because of the high quality of the 2D and 3D seismic data and the location of nearby Rio Chitamena well control. Along the axis of La Florida anticline 3 km northeast of the profile (Figure 2.4) is the producing Rio Chitamena E-1 well and 16 km northeast is the producing Cusiana–2A well (for locations see Figure 2.2). The La Florida profile (Figure 2.4) extends southeastward from the footwall of the Guaicaramo fault across the Cusiana fault. It was created by integrating 3-D seismic inline 489 that covered most of the Florida structure and extending the profile northwestward with 2-D seismic line RC-1991-13.MIG to the footwall of the Guaicaramo thrust fault. To constrain formation tops in the hanging wall, the Rio Chitamena well was projected onto our cross-section ~3 km southwest down plunge along the anticlinal axis (Figure 2.4) using 3D strike-parallel profiles. Footwall formation tops were constrained with well ties to Bromelia-1 (Figure 2.2). The deformation involves sediments above the Early Cretaceous synrift-Late Cretaceous postrift boundary. The Late Cretaceous units thin eastward

toward the Llanos foreland basin, as in the Cusiana field along strike to the northeast (Cooper et al., 1995).

We interpret the La Florida anticline as a thin-skinned fault-bend fold and breakthrough fault. The thrusting ramps up from a bedding plane detachment at the mid-Cretaceous synrift-postrift boundary unconformity at the base of the Une Formation (Figure 2.4B). The position of the Cusiana fault is constrained by hanging wall and footwall cutoffs in the seismic profile (Figure 2.4A). A bedding plane thrust in the lower Carbonera Formation also intersects the Cusiana fault where slip is transferred to the surface as part of late stage breakthrough displacement. Minor back-thrusts on the northwest flank of the La Florida anticline terminate in the Cusiana fault. Total shortening on the La Florida anticline is about 5.7 km, and the total structural relief is 1.5 km.

The 3D seismic reveals a hanging wall anticline at a depth of 5 km at the level of the Mirador Formation with apparent 3-way closure (Figure 2.4B). This anticline is along trend with the hydrocarbon traps to the northeast at Rio Chitamena and Cusiana. Our interpretation is similar to that of Cazier et al. (1995) and Cooper et al. (1995) for the Cusiana field, however, unlike Cazier et al. (1995) and Cooper et al. (1995), our interpretation proposes an early stage ramp anticline and does not require the involvement of pre-Late Cretaceous “basement”. Our interpretation is also similar to that of Mora et al. (2010b) for La Florida anticline, except that with our higher resolution seismic data we were able to image the deeper anticline in the Mirador Formation as well as the detachment in the lower Carbonera Formation. Minor shear fault-bend folding and right-lateral strike-slip out of the plane displacement on the Cusiana fault is not ruled out

by our 2D interpretation. Structural relief on the La Florida anticline and displacement on the Cusiana fault die out to the southwest along strike (Figure 2.2).

2.4.1.2 Retrodeformation of La Florida anticline

A structure's kinematic evolution plays an important role in determining whether the structure will provide migration pathways and traps at the critical moment for a petroleum system. The Florida anticline is a contractional fault-related fold (A – A',

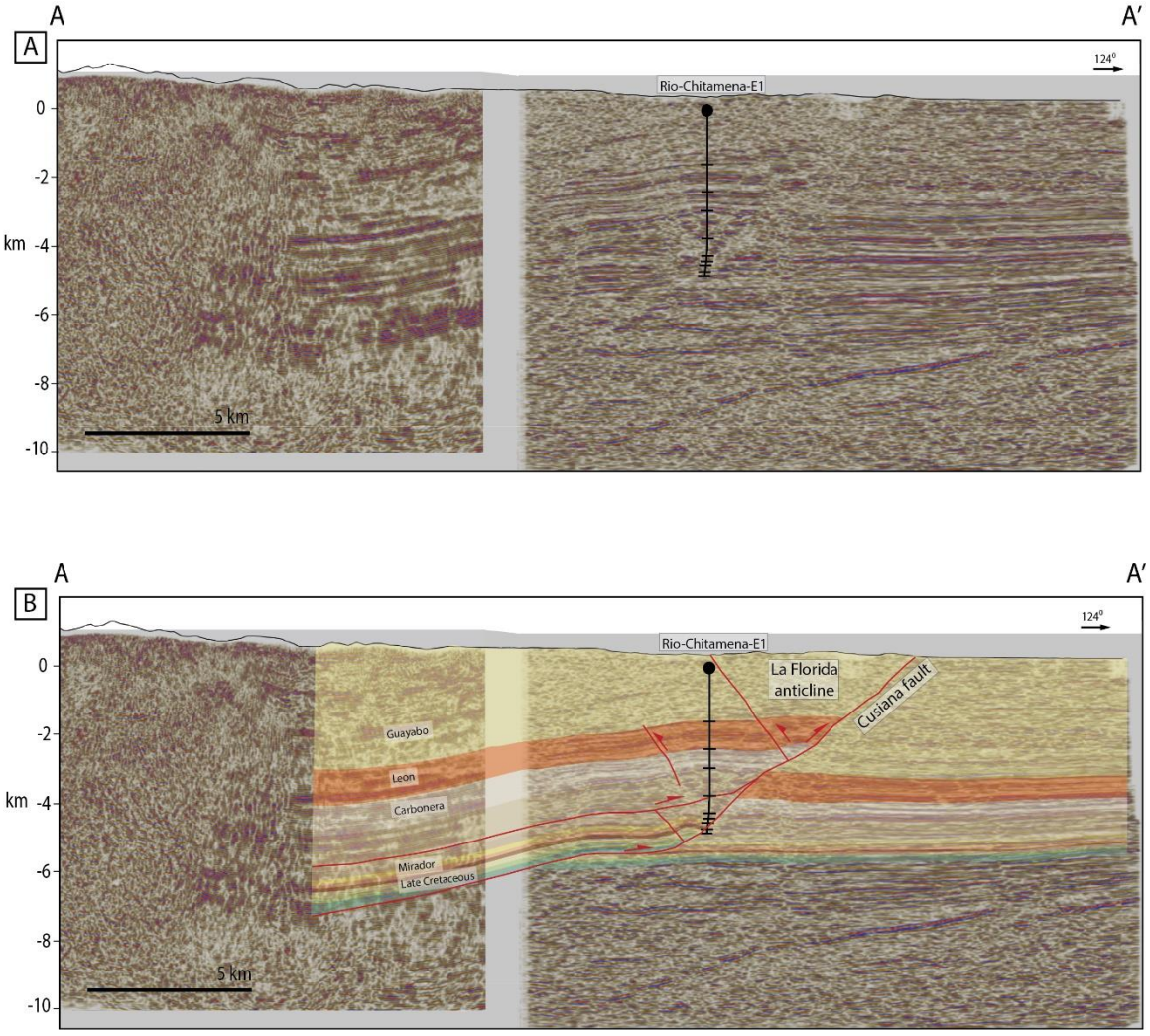

Figure 2.4: (A) Uninterpreted and (B) interpreted seismic lines showing the Florida anticline and Cusiana fault. 3D seismic inline 489 covered most of the Florida structure (right). The northwest side of the profile (left) is 2D seismic line RC-1991-13.MIG. Rio Chitamena well was projected ~3 km southwest along the anticlinal axis to constrain hanging wall formation tops. For location, see A – A' in Figure 2.2.

Figure 2.2, Figure 2.4B). To understand the structural evolution of La Florida anticline and the timing of trap formation relative to hydrocarbon migration, we retrodeformed the structure using the 2D kinematic fault-parallel flow and fault-bend fold algorithms in Move software (Figure 2.5).

Conformable folding and the lack of unconformities in the Guayabo Formation (Figure 2.4B) indicate that the major deformation of La Florida anticline was late Miocene or younger in age. We therefore retrodeformed La Florida profile (Figure 2.4B) to late Miocene time (Figure 2.5A) by flattening on a late Miocene Guayabo Formation horizon, (~7 Ma) assuming a constant sediment deposition rate. Thicknesses of Late Cretaceous and Early Tertiary units gently increase to the northwest. However, no abrupt Early or Late Cretaceous thickness changes associated with normal faulting as proposed by Cooper et al. (1995) can be identified across the Cusiana fault. Rather, the evidence seems to support the Cazier et al. (1995) interpretation that the Cusiana fault is not a reactivated normal fault.

Figure 2.5B shows our interpretation of the first late Miocene-Pliocene deformation event, the formation of a fault-bend fold. We interpret this as the first event, because when we began the retrodeformation by removing the slip on the present day Cusiana fault (Figure 2.5C), a large pre-existing fold resulted. The maximum age for the fold is constrained by the conformable folding and lack of growth strata or unconformities in the late Miocene lower Guayabo Formation (Figure 2.4). The fault-bend fold was formed by a thin-skinned thrust ramping up from a mid-Cretaceous detachment to a Paleocene flat near the base of the Mirador Formation. The lower decollement may be at the base Une Formation at the unconformity marking the

beginning of Late Cretaceous post-rift deposition. The minimum shortening on the ramp anticline was approximately 2.9 km (~ 51% of the total shortening) with vertical relief of 1.1 km. This fold formed an early potential hydrocarbon trap for all reservoir horizons from Late Cretaceous to Pliocene in age.

The present-day model (Figure 2.5C) shows basinward (to southeast) axial displacement of the Florida anticline, which resulted from reverse displacement on the Cusiana breakthrough fault. The displacement ramps up through the forelimb of the earlier fault-bend fold from two bedding-plane faults, the lower one at the base of the Late Cretaceous Une Formation and the upper fault in the Oligocene lower Carbonera (C6-C7). The Cretaceous detachment is near the unconformity marking the initiation of post-rift sedimentation. Approximately 1.8 km of slip is transferred from the Cretaceous detachment to the Cusiana breakthrough reverse fault. The Oligocene detachment may also follow an unconformity (~22 Ma) transferring an additional 1 km of slip to the Cusiana reverse fault. Total shortening on the Cusiana breakthrough fault is 2.8 km resulting in 1.5 km of structural relief on La Florida anticline. Total late Miocene to present thin-skinned shortening on La Florida anticline is 5.7 km.

The bedding plane thrust in the lower Carbonera Formation (Figure 2.4B, and Figure 2.5C) may also indicate an angular unconformity associated with an early Miocene deformation phase. Thus, it is possible that the folding of the Mirador Formation anticline beneath the thrust began in the early Miocene (~22 Ma?). The Mirador anticline is presently being tested for hydrocarbons. Maximum structural relief for this structure along the dip line profile (Figure 2.4B) is about 700 m.

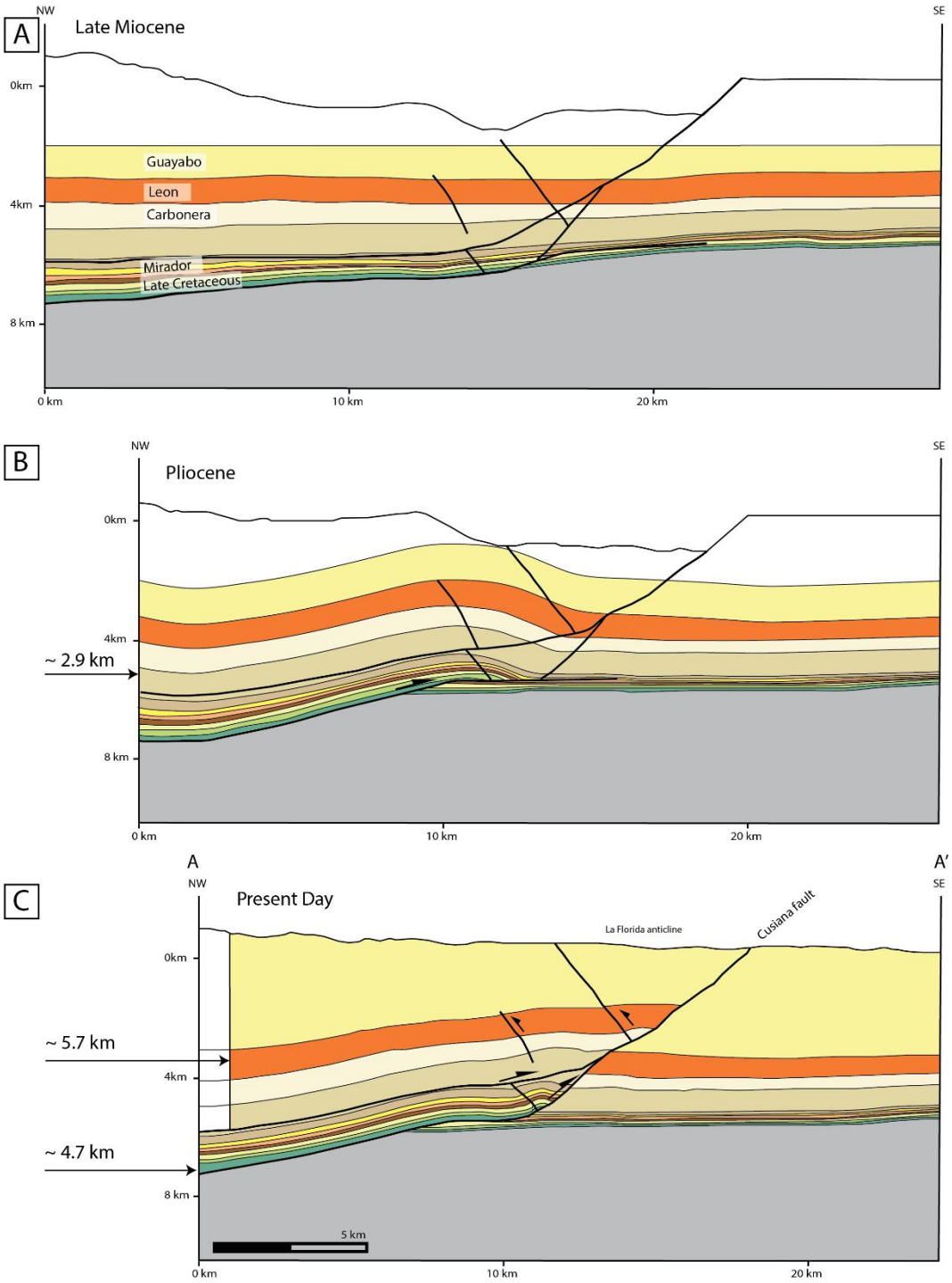

Figure 2.5: Retrodeformed cross-section A – A' across the Florida anticline during (A) late Miocene, (B) Pliocene, and (C) present time, respectively (see Figure 2.2 for location). Color scheme for stratigraphic units is the same as stratigraphic column in Figure 2.3. The Kinematic restoration ′ was performed using the fault-parallel flow and the fault-bend fold algorithms in 2DMove software, from Midland Valley.

2.4.2 Guavio anticline and Guacaramo fault

The Guaicaramo fault separates La Florida anticline and thin-skinned thrusting in the foothills belt to the east from thick-skinned basement involved thrusting in the Medina basin and Guavio anticline to the west. To study the role of basement faulting and the relative timing of thick-skinned and thin-skinned deformation, we interpreted a profile (Figure 2.6) across the northern termination of the Guavio anticline and the Guaicaramo fault (Figure 2.2).

2.4.2.1 Guavio anticline structural interpretation

Relatively little seismic data is available for the Medina basin and Guavio anticline. We interpreted a migrated 2D seismic profile (Figure 2.6A; B – B' in Figure 2.2; RC-1990-07.MIG) that crosses the northern termination of the Guavio anticline and the Guaicaramo fault. Our geologic interpretation (Figure 2.6B) is constrained by surface geology (Montoya et al., 2013) and well data as well as the reflection profile. No previous interpretations have been published for this profile. Previous studies of the Guavio anticline and Medina basin structure have focused on the central and southern part of the basin (e.g., Rowan and Linares, 2000; Branquet et al., 2002; Mora et al., 2009; Mora et al., 2010b; Jimenez et al., 2013; Hafiz et al., 2019). We tied the Guavio anticline seismic reflectors on the Guaicaramo hanging wall to the Medina-1 well (Figure 2.2; Branquet et al., 2002) along a seismic strike-parallel profile (Hafiz et al., 2019). Jimenez et al. (2013) noted that the Guaicaramo fault transitioned from a thin-skinned thrust folding the Guavio anticline in the south to a thick-skinned thrust folding the Tierranegra anticline to the north (Figure 2.2). Profile B – B' (Figure 2.6B) is in the transition zone between the two anticlines and the two structural styles. Just northeast of profile B – B',

rocks are uplifted 3 km along strike, exposing Early Cretaceous units and Late Cretaceous reservoir rocks at the surface in the Tierranegra anticline (Figure 2.2; Jimenez et al., 2013; Mora et al., 2019b).

The surface geology reveals subhorizontal bedding over the Guavio anticline but intense deformation in the Guaicaramo thrust hanging wall extending up to 5 km from the fault (Figure 2.6). An observed offset in the Mirador Formation requires a late stage backthrust offsetting the Gauicaramo fault at the Silbadero anticline (Figure 2.6B). Southeast dipping beds in the Rio Amarillo syncline dip antithetically to the underlying northwest dipping seismic reflectors suggest an early thin-skinned imbricate backthrusting event ramping up from a detachment in the lower Carbonera Formation (Figure 2.6B).

The Guaicaramo thrust ramps to the surface on a thin-skinned bedding plane thrust in the lower levels of the Late Cretaceous Guadalupe Group with a minimum of 4.9 km of slip (Figure 2.6B). Strata are uplifted 2 km in the Guavio anticline relative to similar units in the Guaicaramo footwall to the southeast. We explain this uplift with a thick-skinned fault-bend fold ramping up from deep in the pre-Cretaceous basement to an upper flat at the base of the Late Cretaceous. The basement fault requires approximately 5 km of shortening. We interpret this as a double-wedge fault-bend fold ramping up to the Guaicaramo fault, similar to the interpretation of the Guaicaramo fault 16 km to the south by Hafiz et al. (2019). Our interpretation is based on the observed backthrust offsetting the Guaicaramo fault) and the lack of shortening observed to the east (~ 1 km) in the nearby Parrando anticline. The geometry and kinematics of wedge thrusts are described by Price, 1986 and Medwedeff (1992). At the lower wedge tip, sediments in

the backthrust dip at the same direction as units in the footwall forelimb (Figure 2.6B) similar to the monocline zone in a passive-roof duplex (Jones, 1996).

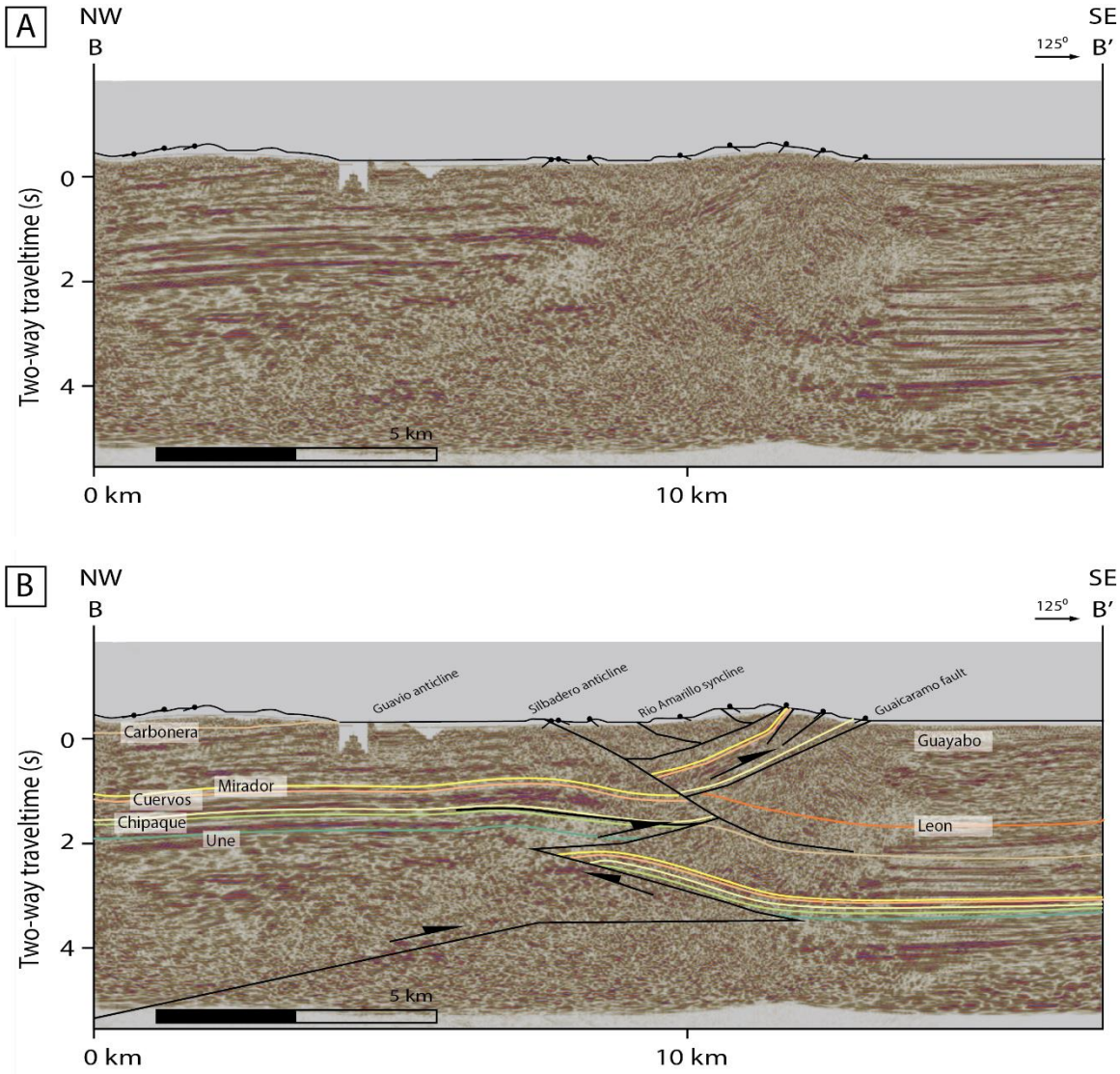

Figure 2.6: (A) Uninterpreted and (B) interpreted migrated seismic profile (RC-1990-07.MIG). Formation tops are labeled. Surface geology is from Montoya et al. (2013). For location see B – B' in Figure 2.2. Average vertical scale equals the horizontal scale.

Based on outcropping sections in the Tierranegra anticline to the northeast of the profile B – B' we estimate that the Cretaceous section thickens rapidly to 4 to 6 km on the Guaicaramo thrust hanging wall (Mora et al., 2010a ,b; Jimenez et al., 2013). We

interpret the Guaicaramo thrust as an inverted Cretaceous normal fault, active during Early Cretaceous rifting (e.g., Jimenez et al., 2013).

2.4.2.2 Retrodeformation of the Guavio anticline profile

To determine the evolution and relative timing of thick-skinned and thin-skinned deformation in the Guavio anticline and Guaicaramo thrust, we retrodeformed profile B – B' (Figure 2.6). The Guavio profile retrodeformation was modeled using 2D kinematic fault-parallel flow and fault-bend fold algorithms (Figure 2.7).

Profile B – B' (Figure 2.6) was first retro-deformed to top Leon Formation in Middle Miocene time (~ 10 Ma) in Figure 2.7A. This horizon was chosen because Leon Formation rocks crop out on the northwest end of the profile with bedding dips conformable to the underlying Tertiary units (Figure 2.6). Also on the southeast end of the profile there are no apparent growth faults or angular unconformities in the Leon Formation indicating that the major deformation occurred in the last 10 Myr after deposition of the Leon Formation. It is always possible that hanging wall unconformities related to earlier thrusting and ramping on the Guaicaramo thrust could have been removed by erosion. Based on the surface geology west of the Tesalia fault (Figure 2.2; Mora et al., 2006; Parra et al., 2009a) and in the Tierranegra anticline (Mora et al., 2010a ,b; Jimenez et al., 2013), we estimate that the Early Cretaceous section is 1.5 to 3 km thick west of the Guaicaramo fault (Figure 2.7A). We therefore interpret the Guaicaramo fault as the southeastern boundary of an Early Cretaceous rift basin. Deposition of post-rift Late Cretaceous sediments was more uniformly distributed during regional thermal subsidence.

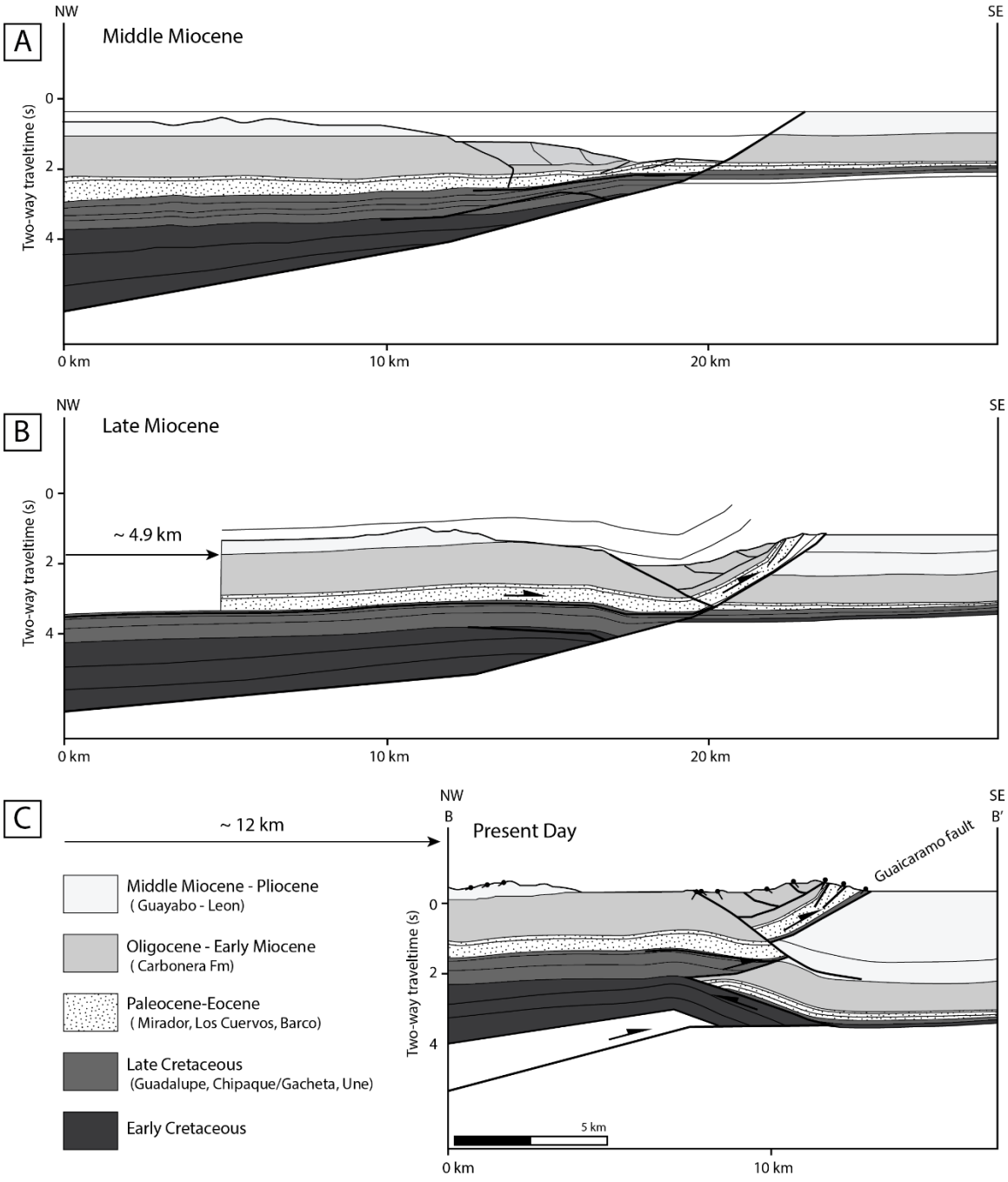

Figure 2.7: Tectonic evolution of the Medina basin (middle Miocene to present) based on retrodeformation of migrated seismic profile RC-1990-07.MIG (Figure 2.6, profile B – B' in Figure 2.2). (A) Middle Miocene showing Early Cretaceous normal fault. (B) Late Miocene thin-skinned thrusting on the Guaicaramo fault. (C) Present showing thick-skinned (basement) inversion of normal fault that produced the Guavio fault-bend fold and double wedge fault.

The first Miocene deformation event was a thin-skinned bedding-plane ramp thrust on the Guaicaramo fault (Figure 2.7B). The thrust had a minimum of 4.9 km of slip on a bedding plane detachment near the base of the Late Cretaceous Guadalupe Group. The tectonic relationships demonstrate that the thin-skinned thrusting had to occur before the thick-skinned basement ramp anticline and prior to the Silbadero backthrust. The lack of hanging wall unconformities in the Leon Formation suggests a late Miocene age or younger for the thrusting. However, earlier thrusting cannot be ruled out, because hanging wall ramp unconformities could have been removed by erosion. The interpretation of the thrust as part of a late stage ramp anticline as proposed for the Guavio anticline further south by Parra et al. (2009a) and Hafiz et al. (2019) is notfeasible on this profile. We therefore think that it is likely that thin-skinned thrusting on the Guaicaramo fault preceeded thick-skinned basement thrusting across the Guavio anticline and Medina basin area. The 4.9 km of thin-skinned shortening represents 40% of the total minimum shortening on profile B – B' (Figure 2.7B).

Thin-skinned thrusting was followed by formation of a broad basement ramp anticline (Figure 2.7C). Compression inverted an Early Cretaceous normal fault, ramping up from pre-Cretaceous basement to an upper flat at the base of the Late Cretaceous. This thick-skinned basement fault-bend fold produced 2 km of vertical relief and 5 km of shortening. We interpret this as a double-wedge fault-bend fold (Medwedeff, 1992) ramping up to the Guaicaramo fault, similar to our interpretation of the Guaicaramo fault 16 km to the south (Hafiz et al., 2019). The conformable folding of Guayabo Formation horizons in the Guaicaramo footwall dates the basement faulting as no older than late Miocene-Pliocene. Finally, the Guaicaramo ramp thrust was offset 700 m by a northeast

dipping backthrust (Figure 2.7C). Total minimum Miocene-Pliocene shortening on the Guavio anticline was 12 km.

2.4.3 Hydrocarbon maturation and burial histories

The timing of source rock oil generation and expulsion relative to trap formation is critical to understanding the evolution of the foothills petroleum system. The main source rock in the Llanos basin is the shallow-marine Late Cretaceous Gacheta Formation and its lateral equivalent, the Chipaque Formation (Ramon and Fajardo, 2006; Sánchez et al., 2015). Mora et al. (2019a) used paleo-geographic maps of potential petroleum systems to show that most hydrocarbons in foothill's traps that charged in the last 3 Myr came from the Gacheta Formation. The Early Cretaceous source rocks in the Fomeque and Macanal formations (Figure 2.3) had expelled their hydrocarbons in the Llanos basin prior to the late Eocene deposition of the main reservoir rocks and long before the formation of Llanos foothills traps in late Miocene-Pliocene (Mora et al., 2010a; Garcia et al., 2015; Sánchez et al., 2015). In this paper we focus 1-D burial models on the Late Cretaceous Gacheta Formation, the main source rock in the foothills zone.

We developed 1-D burial models for two wells in the foothills, Rio Chitamena E-1 and Bromelia-1 (Figure 2.2). Unit thicknesses were derived directly from the well data. One of the most important parameters of the burial history model is the heat-flow, which helps determine the accurate time of oil expulsion (Allen and Allen, 2005; Hantschel and Kauerauf, 2009). The heat-flow estimates range from 35 mW/m2 in the foreland to 45 mW/m2 in the hinterland (Toro et al., 2004). The Sánchez et al. (2015) 1D model assumed exponentially decreasing heat flow ranging from ~ 63 to 33 mW⁄m2 associated with postrift lithospheric thermal contraction, but averaging 46 mW⁄m2 for the last 60 Ma

west of the Tesalia fault. For our 1D models, we chose the heat-flow range 35 - 45 mW/m2, the average heat-flow range of foreland basins worldwide.

2.4.3.1 One-dimensional model of Rio-Chitamena well

Rio-Chitamena E-1 well is located in the hanging wall of the Cusiana fault in La Florida anticline 3 km northeast of profile A – A' (Figure 2.2) southwest of Cusiana oilfield. Rio Chitamena well logs reveal the depth of the Late Cretaceous Gacheta source rock as ~ 4.9 km (15,999 ft). The drilled Guayabo Formation has a thickness of ~ 1.6 km (5,284 ft). Based on 3D seismic data from the Cusiana fault footwall (e.g., A – A' inFigure 2.4) we estimate the average thickness of the Guayabo Formation as ~ 3.1 km (10,000 ft), which means that almost half of the Guayabo Formation, about 1.5 km, was eroded in the Rio Chitamena well location. Assuming a constant heat flow of 35 mW/m2, our 1D model for Rio Chitamena well (Figure 2.8A) predicts that oil generation began in the late Miocene (~ 8.9 Ma) at a burial depth of 4.8 km (~ 15,700 ft). The Gacheta Formation source rock has remained in the oil window until the present. The oil expulsion occurred before the last major cycle of Eastern Cordillera uplift in late Miocene-Pliocene about 6 – 3 Ma (Mora et al., 2013), and the recent anticlinal trap formation in the foothills zone after 3 Ma (Ramirez-Arias et al., 2012; Carrillo et al., 2016).

2.4.3.2 One Dimensional Model of Bromelia Well

Bromelia-1 well, 15 km southwest of La Florida anticline (Figure 2.2), penetrated the Late Cretaceous section in the Cusiana fault footwall and reached Paleozoic basement. The Gacheta Formation source rock in Bromelia-1 is 600 m (~ 2,000 ft) deeper than in the hanging wall in Rio Chitamena E1. We assumed that Miocene-Pliocene

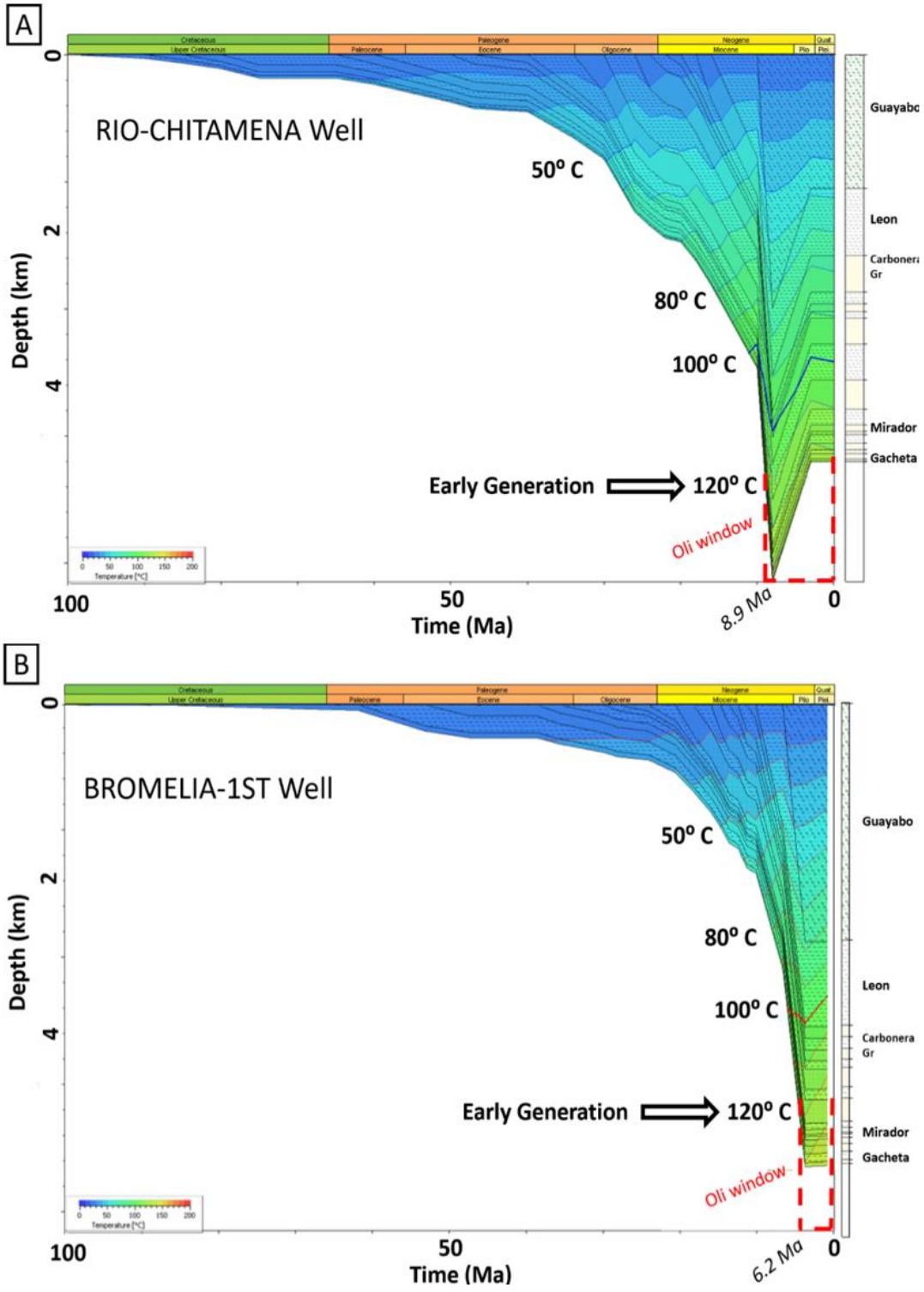

Figure 2.8: One-dimensional models of burial history with constant heat flow of 35 mW/m² in the foothills zone, showing that oil generation began earlier at Rio Chitamena well (A) in the hanging wall of the Cusiana fault (~ 9 Ma) than in the Cusiana fault footwall at Bromelia-1ST well (~ 6 Ma). For the locations of wells, see Figure 2.2.

erosion of the Cusiana footwall was negligible and could be ignored. Assuming a constant heat flow of 35 mW/m2, our 1D model for Bromelia-1 well (Figure 2.8B) predicts that oil generation began in the late Miocene (6.2 Ma) with a burial depth of 5 km (~ 16,400 ft). The slightly later critical moment in the footwall (Figure 2.8B) relative to the hangingwall (Figure 2.8A) reflects the gradual northwestward thickening of the Late Cretaceous and Paleogene sections (see Figure 2.4 and Figure 2.5A). Since the onset of expulsion, temperatures in the Bromelia-1 Gacheta Formation source rocks have remained within the oil window.

2.5 DISCUSSION

2.5.1 Timing of oil expulsion in the Llanos foothills and Medina basin.

The history of oil generation in the Eastern Cordillera and Llanos basin has been comprehensively studied in a number of recent publications (e.g., Garcia et al., 2015; Sánchez et al., 2015; Mora et al., 2019a). The 1-D maturation models by Sánchez et al. (2015) predicted that the first oil generation from the marine Late Cretaceous Chipaque Formation began in the late Paleocene (58 Ma) in the southern part of the present Eastern Cordillera. In the northeast, the Late Cretaceous source rocks entered the oil window in the early Oligocene (Mora et al., 2015).

By the late Oligocene, oil generation ceased as a result of the tectonic inversion of the Eastern Cordillera (Mora et al., 2019a). This deformation event ended the first oil charge event (Garcia et al., 2015) from the largest and most productive kitchen in the present Eastern Cordillera (Sánchez et al., 2015). The migration of petroleum prior to the onset of exhumation of the Eastern Cordillera (Parra et al., 2009b; Mora et al., 2010a)

was updip eastward toward shallow reservoirs in the Llanos basin (Sánchez et al., 2015). However, there may have been no traps available to preserve the pre-late Oligocene hydrocarbons in the Medina basin and Llanos foothills.

In the early Miocene to late Miocene (20 – 9 Ma) kitchens migrated to the northeast, and oil generation was restricted to local sites in the north (Sánchez et al., 2015). The hydrocarbon generation in the Medina basin could be estimated by the 2-D transformation ratios (Sánchez et al., 2015) that show that the organic matter of the Chipaque formation was 49% and 100% converted in the eastern and western kitchen, respectively. One-dimensional burial models from Medina basin suggest that oil expulsion began about 18 – 24 Ma assuming a heat flow range of 35– 46 mW/m2 (Hafiz et al., 2019). Expulsion in the Medina basin began therefore at least 10 Myr before the Guavio anticline trap formed.

In late Miocene to present (9 – 0 Ma), the transformation ratio of the Chipaque source rock organic matter reached 100%, which implies that no active kitchen exists in the Medina basin (Sánchez et al., 2015). A second kitchen, however, located in the foothills to the east generated hydrocarbons throughout the Neogene. Oil generation began ~ 9 Ma in the northern foothills (Cazier et al., 1995; Garcia et al., 2015; Sánchez et al., 2015), and began slightly later in the southern foothills, about 7 - 6 Ma at Parrando-1 (Hafiz et al., 2019) and Bromelia-1 wells (this paper). In this recent pulse, the migration of light fluids followed steep faults and fractures, short migration distances occurred due to the vertical flow, and light oil and gas accumulated in Pliocene age traps (Mora et al., 2019a; this paper). Eventually, active kitchens were limited to small areas in the foothills

and were clearly absent in the Medina basin (Sánchez et al., 2015), which led us to describe the Guavio anticline as a massive dry trap.

2.5.2 Timing of thin-skinned thrusting and thick-skinned basement uplift in the Llanos foothills

This study demonstrates that thin-skinned thrusting on the Guaicaramo fault had to occur before the thick-skinned basement ramp formed the Guavio anticline (Figure 2.7). The lack of hanging wall unconformities in the Leon Formation suggests a late Miocene age or younger for the thrusting. However, earlier thrusting cannot be ruled out, because hanging wall ramp unconformities could have been removed by erosion.

Dengo and Covey (1993) proposed that the Eastern Cordillera is essentially an east-verging structure formed during two main tectonic phases. The first tectonic phase induced a thin-skinned style that created large, east-verging thrust faults, detached into Lower and Upper Cretaceous and Paleogene sequences, with the greatest shortening in the middle-Miocene to Pliocene. During the Pliocene, deformation changed from basement-detached to basement involved as Jurassic and Early Cretaceous normal faults were inverted (Dengo and Covey, 1993).

To better understand the timing of deformation events on the eastern flank of the Eastern Cordillera in the area of the Guavio and La Florida anticlines, we compiled published thermochronometric ages from Oligocene to present in Table 2.1 and Table 2.2. The data in the tables includes apatite fission-track (AFT) and zircon fission-track (ZFT) ages published by Mora et al. (2008); Parra et al. (2009b); Mora et al. (2010a); Ramirez-Arias et al. (2012); Mora et al. (2013). Fission-track sample locations are shown

Table 2.1: Apatite Fission Track Data.

ID	Sample	Longitude (°W)	Latitude (°N)	Elevation (m)	AFT Age	±1 σ Error	References
A 01	A51	- 72° 50' 17.58"	5° 35' 20.88"	1200	9.6	± 2.5	Parra at al 2009b
A 02	A11	- 72° 49' 5.04"	5° 35' 10.02"	1556	14.1	± 2.0	Parra at al 2009b
A 03	MP-27	- 72°31'20.31"	5°30'22.28"	839	11.7	± 2.5	Mora et al 2010a
A 04	MP-40	- 72°30′04.01″	5°29′03.01″	665	8.3	± 1.2	Mora et al 2010a
A 05	MP-18	- 72°28′41.24″	5°28′09.77″	645	6.3	± 1.2	Mora et al 2010a
A 06	MP-12	- 72°28′10.00″	5°27′33.70″	555	9.6	± 2.6	Mora et al 2010a
A 07	MM-005	- 72°31′28.38″	5°28′52.46″	865	11.2	± 1.9	Mora et al 2013
A 08	A10	- 73° 11' 00.48"	5° 18' 25.68"	2215	6.6	± 0.9	Parra at al 2009b
A 09	FF-G1-A11-30	- 72° 44' 01.80"	5° 13' 34.32"	656	16.3	± 1.8	Ramirez-Arias et al 2012
A 10	A26	- 73° 23' 26.46"	5° 1' 55.50"	2954	1.9	± 0.7	Parra at al 2009b
A 11	PM-034	- 72° 53' 35.34"	4° 59' 13.20"	900	14.6	± 1.5	Ramirez-Arias et al 2012
A 12	MA16C	- 73°16'25.33"	4°52'21.18"	800	2.2	± 0.4	Mora et al 2010b
A 13	MA18	- 73°16'23.62"	4°51'42.64"	825	1.7	± 0.4	Mora et al 2010b
A 14	CS-3	- 73°42′55.44″	4°11′53.62″	995	3.1	± 0.5	Mora et al 2013
A 15	16	- 73°39'25.20"	4°29'41.64"	2018	0.8	± 0.3	Mora et al 2008

A 16	13	- 73°40'51.24"	4°29'37.68"	2699	2.8	± 0.4	Mora et al 2008
A 17	11	- 73°43'52.32"	4°29'18.6"	3662	2.7	± 0.7	Mora et al 2008
A 18	17	- 73°33'27.00"	4°28'52.68"	2078	0.9	± 0.2	Mora et al 2008
A 19	14	- 73°41'35.16"	4°28'17.76"	2137	2.3	± 0.8	Mora et al 2008
A 20	12	- 73°42'29.88"	4°27'35.64"	3041	2.4	± 0.7	Mora et al 2008
A 21	15	- 73°40'48.72"	4°25'49.44"	1644	1.2	± 0.4	Mora et al 2008
A 22	A37	- 73° 57' 15.36"	4° 23' 52.32"	2963	2	± 0.7	Parra at al 2009b
A 23	10	73°54'2.88"	4°22'13.8"	1458	3.8	± 0.7	Mora et al 2008
A 24	7	73°46'58.08"	4°17'35.88"	2963	2.6	± 0.5	Mora et al 2008
A 25	8	73°47'0.24"	4°17'33"	2954	2.6	± 1.1	Mora et al 2008
A 26	6	73°48'1.08"	4°16'2.64"	2215	2.3	± 0.6	Mora et al 2008
A 27	9	73°53'38.76"	4°13'28.2"	1556	2.8	± 0.4	Mora et al 2008
A 28	5	73°47'42.36"	4°12'10.44"	1200	1.6	± 0.4	Mora et al 2008
A 29	3	73°38'40.92"	4°11'54.96"	567	3	± 0.4	Mora et al 2008
A 30	4	73°42'44.64"	4°11'46.32"	921	2.9	± 2.1	Mora et al 2008
A 31	2	73°40'8.4"	4°9'44.64"	831	2.6	± 0.3	Mora et al 2008
A 32	1	73°40'12.72"	4°9'41.04"	846	2.7	± 0.3	Mora et al 2008

Table 2.2: Zircon Fission Track Data

ID	Sample	Longitude (°W)	Latitude (°N)	Elevation (m)	ZFT Age	±1 σ Error	Reference
Z 01	MA 16	73°16'2.1"	4°52'23.5812"	990	24.9	± 1.4	Parra at al 2009b
Z 02	Soescol	73°23'3.9012"	4°51'12.3012"	1858	15.7	± 1.5	Parra at al 2009b
Z 03	SJ 1	73°40'51.06"	4°29'37.68"	2748	5.9	± 0.4	Parra at al 2009b
Z 04	FT 1	73°43'52.2012"	4°29'18.4812"	3660	13.1	± 0.9	Parra at al 2009b
Z 05	SJ 5	73°41'35.16"	4°28'17.76"	2251	11.5	± 0.6	Parra at al 2009b
Z 06	BV 126	73°54'31.3812"	4°22'37.74"	1582	13.3	± 1	Parra at al 2009b
Z 07	BV 194	73°46'37.6788"	4°17'51.2988"	3084	9.8	± 0.6	Parra at al 2009b
Z 08	BV 196	73°47'0.1212"	4°17'33"	2862	11.4	± 1.1	Parra at al 2009b
Z 09	BV 86	73°50'4.4988"	4°16'43.9212"	1226	8.3	± 0.5	Parra at al 2009b

in Figure 2.9A. Figure 2.9B is a histogram showing the age distribution for the fission-track data. The ages fall into three broad clusters (Figure 2.9B), one late Oligocene ZFT age at 25Ma, 18 late Miocene ages from 18 to 4 Ma (16 of these from 16 to 6 Ma with a peak of 9 from 12 to 8 Ma), and the sharpest peak of 22 Pliocene-Pleistocene ages from 4 to 1 Ma.

The ZFT age Z 01 in Table 2.2 suggests that deformation and uplift began in late Oligocene (~25 Ma) west of the Tesalia fault (Figure 2.9A) as proposed by numerous recent studies (Parra et al., 2009a; Parra et al., 2009b; Mora et al., 2010b; Bande et al., 2012; Ramirez-Arias et al., 2012; Jimenez et al., 2013; Mora et al., 2013). Corredor (2003) estimated over 50 km of Oligocene ENE-WSW thin-skinned shortening in the northern Eastern Cordillera. The Oligocene age deformation is defined in the eastern foothills by the base of Carbonera (C6) unconformity (Corredor, 2003; Martinez, 2006; Egbue and Kellogg, 2012). A lower Carbonera Formation angular unconformity was also observed in the Guavio anticline by Teixell et al. (2015) and Hafiz et al. (2019) and possibly in La Florida anticline (Figure 2.4B, Figure 2.5C this paper). Saeid et al. (2018) interpret an abrupt change in stream flow directions in Carbonera (C-5) to indicate the rise of incipient foothills in the area of the Guaicaramo thrust at about 22 Ma. Sediment provenance data and reworked pollen samples also show a late Oligocene-early Miocene exhumation of Cretaceous rocks (Horton et al., 2010; Bande et al., 2012; De la Parra et al., 2015).

The fission-track age data (Figure 2.9B) includes a wide distribution of late Miocene ages, with a peak at 12 to 8 Ma. Our interpretation of the Guavio anticline (Figure 2.6) suggests a late Miocene age or younger for thrusting on the Guaicaramo

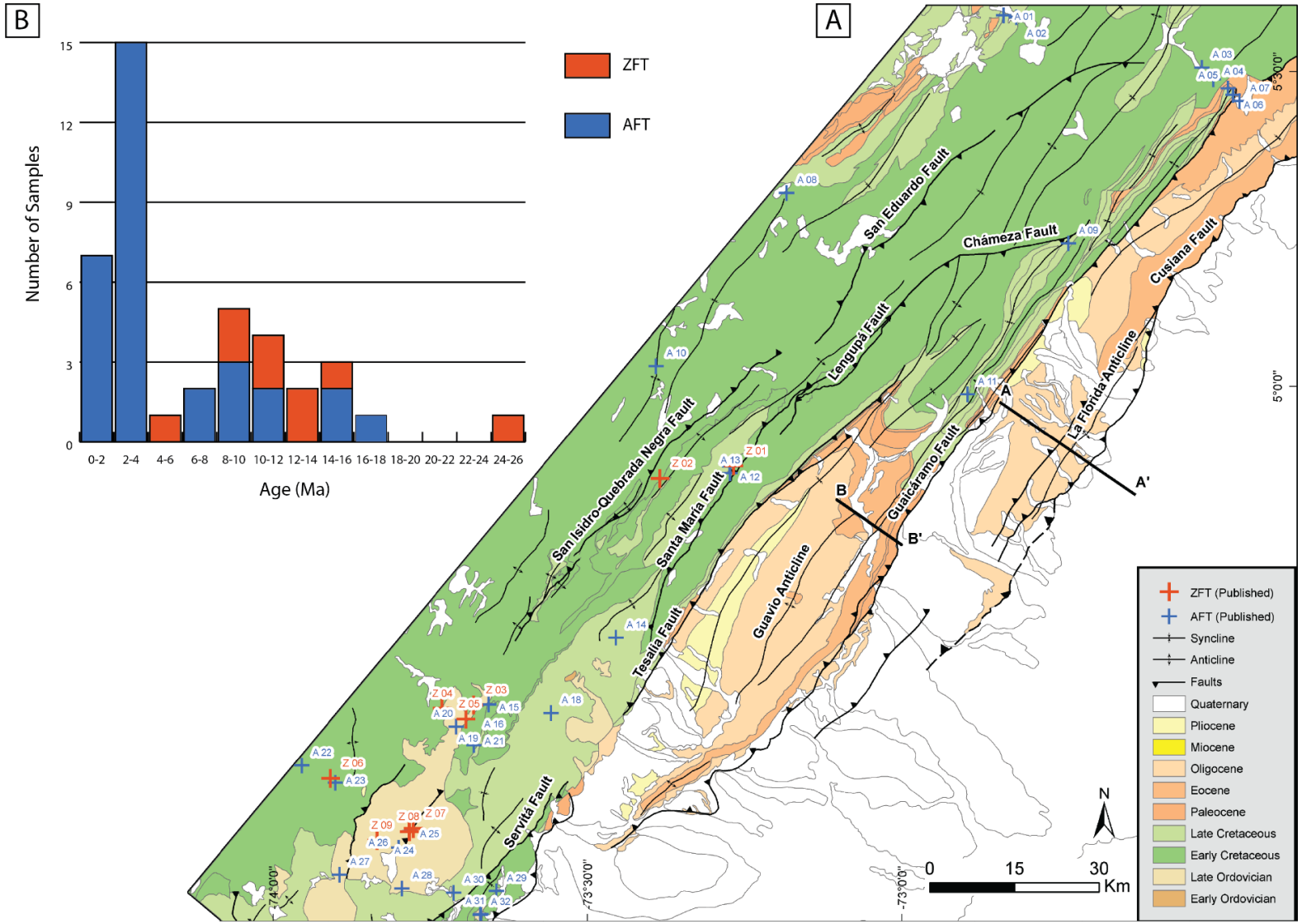
B
Number of Samples
15
12
9
6
3
0
0-2
2-4
4-6
6-8
8-10
10-12
12-14
14-16
16-18
18-20
20-22
22-24
24-26
Age (Ma)
ZFT
AFT
A
San Eduardo Fault
Chámeza Fault
Cusiana Fault
Lengupá Fault
La Florida Anticline
San Isidro-Quebrada Negra Fault
Santa María Fault
Guavio Anticline
Guaicáramo Fault
Tesalia Fault
Servitá Fault
A
A'
B
B'
5°0'0"
-73°30'0"
-74°0'0"
N
0
15
30
Km
ZFT (Published)
AFT (Published)
Syncline
Anticline
Faults
Quaternary
Pliocene
Miocene
Oligocene
Eocene
Paleocene
Late Cretaceous
Early Cretaceous
Late Ordovician
Early Ordovician

Figure 2.9: (A) Geologic map showing the locations of published fission-track samples (map location in Figure 2.1). Apatite fission-track (AFT) in blue and zircon fission-track (ZFT) in red. (B) Histogram shows age distribution. For thermochronometric data values and references, see Table 2.1 and Table 2.2.

fault. The fission-track age data has been interpreted by Bande et al. (2012) and Ramirez-Arias et al. (2012) as showing the onset of exhumation for the Guaicaramo hanging wall in the late Miocene. Branquet et al. (2002) and Teixell et al. (2015) have also interpreted thin-skinned thrusting on the Guaicaramo (Aguaclara) fault as originating in the late Miocene.

The greatest numbers of apatite fission-track ages for the study area (Figure 2.9B) are Pliocene-Pleistocene (4 to 1 Ma). Conformable folding and the lack of unconformities or growth strata in the Guayabo Formation (Figure 2.4B) indicate that Cusiana fault thin-skinned thrusting to form La Florida anticline was late Miocene (~ 7 Ma) or younger in age. Numerous studies suggest that the Cusiana fault and the associated folds in the foothills zone are Plio-Pleistocene in age (Cazier et al., 1995; Cooper et al., 1995; Mora et al., 2010b; Bande et al., 2012; Ramirez-Arias et al., 2012; Carrillo et al., 2016). While Pliocene-Pleistocene thrusting in the foothills east of the Guaicaramo fault was thin-skinned, thick-skinned basement-involved inverse faults were active west of the Guaicaramo fault. Basement-involved reverse faults would be likely to produce more vertical tectonic relief than thin-skinned thrusting alone. Rapid tectonic uplift in the last 5 Myr is supported by the spike in AFT ages from 4 to 1 Ma (Figure 2.9B). It is also in agreement with paleoelevation data from Wijninga (1996) and Gregory-Wodzicki (2000) that show rapid elevation gain from 5 to 2 Ma. The present tectonic relief of the east flank of the Eastern Cordillera is approximately 10 km (Egbue et al., 2014). Dengo and Covey (1993) noted that during the Pliocene, deformation became more basement involved as

Jurassic and Early Cretaceous normal faults were inverted. Egbue and Kellogg (2012) showed that basement-involved thick-skinned uplift was one of the most recent deformation events in the piedemonte area of the foothills. In this paper we also show recent thick-skinned inversion of the Guaicaramo fault to produce the Guavio fault-bend fold (Figure 2.7C). The recent rapid shortening and basement involved uplift of the Eastern Cordillera have been linked to the collision with the Panama-Choco arc and flat slab subduction (e.g., Wagner et al., 2017; Kellogg et al., 2019; Mora-Páez et al., 2019). Across the northern Andes, other basement blocks were also rapidly uplifted 7–12 km in the last 10 Myr, including the Venezuelan Andes (De Toni and Kellogg, 1993), Sierra de Perija (Shagam, 1980; Kellogg and Bonini, 1982), Santander Massif (Amaya et al., 2017), Garzon Massif (Saeid et al., 2017), and the Santa Marta Massif (Villagómez et al., 2011). The spatial distribution of these numerous Laramide-style basement block uplifts correlates with buoyant Caribbean low-angle to flat slab subduction and resultant low heat flow (Kellogg et al., 2019).

2.6 CONCLUSIONS

In this study, we interpreted the geological structures and petroleum systems associated with La Florida anticline and the Cusiana fault system in the Llanos foothills and the Guavio anticline and the Guaicaramo fault system in the Medina basin. We also compiled published AFT and ZFT age data for the study area. We recognize at least three periods of tectonic activity in the last 30 Myr, late Oligocene (25-22 Ma) uplift and thrusting on the Tesalia fault to the west, late Miocene (12-8 Ma) thrusting on the Guaicaramo fault, and Pliocene-Pleistocene (4-1 Ma) thrusting on the Cusiana fault and basement involved inversion of the Guaicaramo fault.

Unlike previous interpretations of the Guavio anticline and Medina basin area, our interpretation shows that thin-skinned thrusting on the Guaicaramo fault preceeded thick-skinned basement thrusting. The first Miocene deformation event was a thin-skinned ramp thrust on the Guaicaramo fault with a minimum of 4.9 km of slip on a bedding plane detachment near the base of the Late Cretaceous Guadalupe Group. This was followed by a Pliocene thick-skinned fault-bend fold ramping up from pre-Cretaceous basement to a double-wedge fault. This inversion of the Cretaceous Guaicaramo normal fault resulted in 5 km of shortening and 2 km of uplift. Total minimum Miocene-Pliocene shortening on the Guavio anticline profile was 12 km.

To the east, all the thrusting on the Cusiana fault and La Florida anticline was thin-skinned. We present the first retrodeformed model for La Florida anticline. We propose a previously unrecognized late Miocene-Pliocene fault-bend fold formed by a thin-skinned thrust ramping up from a mid-Cretaceous detachment with a minimum of 2.9 km of shortening and 1.1 km of uplift. This fold formed an early potential hydrocarbon trap. This was followed by the Cusiana reverse fault, a forelimb breakthrough fault ramping up from two bedding plane faults. Total shortening on the Cusiana breakthrough fault is 2.8 km resulting in 1.5 km of structural relief on La Florida anticline. Total late Miocene-Pliocene shortening on the La Florida anticline was about 5.7 km.

By the late Oligocene, oil generation west of the study area ceased as a result of tectonic inversion along the Tesalia fault. One-dimensional burial models from Medina basin suggest that oil expulsion began about 18 – 24 Ma (Hafiz et al., 2019). Expulsion in the Medina basin began therefore at least 10 Myr before the Guavio anticline trap

formed, thus preventing a commercial hydrocarbon charge. In the late Miocene to present (9 – 0 Ma), no active kitchens existed in the Medina basin however, but source rocks located in the foothills to the east generated hydrocarbons throughout the Neogene. New 1-D burial models for Rio-Chitamena E-1 and Bromelia-1 wells in this paper predict that oil generation began in the La Florida Cusiana foothills ~ 9 to 6 Ma. The La Florida anticline, therefore, has an active petroleum system (source, reservoir, seal, timing of charge, and trap formation) similar to the nearby Cusiana giant field, and source rocks remain in the oil window. The Medina anticline to the southwest of La Florida is isolated from the active Foothills source pods by the major sealing Guaicaramo thrust fault.

CHAPTER 3 MULTI-ATTRIBUTE ANALYSIS USING COHERENCY AND ANT-TRACKING TECHNIQUES FOR FAULT AND FRACTURE DETECTION IN LA FLORIDA ANTICLINE, LLANOS FOOTHILLS, COLOMBIA[2]

[2] Albesher, Z., Kellogg, J., Hafiza, I., Saeid, E., 2020, Multi-Attribute Analysis Using Coherency and Ant-Tracking Techniques for Fault and Fracture Detection in La Florida Anticline, Llanos Foothills, Colombia: Geosciences , v.10, no.4, (Article number:154). doi: https://doi.org/10.3390/geosciences10040154

3.0 OVERVIEW

In the Llanos foothills, Eastern Cordillera, Colombia, high levels of deformation have produced considerable noise in the seismic data. As a result, because of noise sensitivity, seismic attribute analysis has not been commonly used in foothills studies. In this paper, we present techniques to reduce noise and enhance seismic quality, making possible the first multi-attribute analysis of a 3D seismic volume in the Foothills (La Florida anticline) using coherency and ant-tracking techniques for fault and fracture detection. The results could help reduce risk in models of reservoir fracture porosity and permeability. The dominant fracture strike direction in the studied seismic volume (La Florida) is NE-SW (055 ± 20°), parallel to the structural strike of the adjacent Eastern Cordillera Foothills. Ant-tracking fracture results for the reservoir rocks, the Guadalupe Group, Barco and Mirador formations, in the La Florida anticline as well as in the non-folded reservoir rocks to the SE, also reveal the NE-SW fracture set. Late Miocene (10 – 9 Ma) NE-SW normal faulting and fractures may have been produced by lithospheric bending as the mountain front advanced from the northwest. We compared fracture intensity and orientation in folded rocks with the fracture intensity and orientation in non-folded rocks. Our study showed NE-SW, NW-SE, and E-W fracture orientations in the non-folded seismic volume, suggesting that regional stresses could produce these fracture sets, not just folding processes as previously proposed. Azimuthal filtering highlighted secondary fracture trends, including a prominent NNW-SSE (155 ± 15°) trend and a minor E-W (085 ± 10°) trend. The NW-SE and WNW-ESE fracture sets are only found in the Guayabo Fm (11 Ma – Present) synchronous with the greatest orogenic shortening. Right-lateral strike-slip displacement on the nearby Algeciras fault system in the last 2

m.y. may have generated WNW-ESE and NW-SE Riedel-type shear fractures in the Foothills study area.

3.1 INTRODUCTION

La Florida anticline is located in the Llanos foothills (Figure 3.1) bounded by the Cusiana thrust fault system and the Llanos basin to the southeast, and by the Guaicaramo fault system and the Eastern Cordillera to the northwest. The eastern foothills of the Eastern Cordillera of Colombia contains important oil fields in a complex foreland fold and thrust belt (e.g., Cazier et al., 1995; Cooper et al., 1995). The main reservoirs of the giant Cusiana oilfield, the Mirador, Barco, and Guadalupe formations have low porosity but are highly fractured in the fold traps (Cazier et al., 1995; Tamara et al., 2015). Fracture systems are critically important, creating fracture porosity as well as pathways for hydrocarbon migration and production (Cazier et al., 1995; Ortiz and Beltran, 2008; Engelder et al., 2009; Tamara et al., 2015).

La Florida anticline (Figure 3.1) is located on the trend of anticlinal traps associated with the Yopal-Cusiana fault system, including Rio Chitamena 3 km to the northeast and the giant Cusiana oilfield 16 km to the northeast (Cazier et al., 1995). Mora et al. (2010b) interpreted La Florida anticline as produced by slip on the Cusiana fault, a listric high angle reverse fault. Both Cooper et al. (1995) and Cazier et al. (1995) also interpreted the Cusiana fault as a listric reverse fault involving Early Cretaceous and older basement. Albesher et al. (2019) reinterpreted all the thrusting on the Cusiana fault and La Florida anticline as thin-skinned and presented the first retrodeformed model for La Florida anticline, proposing a previously unrecognized late Miocene-Pliocene fault-

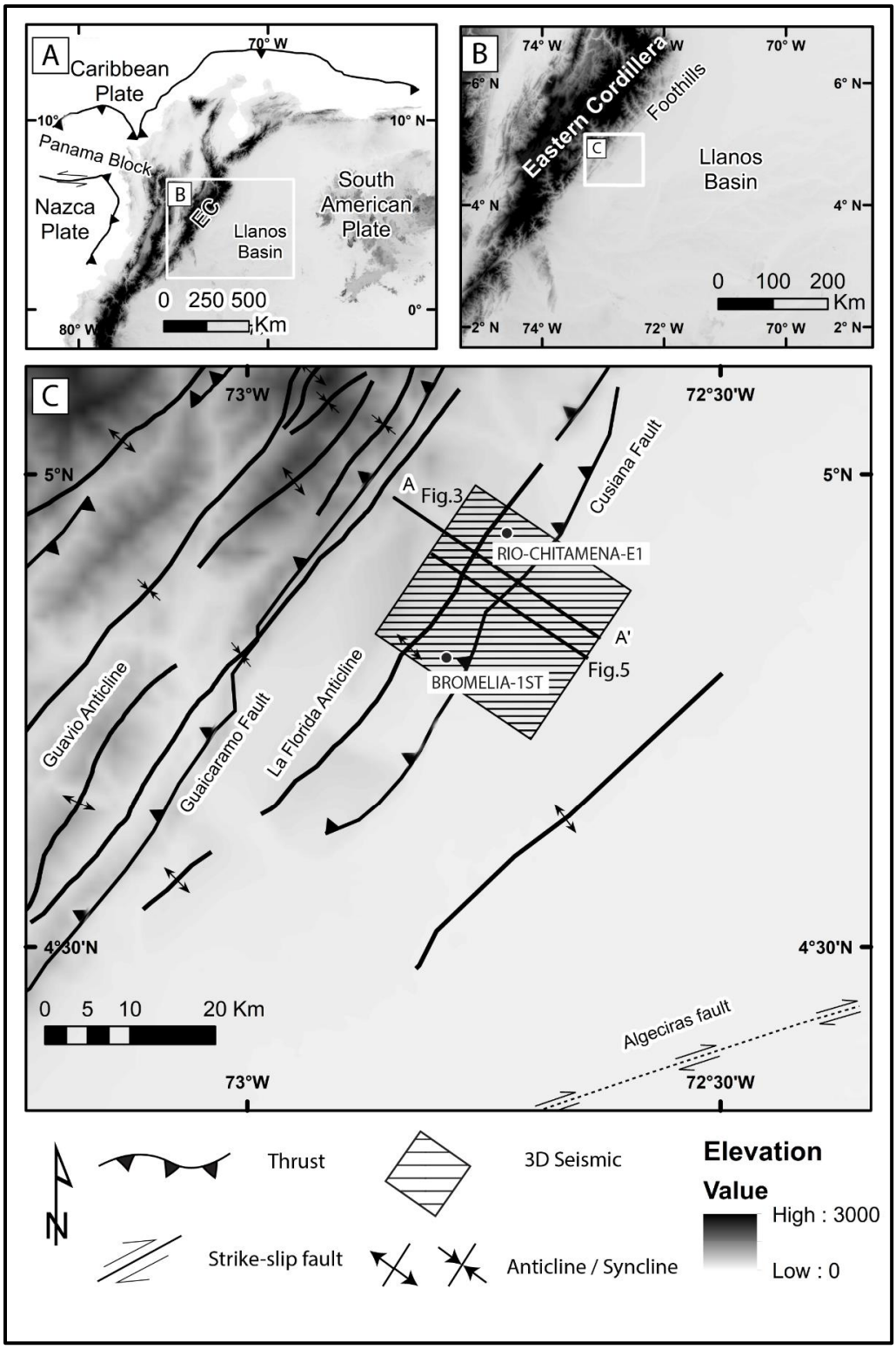

Figure 3.1: Shaded relief maps for (A) northwest South America, (B) Eastern Cordillera, and (C) structural features for the study area.

bend fold formed by a thin-skinned thrust ramping up from a mid-Cretaceous detachment.

Previous studies of fracture systems in the Eastern Cordillera Foothills related their distribution to fold types and geometries based on field mapping and subsurface borehole imager logs. Seismic attribute analysis has not been commonly used in foothills studies, because it is sensitive to high noise levels in the seismic data produced by strong deformation and high topographic relief. In this paper, we present techniques to reduce noise and enhance seismic quality, making possible the first multi-attribute analysis of a 3D seismic volume in the Foothills using coherency and ant-tracking techniques for fault and fracture detection. Because we were able to image an non-folded seismic volume for fractures, we could identify fractures produced by regional stress fields apart from folding processes. Furthermore, we studied a post-rift sedimentary volume from Late Cretaceous to Present, and we were able to make some inferences about the relative timing and orientation of regional fracture sets. The results could help reduce risk in models of reservoir fracture porosity and permeability.

3.2 GEOLOGICAL SETTING

3.2.1 Stratigraphic setting and petroleum system

The Llanos foothills separate the Eastern Cordillera from the Llanos basin and constitute a modern foredeep in the foreland basin system (Parra et al., 2009a). The sedimentary sequence in the Llanos foothills basin study area and adjacent Guavio anticline (Figure 3.1and Figure 3.2) is up to 12 km thick, including at least 6 km of

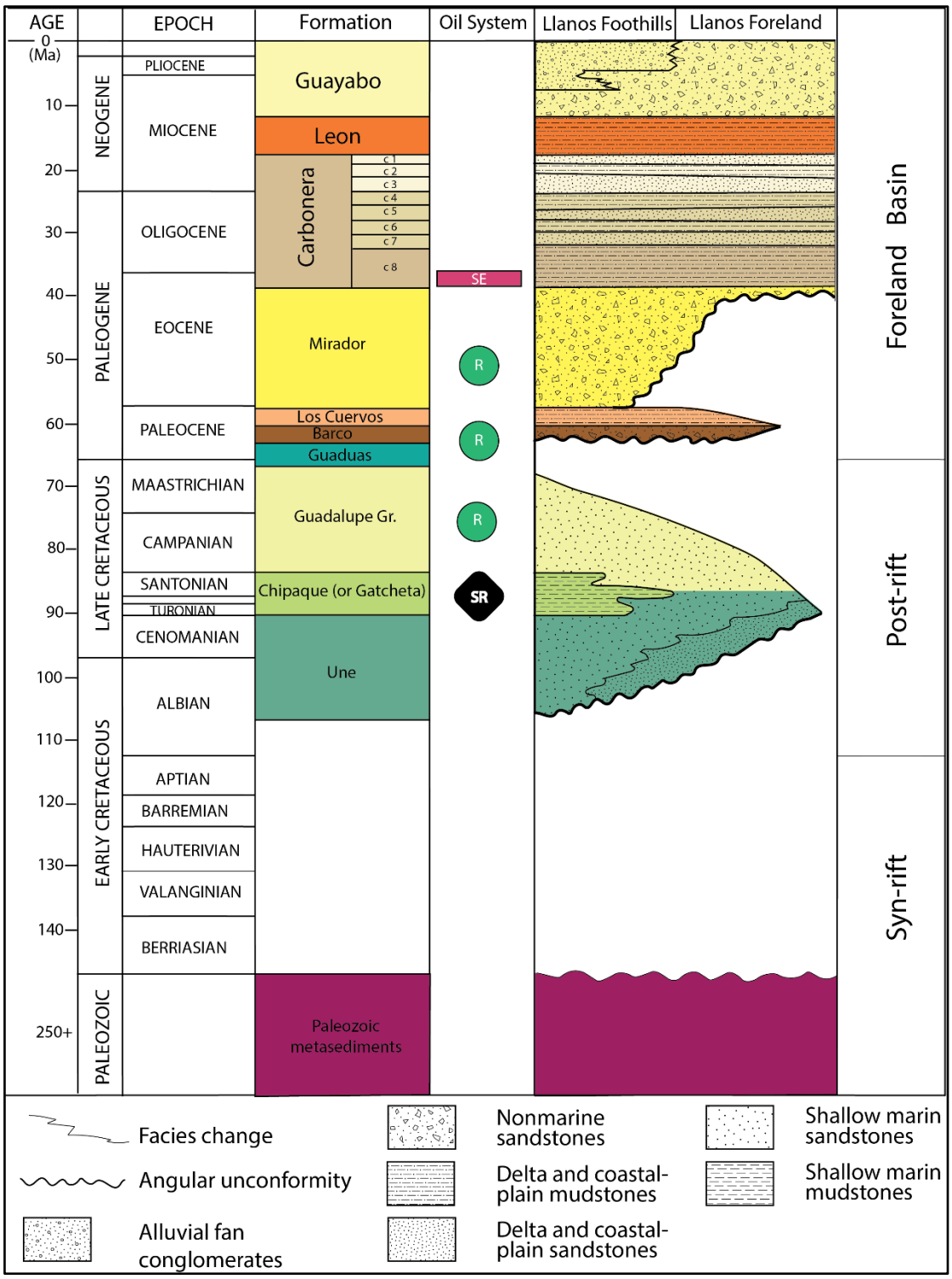

Figure 3.2: Chronostratigraphic diagram of Paleozoic-Cenozoic strata in the Llanos foothills (after Ramon and Fajardo, 2006; Parra et al., 2009a).

Cenozoic synorogenic sediments (Parra et al., 2009b; Teixell et al., 2015). The stratigraphic column (Figure 3.2) after Cooper et al. (1995); Ramon and Fajardo (2006); Parra et al. (2009b) shows Llanos foothills oil system, and post-rift and foreland basin sedimentation. Basement is Paleozoic metamorphic rock overlain by Albian-Cenomanian sandstones of Une Formation during Late Cretaceous post-rift thermal subsidence. The Turonian-Santonian Gacheta Formation, the main source rock in the area, was deposited as thermal subsidence continued (Toro et al., 2004). The Gacheta Formation was overlain by shallow marine sandstones and interbedded mudstones of the Campanian-Maastrichtian Guadalupe Group, a deep valuable reservoir in the Cusiana oilfield (Cazier et al., 1995). The second important reservoir in the Llanos foothills is the fluvial sandstone of the Paleocene Barco Formation. The Guadalupe Group reservoir is sealed by the Upper Paleocene mudstone of Los Cuervos Formation (Reyes-Harker et al., 2015; Sánchez et al., 2015). The Eocene sandstones of the Mirador Formation are the main reservoir that preserves more than half of the hydrocarbons in the Llanos foothills and are considered the most important oil exploration target (Ramon and Fajardo, 2006). The late Eocene to early Miocene Carbonera Formation comprises interlayered transgressive shales and sandstone intervals, with the lower muddy interval C8 forming the regional top seal for the underlying Mirador Fm reservoir (Ramon and Fajardo, 2006). The shaly middle Miocene Leon Formation deposition coincided with uplift of the Eastern Cordillera that isolated the Llanos basin from the Magdalena Valley (Cooper et al., 1995). The Miocene–Holocene Guayabo Formation coarse to fine fluvial gravels interbedded with variegated floodplain deposits were produced by the rapid late Miocene Andean uplift (Parra et al., 2010).

3.2.2 Structural evolution of La Florida anticline

La Florida anticline (Figure 3.1) was formed in the last 7 my by displacement on the underlying Cusiana thrust fault and the nearby Guaicaramo fault (Parra et al., 2009a; Carrillo et al., 2016). Mora et al. (2010b) interpreted La Florida anticline as produced by slip on the Cusiana fault, a listric high angle reverse fault involving pre-Late Cretaceous basement rocks. Cooper et al. (1995) and Cazier et al. (1995) interpreted the Cusiana fault as an inverted listric normal fault involving Early Cretaceous and older basemen. Total slip on the Yopal-Cusiana high angle reverse faults is over 4 km. Based on thermochronometric data and kinematic restorations, Bande et al. (2012) and Carrillo et al. (2016) suggest that the folds associated with the Cusiana fault originated in the last 3 Myr. Mora et al. (2010b) also noted that Pliocene-Pleistocene units on the back-limb of the Florida anticline are folded conformably with no significant growth strata. None of these interpretations, however, explained the Cusiana hanging wall anticline.

Albesher et al. (2019) used higher resolution seismic data than previous studies and were able to image the deeper anticline in the Mirador Formation as well as the detachment in the lower Carbonera Formation. Albesher et al. (2019) also presented the first retrodeformed model for La Florida anticline (Figure 3.3). They reinterpreted the thrusting on the Cusiana fault and La Florida anticline as thin-skinned. Their model also explained the La Florida anticline as a previously unrecognized late Miocene-Pliocene fault-bend fold formed by a thin-skinned thrust ramping up from a mid-Cretaceous detachment (Figure 3.3b). The fault-bend fold formed an early potential hydrocarbon trap. This was followed by thrusting on the Cusiana reverse fault, a forelimb breakthrough fault ramping up from two bedding plane faults in the Late Cretaceous Une

Formation and in the Oligocene lower Carbonera Formation (Figure 3.3c). Total late Miocene-Pliocene shortening on the La Florida anticline was about 5.7 km.

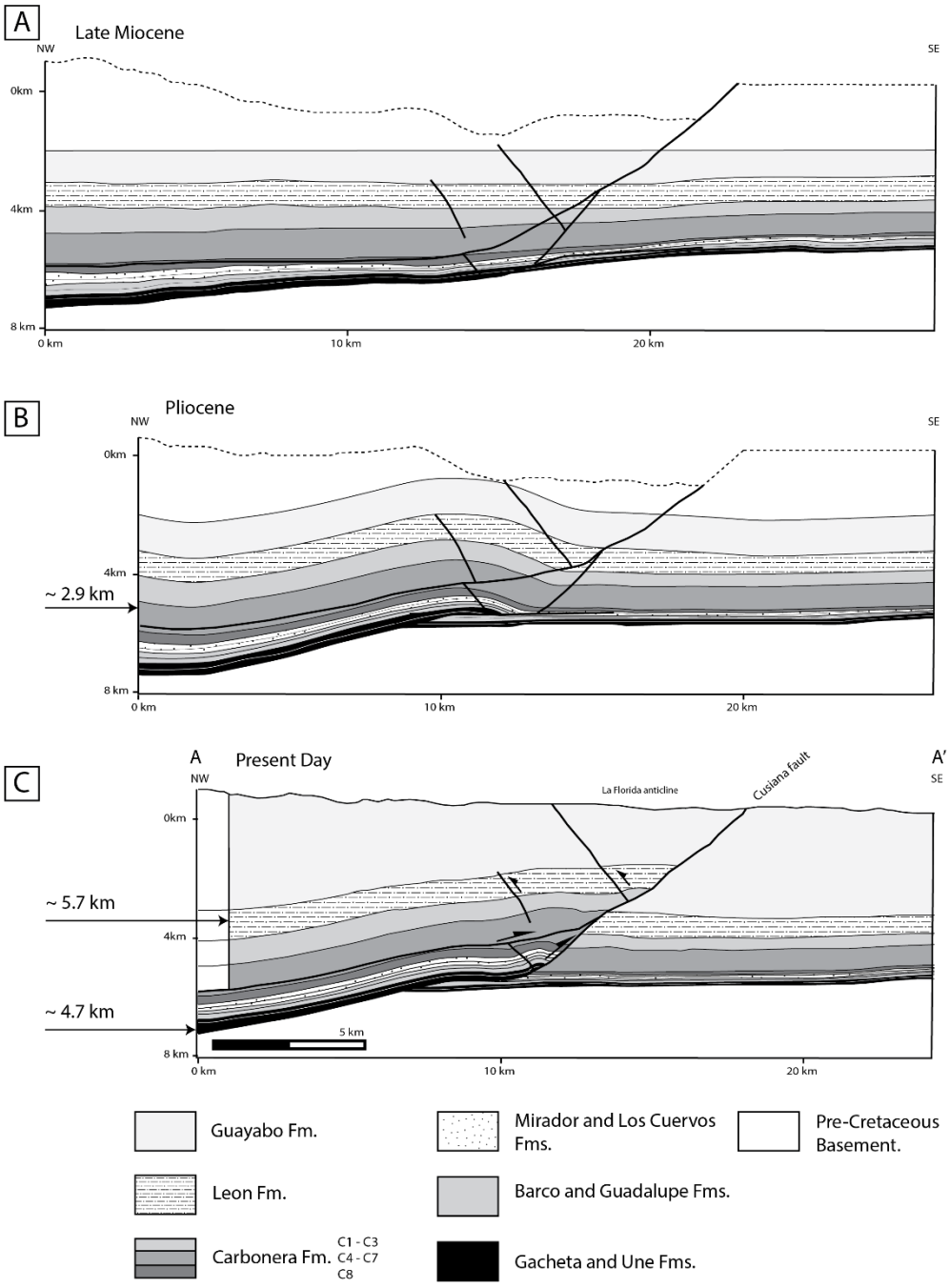

Figure 3.3: Retrodeformed model of La Florida anticline (Albesher et al., 2019). See the location in Figure 3.1.

3.2.3 Previous fracture analysis in Foothills and Cusiana

Fractures may enhance permeability in reservoirs, increasing productivity and recovery efficiency (Chopra and Marfurt, 2010). In the Llanos foothills, Cazier et al. (1995) found the Eocene Mirador Fm (the main reservoir) has low porosity but good permeability in the giant Cusiana oilfield northeast of La Florida anticline. Well tests indicated that the type of permeability was primarily matrix related (Cazier et al., 1995), however, fluid flow is likely also influenced by augmented fracture permeability (Matthäi and Belayneh, 2004). Tamara et al. (2015) studied the fracture systems in the Cusiana anticline using subsurface well data. They divided the Cusiana anticline into three segments, documented four fracture systems (NE-SW, NW-SE, E-W, and N-S) and related their distribution and intensity to fold geometry and folding mechanism. They noted that the NE-SW fracture set was present everywhere in the Cusiana reservoir rocks with high intensities in the hinge region of the anticline. They also correlate the general fracture distribution with changes in structural style in the Cusiana anticline along strike. Their study was also based on field mapping of outcrops in the Foothills to determine the relative timing of fracture sets, as well as using subsurface borehole imager logs for the Cusiana, Cupiagua, and Piedemonte oil fields.

Small faults not detected in traditional seismic reflection data may also cut migration pathways and reduce fluid pressure in basin models (Chopra and Marfurt, 2007). Seismic attributes can detect cracks and low displacement faults that are difficult to see in seismic amplitude data. In this study we use geometric attributes, especially the reflector continuity edge detect tool, “coherence” (Liner et al., 2004). Image log analysis, a traditional method to detect subsurface fractures, is reliable and derived from direct

observation. It is limited to wells where image logs are available and does not sample the rock volume between wells. In this study, we took advantage of a high resolution 3D seismic volume and applied the swarm intelligence algorithm attribute, known commercially as ant-tracking (Marfurt, 2018). In Sabriyah oil field (northern Kuwait), Singh et al. (2008) showed that the ant-tracker attribute effectively detected fracture orientations and provided similar results to fracture orientations found in well image logs. We note that results extracted from the La Florida seismic volume by ant-tracking attributes in this study are also similar to those obtained in reservoir rocks from the nearby Cusiana wells (Tamara et al., 2015).

3.3 RESEARCH METHODS

3.3.1 Post-Migration Data Conditioning and Image Enhancement

Synthetic seismograms were created for the Rio Chitamena and Bromelia wells along the 3-D seismic volume of La Florida anticline (see Figure 3.1 and Figure 3.6 for locations). The Rio Chitamena well constrained the northern part of the Cusiana thrust hanging wall, and the Bromelia well constrained the Cusiana footwall to the south. Well logs were used to create synthetic seismogram traces. The seismic cross-sections were then tied to the wells using velocities from well check-shots surveys, and adjusting the time-depth function by stretching and squeezing the wavelet until the seismic matched the synthetic seismogram (Figure 3.4). The Eocene Mirador Formation (the main reservoir in the Llanos foothills) reflectors can be seen at 2.34 to 2.39 sec TWT in Rio Chitamena well in the hanging wall (Figure 3.4).

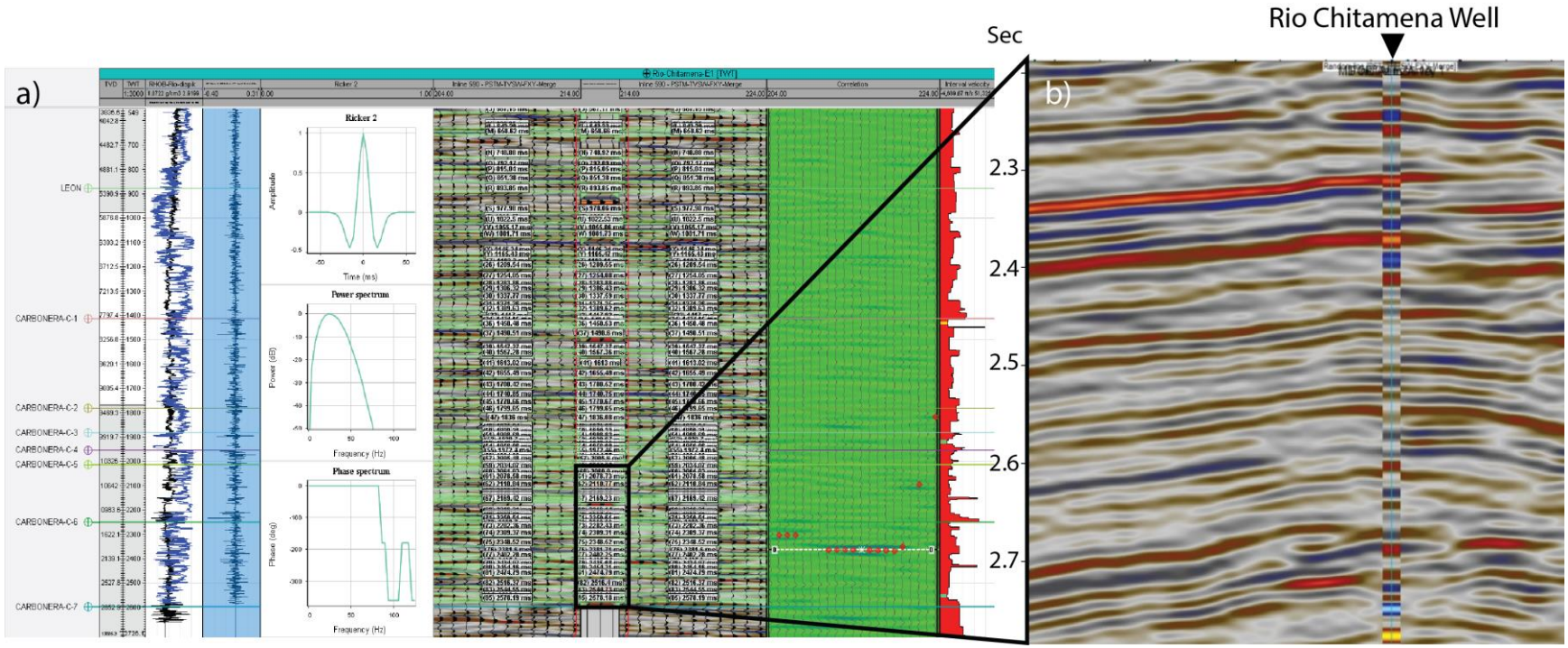

Figure 3.4: a) Synthetic seismogram with sonic and density logs. b) Synthetic seismogram for Rio Chitamena well displayed on a seismic section.

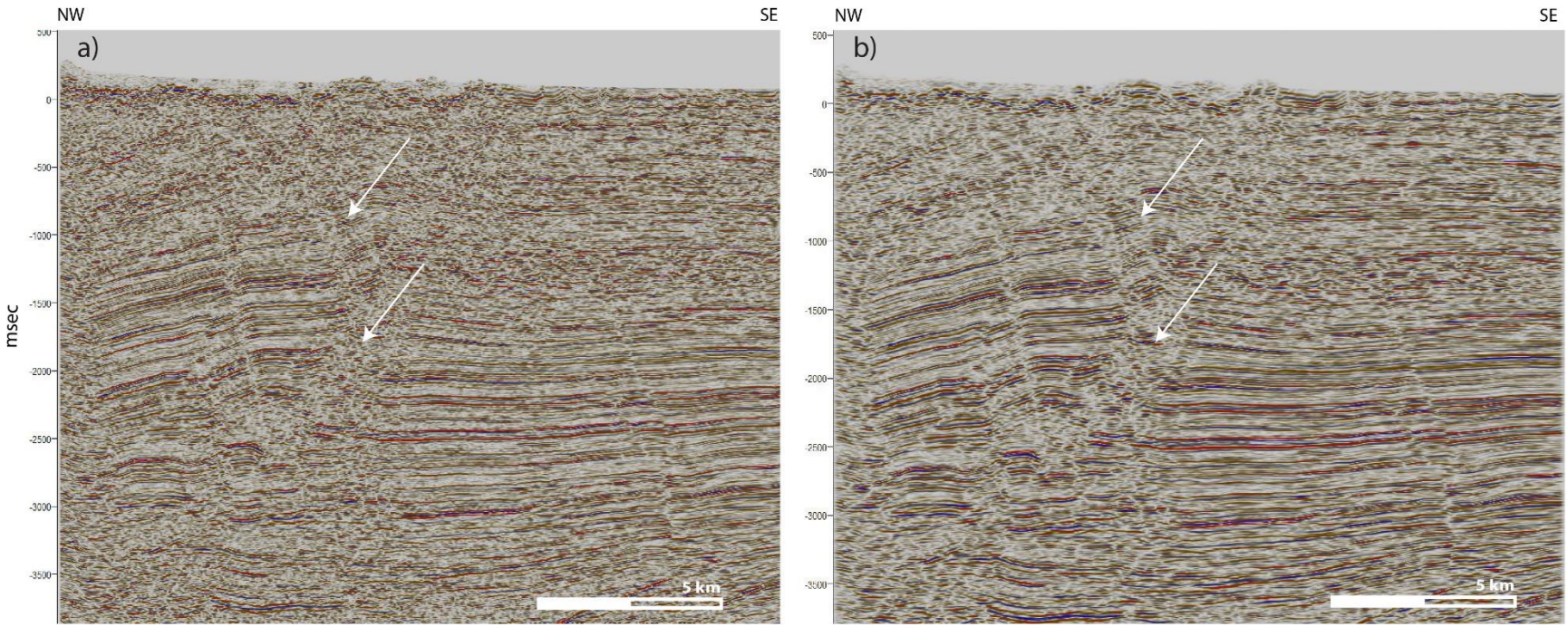

Figure 3.5: a) Amplitude seismic cross-section before applying the structure smoothing filter. b) After applying the structure smoothing filter. The white arrows indicate areas of increased reflector resolution and reduced noise near the Cusiana fault plane after filtering in Fig. 5b. For profile location see Figure 3.1.

The interpretation of critical features such as faults and fractures in seismic amplitude data is complicated in the Foothills by noise introduced to the data by structural and topographic complexity. Randen et al. (2003) suggested a way to suppress the noise by applying a "structure-oriented filter", using the principles of scale-space theory to smooth the seismic volume and detect geological features at different stages of resolution. Depending on the feature of interest, large smoothing leaves primarily major features, while low smoothing leaves minor features. Figure 3.5 shows the effects of using the structure smoothing filter on our 3D seismic volume, where resolution was increased by enhancing the horizontal continuity of the seismic reflectors. The structure smoothing filter decreases data noise level and makes accurate seismic attribute analysis possible.

3.3.2 Coherence and ant-tracking seismic attribute analysis

A seismic attribute is a measurement derived or extracted from seismic data (Marfurt, 2018), which helps to visually enhance or focus on the geological features of greatest interest. The optimal results from seismic attributes depend on data conditioning and the quality of the seismic data. Deformation in the Llanos Foothills is intense, especially in the northeast where it is difficult to apply seismic attribute analysis because of the deformation noise. Fortunately, the La Florida structure is a gentle anticline (Mora et al., 2010b; Parra et al., 2010; Albesher et al., 2019), and the La Florida footwall is relatively undeformed, which means that we are able to apply seismic attribute analysis to the La Florida 3D seismic volume (Figure 3.6). For this study, we used Petrel 2019.3 software from Schlumberger for seismic interpretation, and we produced the seismic attributes by following the fault imaging workflow (Figure 3.7).

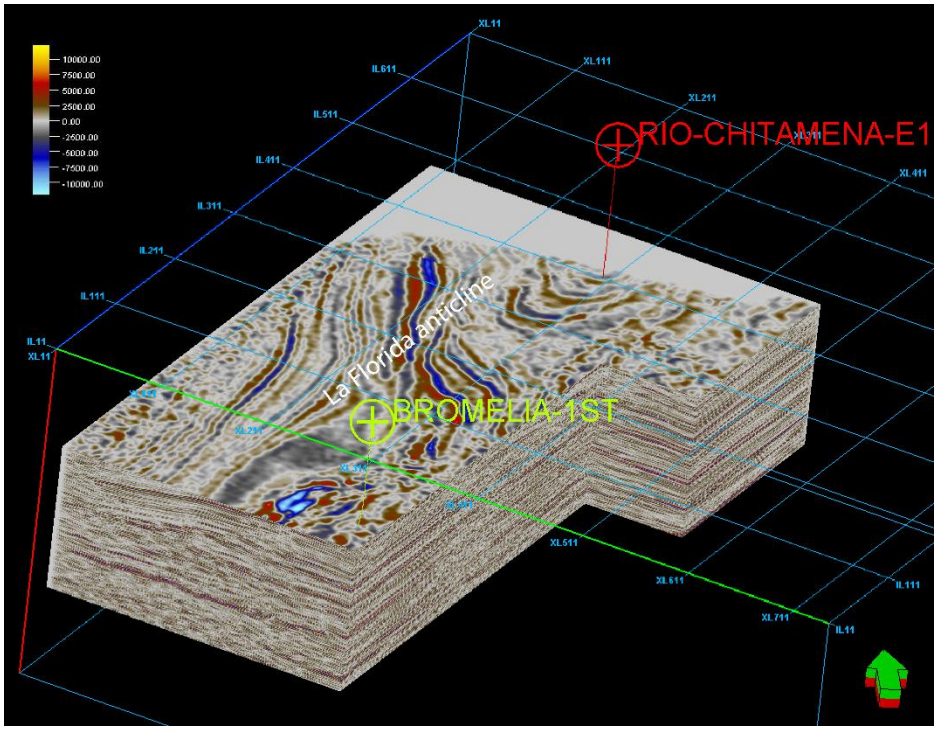

Figure 3.6: 3D Seismic amplitude volume of La Florida anticline showing well locations.

The coherence attribute enhances the ends of reflectors, where these edges can delineate faults or even fault damage zones in fractures (Liner et al., 2004). Through the evolution of eigen-decomposition algorithms, coherence can enhance lateral resolution and produce relatively sharp definition for faults and fractures (Chopra and Marfurt, 2010). For that purpose, we applied the coherence attribute on the 3D seismic cube after applying the structure smoothing filter to reduce noise and extract faults and fractures that are not readily visible in the seismic amplitude data.

Ant-tracking is an advanced attribute that uses the swarm intelligence algorithm to enhance discontinuities (Pedersen et al., 2002). The ant-trackers mission is to find all the discontinuity traces in three dimensions in the volume and enhance those traces that represent possible faults and fractures. In this approach, we set azimuthal parameters before allowing the "artificial ants" to search for the discontinuities in the edge-detection volume. We first force the ant-trackers to search for all direction by applying all azimuths

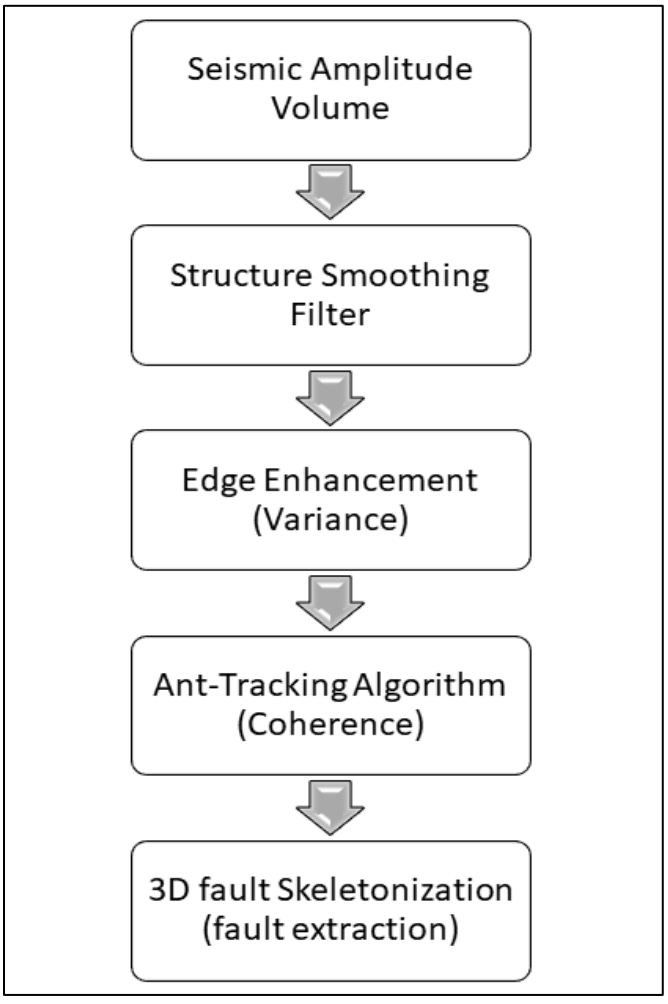

Figure 3.7: Workflow illustrating the steps used in our attribute analysis, which involved the generation of ant-tracking and fault extraction volumes.

at -180° < ϕ < 180° to capture features that are continuous and likely to be faults and to ignore other features with short continuity such as noise or channels. Therefore, the first result will show faults and fracture zones of all azimuths distributed throughout the whole volume. In the second step, we use an azimuthal filter to hide the dominant fracture orientation and allow the ants to search in the remaining directions to detect secondary faults and fractures that may have been hidden. Finally, 3D visualization of faults and fractures in the ant-tracking attribute volume prepares the data for automatic fault extraction (Pedersen et al., 2002). The fractures can then be displayed as dip azimuth points and strike azimuth rose diagrams (Wells, 2000).

3.4 RESULTS

3.4.1 3D seismic visualization of La Florida anticline

Figure 3.8a shows the ant-tracking results for the La Florida 3D seismic volume including the Cusiana fault hangingwall and footwall. Parameters and filters were applied to the ant-tracking volume to reduce the signal of non-fracture features, such as channels and bedding. For example, we only mapped fracture patches dipping over 75 degrees to filter out bedding plane effects. Figure 3.8b shows the fault and fracture patches for the 3D ant-tracking volume with no azimuthal filter applied. The fault patches volume clearly shows greater fracture intensity in the folded Cusiana hanging wall than in the non-folded footwall. One way to quality control (QC) the ant-tracking fault and fracture patch predictions is to compare to structural features in the seismic amplitude volumes. Figure 3.9 is a 3D window showing an ant-tracker time slice and a seismic reflection profile. The white arrows point to faults or fractures visible in the seismic amplitude vertical section that match fractures predicted in the ant-tracker time-slice.

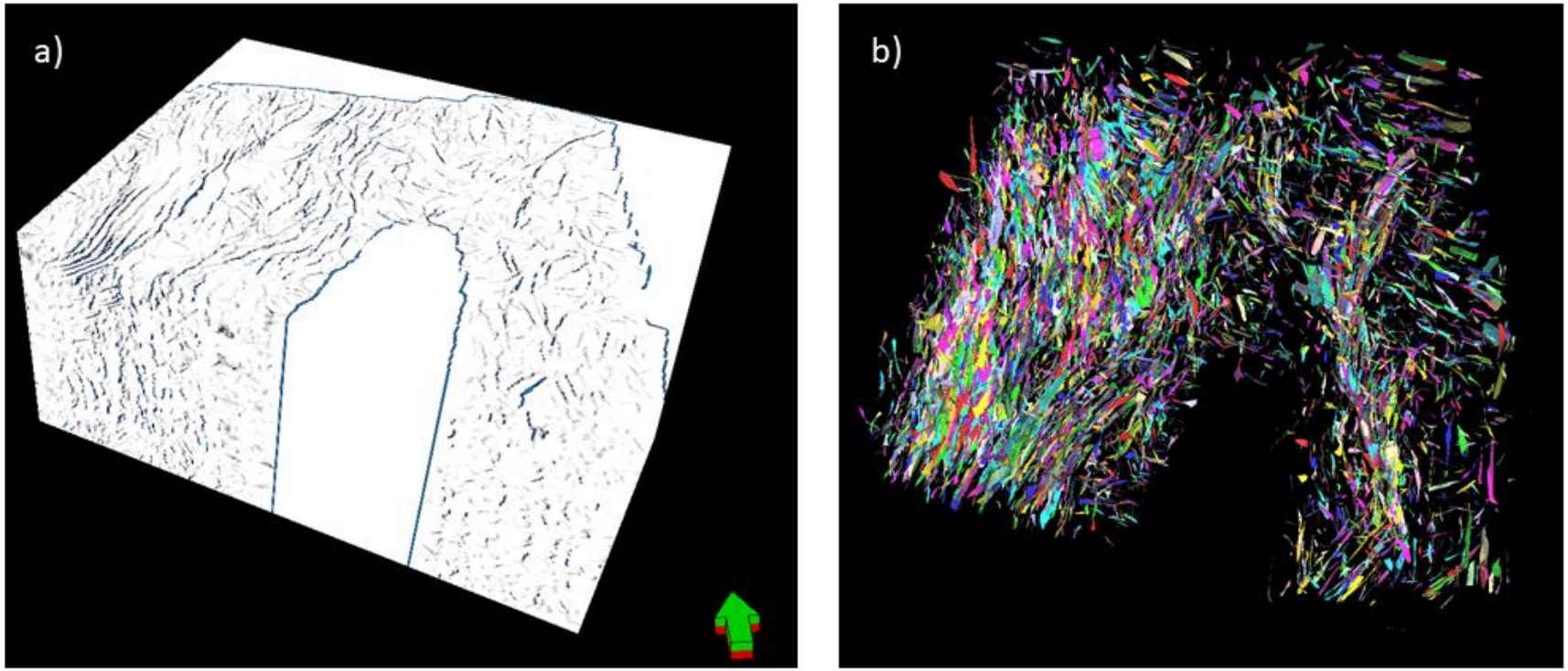

Figure 3.8: a) The Ant-tracking results for the whole 3D seismic volume including La Florida anticline (left side) and the Cusiana fault footwall block (right side). b) The fault patches volume shows greater fracture intensity in the folded Cusiana hanging wall than in the footwall.

Figure 3.10 shows the dip azimuths and strike azimuths for the fractures extracted from the total ant-tracking volume (Figure 3.8). The dominant fracture strike direction is NE-SW (055 ± 20°), approximately parallel to the structural strike of the adjacent Eastern Cordillera Foothills (055°). For the Foothills fold and thrust belt, these fractures are parallel to the intermediate stress direction and perpendicular to the maximum principal stress direction. In the total volume, which includes the Cusiana fault hangingwall and footwall, other secondary fracture orientations are less common and difficult to statistically differentiate. When the non-folded footwall volume is considered separately however, secondary fracture orientations are resolvable.

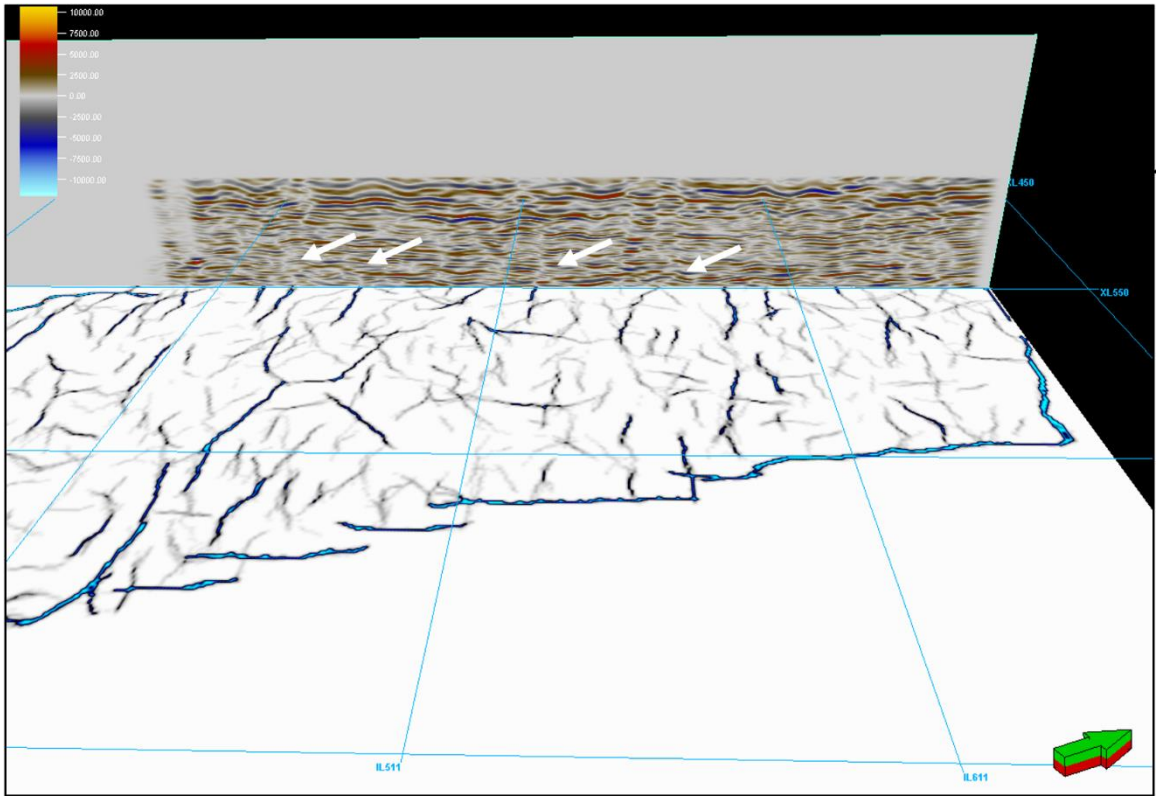

Figure 3.9: In 3D window, we QC to validate the fractures in time slice (-380 msec) and seismic profile – 465 (strike line). The white arrows point to fractures visible in the seismic amplitude vertical section corresponding to fractures predicted in the ant-tracker time-slice.

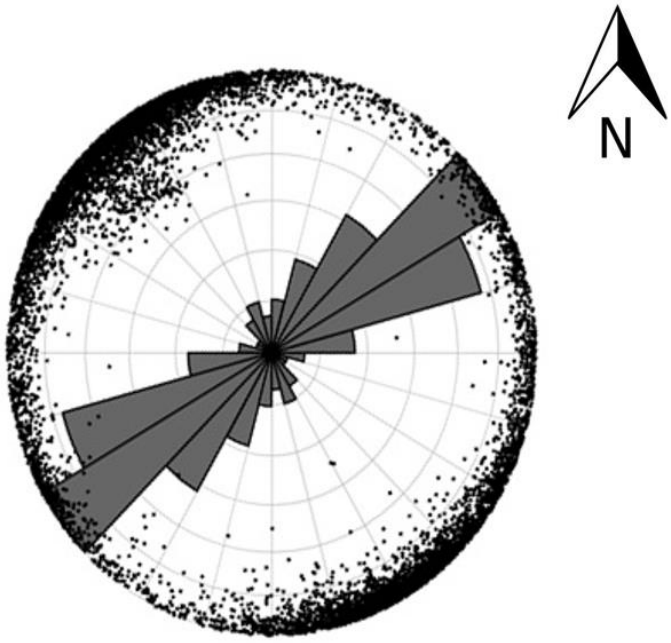

Figure 3.10: Rose diagram shows fracture dip azimuths (dark points) and fracture strike azimuths (rose petals).

3.4.2 Comparison of fracture systems in folded and non-folded rocks near the Cusiana fault

In this study we were able to compare fracture intensity and orientation in folded rocks with the fracture intensity and orientation in non-folded rocks. The fracture orientations in the non-folded footwall block may help us to recognize the regional stress fields not associated with folding that are responsible for fracture formation. We divided the seismic volume into folded units in the La Florida anticline in the hangingwall block of the Cusiana fault to the northwest and non-folded units in the footwall block to the

southeast. Basement, defined as pre-Late Cretaceous rocks (i.e., pre-Une Fm), were omitted from the seismic volume. Rose diagrams (Figure 3.11) show the dip azimuths and strike azimuths for fractures in the folded Cusiana fault hanging wall and the non-folded footwall. Fracture strike azimuths in the folded rocks of the hangingwall are predominantly NE-SW (055°), the main structural trend in the Foothills. No secondary

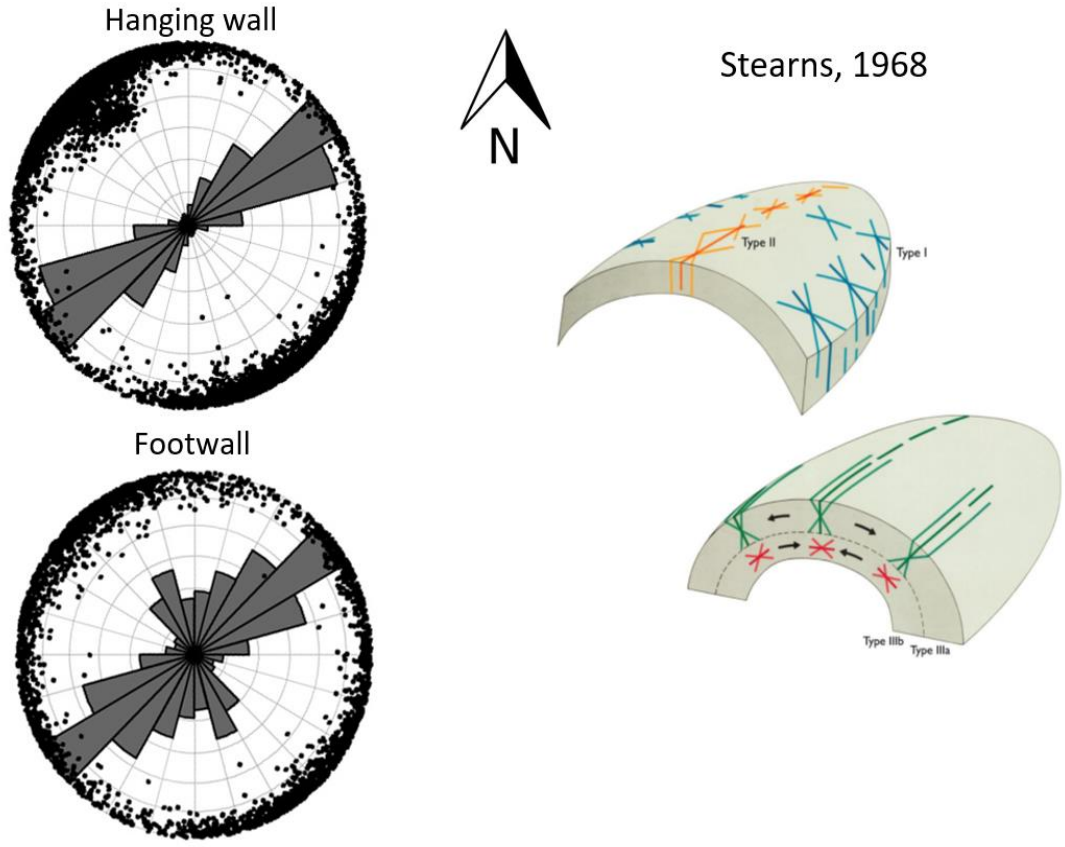

Figure 3.11: Rose diagrams (left) show the dip azimuths (dots) and strike azimuths (rose petals) for fractures in the Cusiana fault hanging wall and footwall. Schematic diagrams (right) show fracture types associated with folding (Stearns, 1968).

orientations are distinguishable. Fracture strike azimuths in the non-folded rocks of the footwall (Fig. 11) are also primarily NE-SW trending. However, a NNW-ESE secondary fracture strike orientation is also apparent. Schematic diagrams (Fig. 11) show fracture types associated with folding (Stearns, 1968). The primary fracture orientation (NE-SW) is sub-parallel to the fold axis, the trend of type 2 or type 3 fracture sets (Stearns, 1968).

Both type 2 and type 3 fracture sets are predicted for an elastic plate subjected to pure bending. The minimum principal stress direction during fracture formation was parallel to the fold dip direction and perpendicular to the fracture planes.

3.4.3 Secondary fracture orientations in non-folded rocks of the Cusiana footwall

The non-folded footwall block of the Cusiana thrust fault shows a NW-SE secondary fracture orientation. To highlight secondary fracture orientations, we edited the ant-tracking attribute parameters to hide the primary NE-SW fracture sets with an "azimuthal filter" (Fig. 12). The resulting filtered rose diagram (Fig. 12) shows a prominent NNW-SSE (155 ± 15°) fracture strike trend. Another minor E-W (085 ± 10°) fracture trend is also visible. Both the NNW-ESE and E-W fracture trends are oblique (80° and 30°respectively) to the regional foothills structural trend. They can be grouped as Type 1 fracture sets (Stearns, 1968) resulting from a vertical intermediate stress and

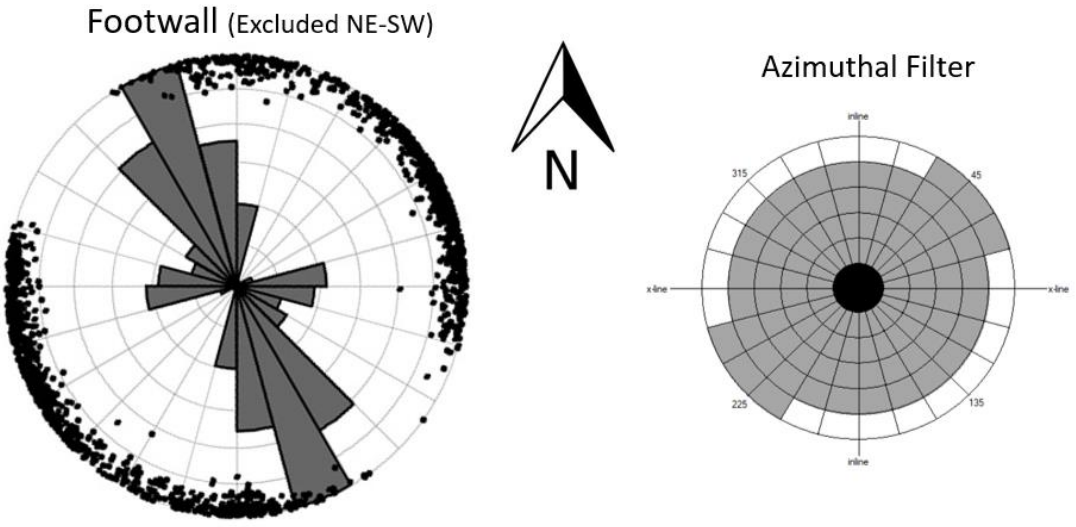

Figure 3.12: Rose diagram (left) after applying the azimuthal filter (right) to remove the dominant NE-SW striking orientation, forcing the artificial ants to detect fractures with secondary orientations.

maximum compressive stress parallel to the dip direction of bedding. Stearns (1968) suggests that type 1 fractures form early during folding with the regional maximum compressive stress normal to the advancing mountain front.

3.4.4 Fracture systems for the Guadalupe Group–Barco-Mirador formation reservoir rocks

Understanding the orientation and spatial density of fractures where outcrops are sparse or absent is useful for modeling hydrocarbon flow, spatial density, fracture porosity, and fracture permeability in fractured reservoirs. In this study we use multi-attribute analysis of the La Florida 3D seismic volume using coherency and ant-tracking techniques for fault and fracture detection in reservoir rocks of the Guadalupe Group, Barco Fm, and Mirador Fm. We were able to isolate the reservoir fractures (Fig. 13) by cropping the ant-tracking volume between the base of the Guadalupe Group and the top of the Mirador Formation. The insets (Fig. 13) are rose diagrams showing the orientations of reservoir fractures in the hanging wall and footwall of the Cusiana fault. Only one fracture orientation is apparent in both hanging wall and footwall, the NE-SW trend prominent throughout the sedimentary volume, 060° ± 15° in the hanging wall and 055° ± 15° in the footwall. The fracture intensity in the reservoir rock is low relative to the total sedimentary volume, and the spatial density of fractures is similar on the hanging wall and footwall of the La Florida fault-bend fold (Fig. 3). The primary fracture orientation (NE-SW) is sub-parallel to the fold axis, the trend of type 2 or type 3 fracture sets (Stearns, 1968) predicted for an elastic plate subjected to pure bending. The minimum principal stress direction during fracture formation was parallel to the fold dip direction and perpendicular to the fracture planes.

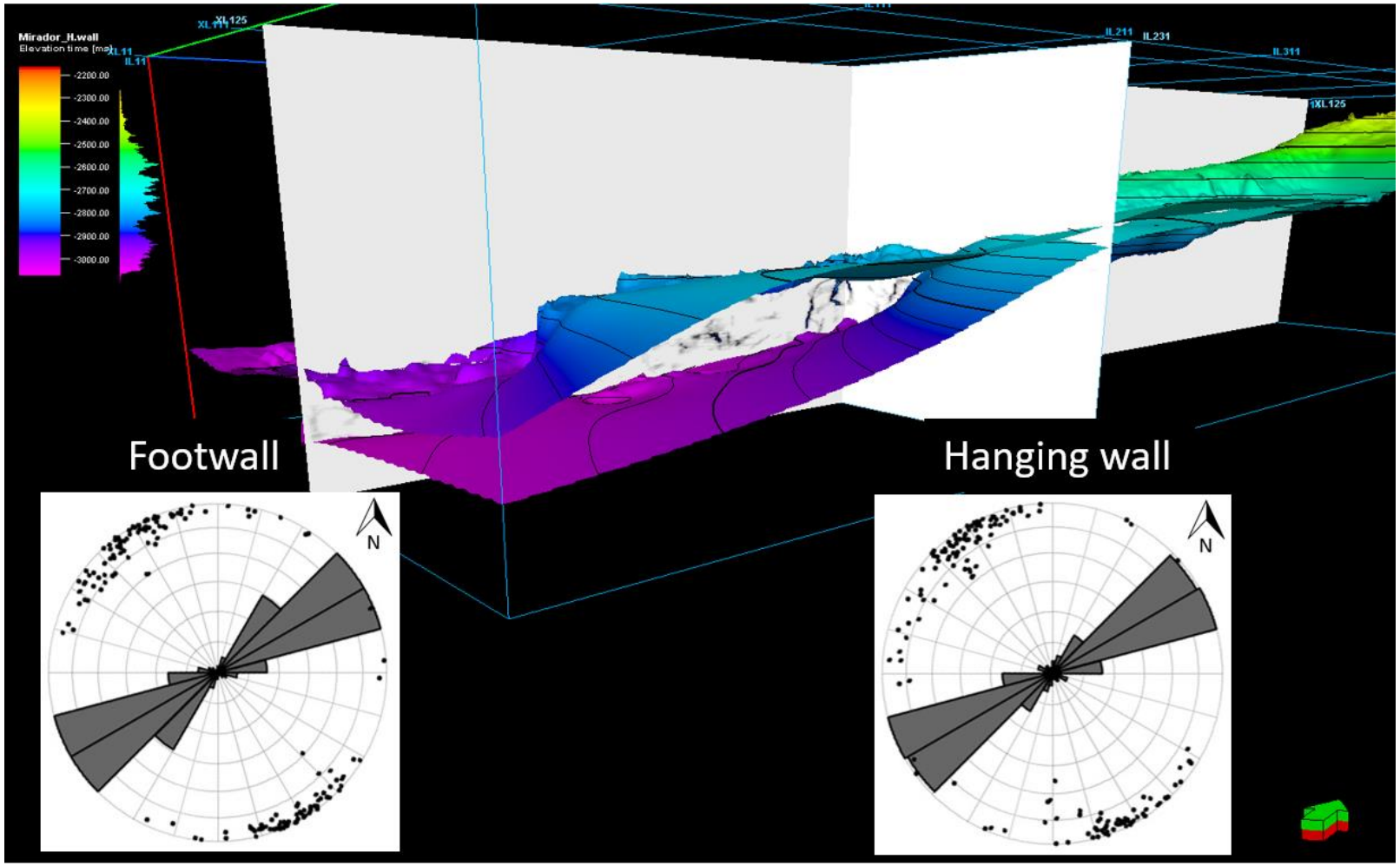

Figure 3.13: Ant-tracking data cropped between two surfaces to extract fractures in Mirador Fm. The insets are rose diagrams showing the orientation of the reservoir fractures in the hanging wall and the footwall.

3.4.5 Regional stress field – timing and orientation of footwall block fractures

The fracture orientations in the non-folded footwall block may help us to recognize the regional stress fields not associated with folding that are responsible for fracture formation. If we can associate fractures with faults that show measurable displacement, this will support regional stress field predictions and may also help determine the timing of fracture set formation.

3.4.5.1 Northeast-southwest trending normal faulting.

Figure 3.14 shows a seismic amplitude profile and ant-tracking time-slice at 1940 msec in the footwall block. The ant-tracking time slice reveals a NE-SW trending system of arcuate en-echelon fractures. The seismic profile demonstrates that the fractures form a normal fault system with minor down to the SE displacement. The displacement is uniform downsection indicating that it was not a growth fault. It dies out above 1000 msec TWT (Figure 3.5 and Figure 3.15) in the lower Guayabo Formation suggesting a 10 Ma late Miocene age for faulting early in the latest Andean orogenic event. The NE-SW normal fault/fracture orientation indicates a NW-SE minimum principal stress direction and vertical maximum principal stress at the time of displacement. This is compatible with lithospheric loading by the advancing mountain front of the rising Eastern Cordillera.

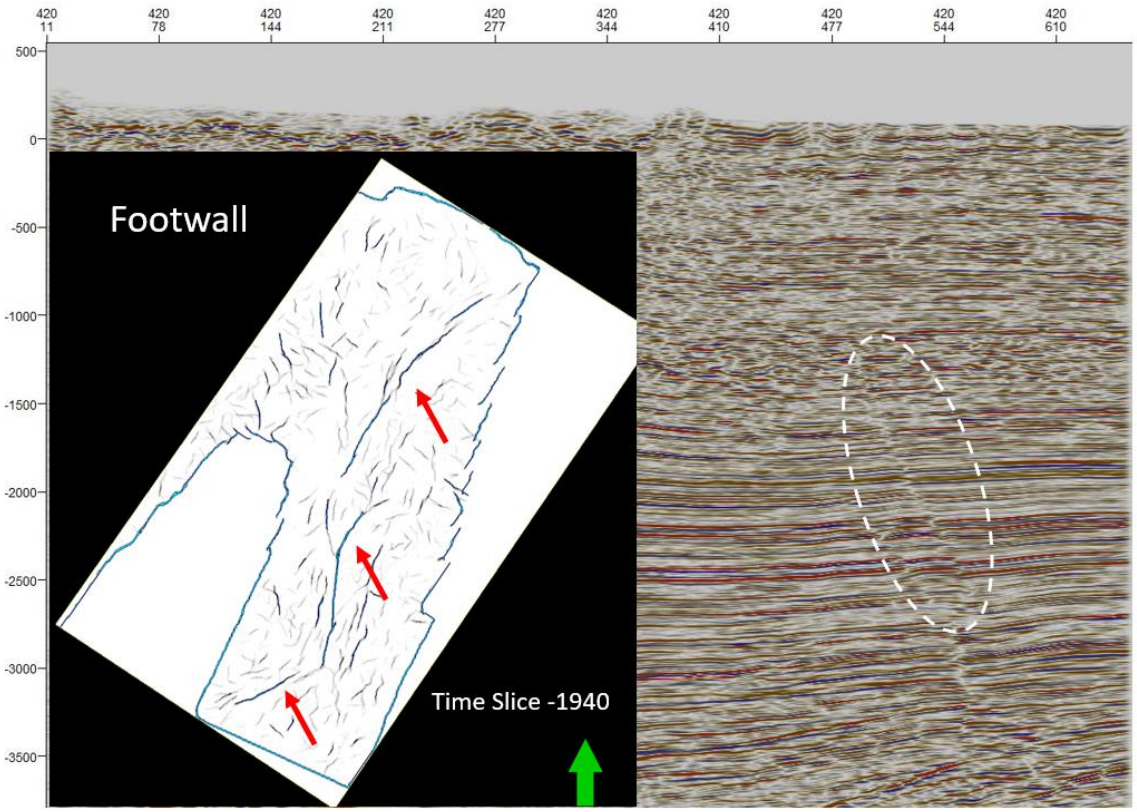

Figure 3.14: Seismic amplitude profile showing normal fault (dashed white oval on the right), and ant-tracking time-slice (left) at 1940 msec showing the normal fault (red arrows).

3.4.5.2 Northwest-southeast trending fracture sets – Riedel shears?

An ant-tracker time-slice at 380 msec in the footwall block (Figure 3.15) shows a prominent WNW-ESE (125° ± 5°) fracture set in the Guayabo Fm. Figure 3.9 shows that this fracture set corresponds to fractures observed in a seismic profile. Displacement cannot be determined from the seismic profile. However, we note that the intensity of WNW-ESE and NW-SE fracture sets is greatest in the sediments of the Guayabo Fm (11 Ma – Present) and hence, roughly synchronous with the latest Andean tectonic phase. The least principal stress direction during at least part of this time period has been NE-SW, compatible with regional NW-SE maximum principal stresses during formation of

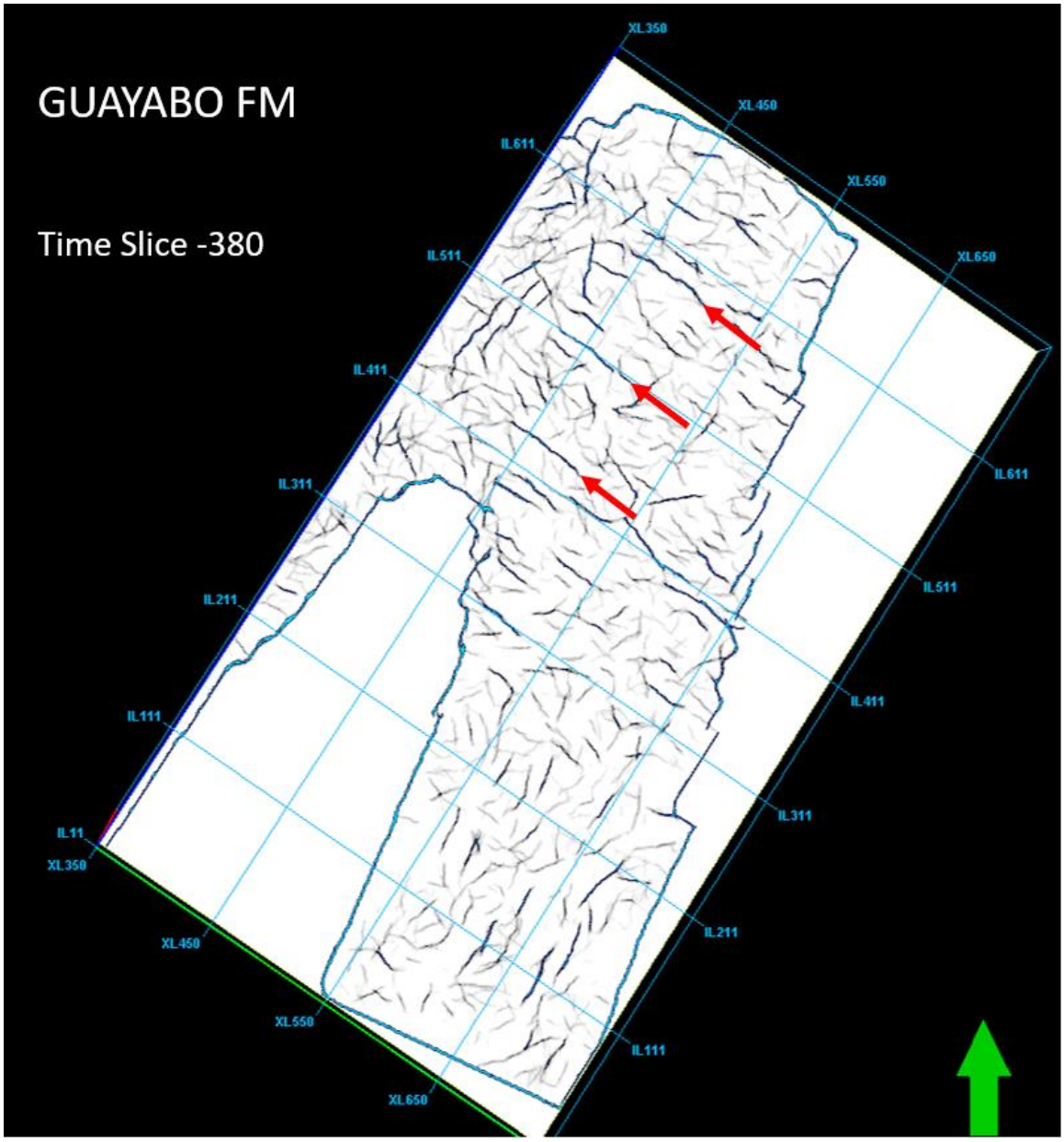

Figure 3.15: Time-slice at 380 msec showing the WNW-ESE fracture direction in the Guayabo Fm in the footwall block.

the advancing Eastern Cordillera Foothills. We also note recent right-lateral displacement on the nearby Algeciras fault (Figure 3.1 and Figure 3.16). The regional minimum

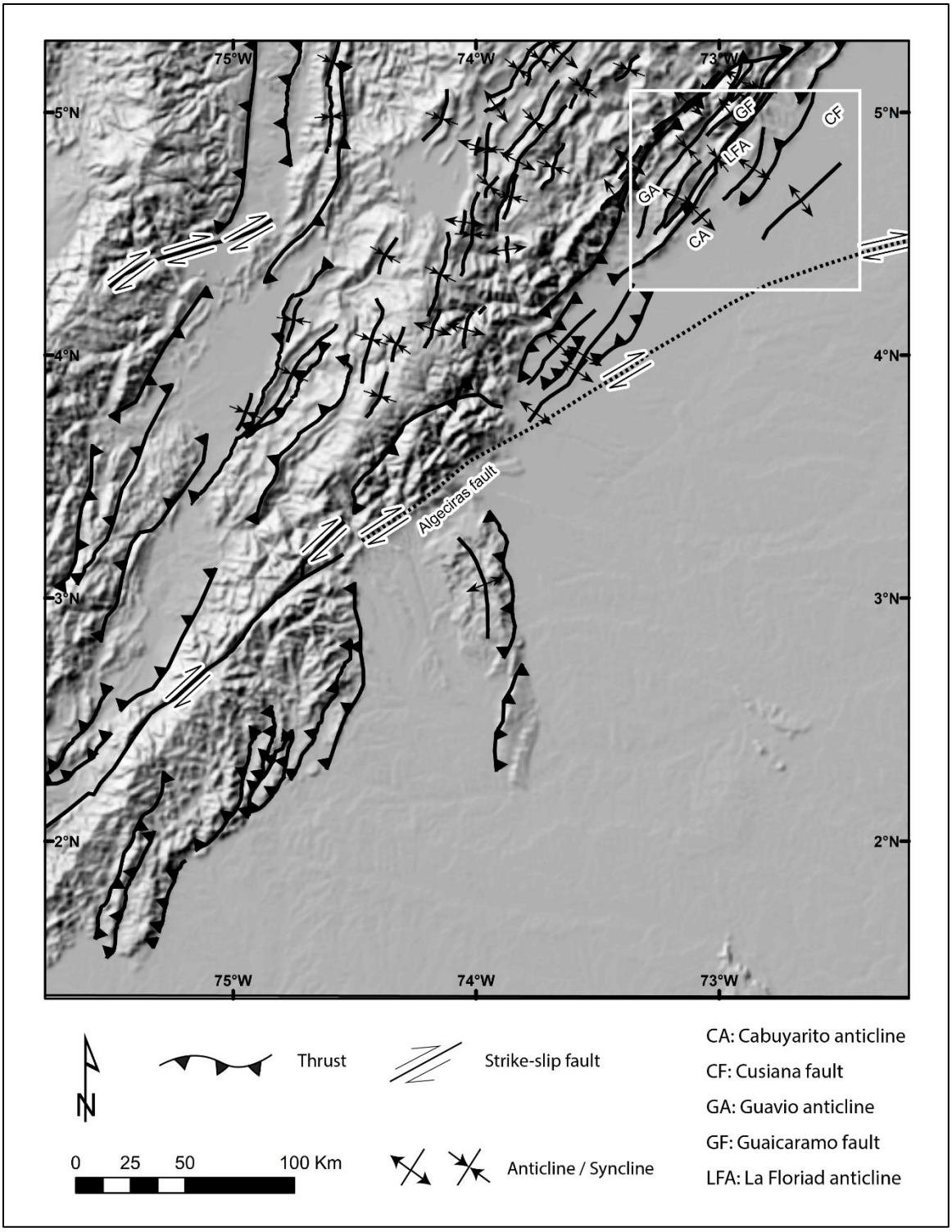

Figure 3.16: Topographic map with structural elements of the southeastern flank of the Eastern Cordillera and Llanos basin. Note the proximity of the Algeciras fault to the study area (white box, Figure 3.1).

principal stress direction for the Algeciras fault would also be NE-SW, and the NW-SE fracture sets could be interpreted as a Riedel shear set associated with this fault system.

3.5 DISCUSSION

3.5.1 Comparison of seismic attribute ant-tracking results with previous surface mapping and well borehole imager log results

Tamara et al. (2015) published a comprehensive study of fractured reservoirs in the Eastern Foothills, focusing on their relationship with fold kinematics. Tamara et al. (2015) documented four fracture systems and related their distribution to fold geometry and folding mechanism. Their study was based on field mapping of outcrops to determine the relative timing of fracture sets, and subsurface borehole imager logs for the Cusiana, Cupiagua, and Piedemonte oil fields. Our study complements this work with the first multi-attribute analysis of a 3D seismic volume in the Foothills using coherency and ant-tracking techniques for fault and fracture detection. In this study we compared fracture intensity and orientation in folded rocks with the fracture intensity and orientation in non-folded rocks. The fracture orientations in the non-folded seismic volume helped us recover the regional stress field responsible for non-fold related fracture formation. Furthermore, we included the entire post-rift sedimentary volume above pre-Late Cretaceous “basement”, so that we were able to predict the relative timing and orientation of several fracture sets.

Tamara et al. (2015) found four fracture sets in the Foothills folded reservoir rocks from surface mapping and well data: NE-SW, NW-SE, E-W, and N-S. Our study

confirmed the first three of these sets in the seismic volume using attribute analysis: NE-SW, NW-SE, and E-W.

The Cusiana oil field is located just 15 km to the northeast of the La Florida anticline along structural strike. Using well data, Tamara et al. (2015) note that the NE-SW fracture set is present everywhere in the Cusiana reservoir rocks with high intensities in the hinge region of the anticline. They also correlate the general fracture distribution with changes in structural style in the Cusiana anticline along strike. Ant-tracking fracture results for the Guadalupe Group, Barco and Mirador formations in the La Florida anticline as well as the non-folded reservoir rocks to the SE (Figure 3.13) also reveal the prominent NE-SW fracture set. Our study was not able to resolve NW-SE, E-W, or N-S fracture sets in the reservoir units, although the depth may limit the resolution of the seismic attribute analysis. We also note that the fracture intensities in the folded La Florida reservoir units were similar to the fracture intensities in the non-folded reservoir units.

Our fracture orientations in the whole post-rift non-folded seismic volume suggest that regional stresses as well as folding could produce the NE-SW, NW-SE, and E-W fracture sets. In particular, late Miocene (10 – 9 Ma) NE-SW normal faulting may have been produced by lithospheric bending as the mountain front advanced from the northwest. However, in the whole volume, the NE-SW fracture intensity is greater in the folded rocks than in the non-folded footwall.

3.5.2 Algeciras fault system, regional shear stresses, and NW-SE and WNW-ESE fracture sets

The NW-SE and WNW-ESE fracture sets (Figure 3.9 and Figure 3.15) are only found in the Guayabo Fm (11 Ma – Present) synchronous with the greatest orogenic shortening. The regional NW-SE maximum principal stress that produced the orogenic shortening in the Foothills also produced the nearby right-lateral Algeciras fault system (Figure 3.16). The Garzón/Algeciras fault system has accommodated both dip slip and strike-slip displacement in Miocene-Pliocene time. In the Garzón Massif, Saeid et al. (2017) demonstrated 10 to 17 km of northwestward thrust faulting over Miocene sediments for the Garzón/Algeciras fault system. Egbue and Kellogg (2010) and Anderson et al. (2016) proposed a transition from shortening to strike-slip deformation along the Garzón/Algeciras fault system approximately 2 m.y. ago. Using Landsat TM images, Chorowicz et al. (1996) and Velandia et al. (2005) estimated 3 to 5 km of right lateral shear in the last 2 m.y. on the Algeciras fault system. Right-lateral strike-slip displacement on the Algeciras fault system (Egbue and Kellogg, 2010), could have generated N-S and WNW-ESE Riedel-type shear fractures in the Foothills study area. Riedel structures are networks of shear bands, commonly developed in zones of simple shear during the early stages of faulting (Riedel, 1929).

3.6 CONCLUSIONS

Previous studies of fracture systems in the Eastern Cordillera Foothills have related their distribution to fold types and geometries based on field mapping and subsurface borehole imager logs. In the Llanos foothills high levels of deformation have produced considerable noise in the seismic data and as a result, seismic attribute analysis

has not been commonly used. In this paper, we present techniques to reduce noise and enhance seismic quality, making possible the first multi-attribute analysis of a 3D seismic volume in the Foothills using coherency and ant-tracking techniques for fault and fracture detection. In this study we compared fracture intensity and orientation in folded rocks with the fracture intensity and orientation in non-folded rocks. The fault patches volume clearly shows greater fracture intensity in the folded Cusiana hanging wall than in the non-folded footwall. The dominant fracture strike direction is NE-SW (055 ± 20°), approximately parallel to the structural strike of the adjacent Eastern Cordillera Foothills (055°). For the Foothills fold and thrust belt, these fractures are parallel to the intermediate stress direction and perpendicular to the maximum principal stress direction. Ant-tracking fracture results for the reservoir rocks, the Guadalupe Group, Barco and Mirador formations, in the La Florida anticline as well as in the non-folded reservoir rocks to the SE, also reveal the NE-SW fracture set.

The fracture orientations in the non-folded seismic volume helped us recover the regional stress field responsible for non-fold related fracture formation. Our fracture orientations in the whole post-rift non-folded seismic volume suggest that regional stresses as well as folding could produce the NE-SW, NW-SE, and E-W fracture sets. The NE-SW trending type 2 and type 3 fracture sets are predicted for an elastic plate subjected to pure bending. Late Miocene (10 – 9 Ma) NE-SW normal faulting may have been produced by lithospheric bending as the mountain front advanced from the northwest.

To highlight secondary fracture orientations, we edited the ant-tracking attribute parameters to hide the primary NE-SW fracture sets with an “azimuthal filter”. The

resulting filtered rose diagram shows a prominent NNW-SSE (155 ± 15°) fracture strike trend and another minor E-W (085 ± 10°) fracture trend. Both the NNW-ESE and E-W fracture trends are oblique (80° and 30°respectively) to the regional foothills structural trend. They can be grouped as Type 1 fracture sets (Stearns 1968) resulting from a vertical intermediate stress and maximum compressive stress parallel to the dip direction of bedding. The NW-SE and WNW-ESE fracture sets are only found in the Guayabo Fm (11 Ma – Present) synchronous with the greatest orogenic shortening. Right-lateral strike-slip displacement on the Algeciras fault system could have generated WNW-ESE Riedel-type shear fractures in the Foothills study area.

In this paper we show the utility of coherency and ant-tracking techniques for detection of fractures and faults in an active mountain foreland. The authors encourage further work to apply the method to a foreland structure, such as the Cusiana anticline, with both 3D seismic and borehole imager logs available. This could both validate and calibrate the coherency and ant-tracking method with well data as well as help visualize the complex 3D fracture patterns between wells. The resulting study could help reduce risk in 3D models of reservoir fracture porosity and permeability.

CHAPTER 4 CONCLUSIONS

The studies presented in Chapters 2 and 3 provide new solutions for the structural evolution and natural fracture formation in the Llanos Foothills. The new interpretations of the geological structures and petroleum systems associated with La Florida anticline and the Cusiana fault system in the Llanos foothills and the Guavio anticline and the Guaicaramo fault system in the Medina basin help resolve controversies regarding the timing of thin-skinned and thick-skinned thrusting in the area. Unlike previous interpretations of the Guavio anticline and Medina basin (e.g., Rowan and Linares, 2000; Branquet et al., 2002; Parra et al., 2009a), the interpretation presented in this study shows that thin-skinned thrusting on the Guaicaramo fault preceeded thick-skinned basement thrusting which included wedge faulting. To the northeast, all the thrusting on the Cusiana fault and La Florida anticline is interpreted as thin-skinned, rather than previous interpretations of the Cusiana thrust as an inverted normal fault (Cooper et al., 1995; Mora et al., 2010b). Also, the first retrodeformed model for La Florida anticline, presented in this study, proposes a previously unrecognized late Miocene-Pliocene fault-bend fold formed by a thin-skinned thrust ramping up from a mid-Cretaceous detachment.

A new radiometric age map was compiled from published apatite and zircon fission-track samples from the Medina basin area (Mora et al., 2008; Parra et al., 2009b; Mora et al., 2010a; Mora et al., 2010b; Ramirez-Arias et al., 2012; Mora et al., 2013).

These ages cluster in three groups in the last 25 myr; late Oliocene (25-22 Ma) uplift and thrusting on the Tesalia fault to the west, late Miocene (12-8 Ma) thrusting on the Guaicaramo fault, and Pliocene-Pleistocene (4-1 Ma) thrusting on the Cusiana fault and basement involved inversion of the Guaicaramo fault. New 1-D burial history models for two wells in the La Florida – Chitamena anticline (Rio-Chitamena E-1, and Bromelia-1) predict that oil generation began in the hangingwall of the Cusiana fault ~ 9 Ma, and ~ 6 Ma in the footwall.

Chapter3 focused on the natural fracture distribution, orientation, and intensity in the hangingwall and footwall of the Cusiana fault. Seismic attribute analysis was applied in this study for the first time in the Llanos foothills to detect small faults and fractures. The advanced coherence attribute and ant-tracking algorithm were used to produce a fault/fracture patch model for the 3D seismic volume (Marfurt, 2018). A noise reduction process (Randen et al., 2003) applied to the seismic amplitude volume made seismic attribute analysis feasible in the area. The fault patches volume revealed that the folded Cusiana hangingwall has greater fracture intensity than the non-folded Cusiana footwall. Northeast-southwest was the dominant orientation of fractures in La Florida anticline parallel to the structural trend of the adjacent Eastern Cordillera Foothills. Secondary orientations were not distinguished in the hangingwall or in the reservoir rocks (Late Cretaceous to late Eocene).

Fracture orientations in the non-folded footwall seismic volume included NE-SW, NW-SE, and E-W fracture sets. These first results for an undeformed seismic volume in the Foothills suggests the importance of regional stress fields in fracture set formation in addition to the widely studied role of folding mechanisms for fracture formation. Some

NE-SW oriented fractures may have been inherited from Early Cretaceous rifting and normal faulting such as the Guaicaramo fault (Horton 2010, Cooper 1995). Compressional stresses and uplift of the Central Cordillera from middle Eocene to middle Miocene times (Gómez et al., 2005; Horton et al., 2010) was followed by rapid Miocene-Pliocene uplift of the southeast flank of the Eastern Cordillera (Duque-Caro, 1990; Kellogg and Vega, 1995; Taboada et al., 2000; Cediel et al., 2003). New NE-SW fracture sets formed in response to Miocene-Pliocene folding of La Florida anticline. The NW-SE and WNW-ESE fracture sets that are only found in the younger deposits (Guayabo Fm) from middle-Miocene until present day, which coincides with the time of maximum orogenic shortening. These fractures are oriented parallel to the maximum compressive stress direction associated with the mountain building. Also, right-lateral strike-slip displacement on the Algeciras fault system (Egbue and Kellogg, 2010, Anderson et al.2016) could have generated WNW-ESE Riedel-type shear fractures in the Foothills study area.

The applications of coherency and ant-tracking techniques for detection of fractures and faults in an active mountain foreland has been demonstrated to be an effective way to predict natural fractures for any potential well (Marfurt, 2018). The ability to reduce noise and enhance the 3-D image signal are critical in order to apply attribute analysis successfully (Randen et al., 2003). The ant-tracking attribute has numerous potential applications for studies of the effect of fractures on fluid flow such as hydrology (Singh et al., 2008), the movement of pollutants, etc. I hope that this research inspires future work to validate the results from coherency attribute analysis with 3D

porosity and permeability modeling in an active hydrocarbon producing field with downhole fracture data.

REFERENCES

Albesher, Z., Kellogg, J., Hafiz, I., and Saeid, E., Structural Evolution of La Florida Anticline and Petroleum System in a Foreland Fold Belt, Eastern Cordillera Foothills, Colombia, *in* Proceedings 2019 AAPG Annual Convention and Exhibition, San Antonio, Texas, May 19-22, 2019 2019, AAPG Search and Discovery. doi:10.1306/30623Albesher2019.

Allen, P. A., and Allen, J. R., 2005, Basin analysis: Principles and application, Oxford, UK, Blackwell Publishing, 549 p.:

Amaya, S., Zuluaga, C. A., and Bernet, M., 2017, New fission-track age constraints on the exhumation of the central Santander Massif: Implications for the tectonic evolution of the Northern Andes, Colombia: Lithos, v. 282-283, p. 388-402. doi:https://doi.org/10.1016/j.lithos.2017.03.019.

Anderson, V. J., Horton, B. K., Saylor, J. E., Mora, A., Tesón, E., Breecker, D. O., and Ketcham, R. A., 2016, Andean topographic growth and basement uplift in southern Colombia: Implications for the evolution of the Magdalena, Orinoco, and Amazon river systems: Geosphere, v. 12, no. 4, p. 1235-1256. doi:https://doi.org/10.1130/GES01294.1.

Baby, P., Hérail, G., Salinas, R., and Sempere, T., 1992, Geometry and kinematic evolution of passive roof duplexes deduced from cross section balancing: Example from the foreland thrust system of the southern Bolivian Subandean Zone: Tectonics, v. 11, no. 3, p. 523-536. doi:https://doi.org/10.1029/91TC03090.

Bachu, S., Ramon, J. C., Villegas, M. E., and Underschultz, J. R., 1995, Geothermal regime and thermal history of the Llanos Basin, Colombia: AAPG bulletin, v. 79, no. 1, p. 116-128.

Bande, A., Horton, B. K., Ramirez, J. C., Mora, A., Parra, M., and Stockli, D. F., 2012, Clastic deposition, provenance, and sequence of Andean thrusting in the frontal Eastern Cordillera and Llanos foreland basin of Colombia: Geological Society of America Bulletin, v. 124, no. 1-2, p. 59-76. doi:https://www.doi.org/10.1130/b30412.1.

Bayona, G., Cortes, M., Jaramillo, C., Ojeda, G., Aristizabal, J. J., and Reyes-Harker, A., 2008, An integrated analysis of an orogen-sedimentary basin pair: Latest

Cretaceous-Cenozoic evolution of the linked Eastern Cordillera orogen and the Llanos foreland basin of Colombia: Geological Society of America Bulletin, v. 120, no. 9-10, p. 1171-1197. doi:https://doi.org/10.1130/B26187.1.

Bayona, G., Cardona, A., Jaramillo, C., Mora, A., Montes, C., Caballero, V., Mahecha, H., Lamus, F., Montenegro, O., Jimenez, G., Mesa, A., and Valencia, V., 2013, Onset of fault reactivation in the Eastern Cordillera of Colombia and proximal Llanos Basin; response to Caribbean–South American convergence in early Palaeogene time: Geological Society, London, Special Publications, v. 377, no. 1, p. 285-314. doi:https://doi.org/10.1144/SP377.5.

Boschman, L. M., van Hinsbergen, D. J. J., Torsvik, T. H., Spakman, W., and Pindell, J. L., 2014, Kinematic reconstruction of the Caribbean region since the Early Jurassic: Earth-Science Reviews, v. 138, p. 102-136. doi:https://doi.org/10.1016/j.earscirev.2014.08.007.

Branquet, Y., Cheilletz, A., Cobbold, P. R., Baby, P., Laumonier, B., and Giuliani, G., 2002, Andean deformation and rift inversion, eastern edge of Cordillera Oriental (Guateque–Medina area), Colombia: Journal of South American Earth Sciences, v. 15, no. 4, p. 391-407. doi:10.1016/S0895-9811(02)00063-9.

Campbell, C. J., and Burgl, H., 1965, Section through the Cordillera Oriental of Colombia, South America: GSA Bulletin, v. 76, p. 567-590.

Campbell, C. J., 1974, Colombian Andes: Geological Society, London, Special Publications, v. 4, no. 1, p. 705-724. doi:https://doi.org/10.1144/GSL.SP.2005.004.01.43.

Cardozo Puentes, A., 1988, Structural Style of the Central Western Flank of the Cordillera Oriental West of Bogota, Colombia. M.S. thesis, University of South Carolina, pp. 146.

Carrillo, E., Mora, A., Ketcham, R. A., Amorocho, R., Parra, M., Costantino, D., Robles, W., Avellaneda, W., Carvajal, J. S., and Corcione, M. F., 2016, Movement vectors and deformation mechanisms in kinematic restorations: A case study from the Colombian Eastern Cordillera: Interpretation, v. 4, no. 1, p. T31-T48. doi:https://doi.org/10.1190/INT-2015-0049.1.

Cazier, E. C., Hayward, A. B., Espinosa, G., Velandia, J., Mugniot, J. F., and Leel Jr, W. G., 1995, Petroleum geology of the Cusiana field, Llanos Basin foothills, Colombia: AAPG bulletin, v. 79, no. 10, p. 1444-1462.

Cediel, F., Shaw, R. P., and Cceres, C., 2003, Tectonic assembly of the northern Andean block: The Circum-Gulf of Mexico and the Caribbean: Hydrocarbon habitats, basin formation, and plate tectonics, v. 79, p. 815-848.

Chapple, W. M., 1978, Mechanics of thin-skinned fold-and-thrust belts: Geological Society of America Bulletin, v. 89, no. 8, p. 1189-1198. doi:https://doi.org/10.1130/0016-7606(1978)89<1189:MOTFB>2.0.CO;2.

Chopra, S., and Marfurt, K. J., 2007, Seismic attributes for prospect identification and reservoir characterization, *in* Hill, S. J., ed., Seismic Attributes for Prospect Identification and Reservoir Characterization, Society of Exploration Geophysicists and European Association of Geoscientists and Engineers, p. 1-464. doi:https://doi.org/10.1190/1.9781560801900.fm.

Chopra, S., and Marfurt, K. J., 2010, Interpreting fractures through 3-D seismic discontinuity attributes and their visualization: CSEG Recorder, v. 34, p. 5-14.

Chorowicz, J., Chotin, P., and Guillande, R., 1996, The Garzon fault: active southwestern boundary of the Caribbean plate in Colombia: Geologische Rundschau, v. 85, no. 1, p. 172-179. doi:https://doi.org/10.1007/BF00192075.

Colletta, B., Hebrard, F., Letouzey, J., Werner, P., and Rudkiewicz, J. L., 1990, Tectonic Style and Crustal Structure of the Eastern Cordillera (Colombia) from a Balanced Cross-Section: Petroleum and Tectonics in Mobile Belts, v. 47, p. 81-100.

Cooper, M. A., Addison, F. T., Alvarez, R., Coral, M., Graham, R. H., Hayward, A. B., Howe, S., Martinez, J., Naar, J., and Peñas, R., 1995, Basin development and tectonic history of the Llanos Basin, Eastern Cordillera, and middle Magdalena Valley, Colombia: AAPG bulletin, v. 79, no. 10, p. 1421-1442.

Corredor, F., 2003, Seismic strain rates and distributed continental deformation in the northern Andes and three-dimensional seismotectonics of northwestern South America: Tectonophysics, v. 372, no. 3-4, p. 147-166. doi:https://doi.org/10.1016/S0040-1951(03)00276-2.

Cortés, M., Colletta, B., and Angelier, J., 2006, Structure and tectonics of the central segment of the Eastern Cordillera of Colombia: Journal of South American Earth Sciences, v. 21, no. 4, p. 437-465. doi:https://doi.org/10.1016/j.jsames.2006.07.004.

De la Parra, F., Mora, A., Rueda, M., and Quintero, I., 2015, Temporal and spatial distribution of tectonic events as deduced from reworked palynomorphs in the eastern Northern Andes: AAPG Bulletin, v. 99, no. 08, p. 1455-1472. doi:https://www.doi.org/10.1306/02241511153.

De Toni, B., and Kellogg, J., 1993, Seismic evidence for blind thrusting of the northwestern flank of the Venezuelan Andes: Tectonics, v. 12, no. 6, p. 1393-1409. doi:https://www.doi.org/10.1029/93tc01893.

Delgado, A., Mora, A., and Reyes-Harker, A., 2012, Deformation partitioning in the Llanos foreland basin during the Cenozoic and its correlation with mountain

building in the hinterland: Journal of South American Earth Sciences, v. 39, p. 228-244. doi:https://doi.org/10.1016/j.jsames.2012.04.011.

Dengo, C. A., and Covey, M. C., 1993, Structure of the Eastern Cordillera of Colombia - Implications for Trap Styles and Regional Tectonics: Aapg Bulletin-American Association of Petroleum Geologists, v. 77, no. 8, p. 1315-1337.

Duque-Caro, H., 1990, The choco block in the northwestern corner of South America: Structural, tectonostratigraphic, and paleogeographic implications: Journal of South American Earth Sciences, v. 3, no. 1, p. 71-84. doi:https://doi.org/10.1016/0895-9811(90)90019-W.

Egan, S. S., Kane, S., Buddin, T. S., Williams, G. D., and Hodgetts, D., 1999, Computer modelling and visualisation of the structural deformation caused by movement along geological faults: Computers & Geosciences, v. 25, no. 3, p. 283-297. doi:https://doi.org/10.1016/S0098-3004(98)00125-3.

Egbue, O., and Kellogg, J., 2010, Pleistocene to Present North Andean "escape": Tectonophysics, v. 489, no. 1, p. 248-257. doi:https://doi.org/10.1016/j.tecto.2010.04.021.

-, 2012, Three-dimensional structural evolution and kinematics of the Piedemonte Llanero, Central Llanos foothills, Eastern Cordillera, Colombia: Journal of South American Earth Sciences, v. 39, p. 216-227. doi:https://doi.org/10.1016/j.jsames.2012.04.012.

Egbue, O., Kellogg, J., Aguirre, H., and Torres, C., 2014, Evolution of the stress and strain fields in the Eastern Cordillera, Colombia: Journal of Structural Geology, v. 58, p. 8-21. doi:https://doi.org/10.1016/j.jsg.2013.10.004.

Engelder, T., Lash, G. G., and Uzcátegui, R. S., 2009, Joint sets that enhance production from Middle and Upper Devonian gas shales of the Appalachian Basin: AAPG Bulletin, v. 93, no. 7, p. 857-889. doi:10.1306/03230908032.

Fan, M., and Carrapa, B., 2014, Late Cretaceous–early Eocene Laramide uplift, exhumation, and basin subsidence in Wyoming: Crustal responses to flat slab subduction: Tectonics, v. 33, no. 4, p. 509-529. doi:https://doi.org/10.1002/2012TC003221.

Garcia, D. F., dos Santos Neto, E. V., and Penteado, H. L. d. B., 2015, Controls on petroleum composition in the Llanos basin, Colombia: Implications for exploration: AAPG Bulletin, v. 99, no. 8, p. 1503-1535. doi:https://www.doi.org/10.1306/10231411111.

Gómez, E. a., Jordan, T. E., Allmendinger, R. W., and Cardozo, N., 2005, Development of the Colombian foreland-basin system as a consequence of diachronous exhumation of the northern Andes: GSA Bulletin, v. 117, no. 9-10, p. 1272-1292. doi:https://doi.org/10.1130/B25456.1.

Gómez, J., Montes, N. E., Nivia, Á., and Diederix, H., 2015, Geological Map of Colombia 2015: Servicio Geológico Colombiano, 2 sheets, scale 1:1 000 000.

Gregory-Wodzicki, K. M., 2000, Andean paleoelevation estimates: a review and critique: Geological Society of America Bulletin, v. 112, p. 1091-1105.

Hafiz, I., Kellogg, J., Saeid, E., and Albesher, Z., 2019, Thin-skinned and thick-skinned structural control on the evolution of a foreland basin petroleum system - Parrando and Guavio anticlines, Eastern Cordillera Llanos foothills, Colombia: Journal of South American Earth Sciences, v. 96, p. 102373. doi:https://doi.org/10.1016/j.jsames.2019.102373.

Hantschel, T., and Kauerauf, A. I., 2009, Fundamentals of basin and petroleum systems modeling, Springer, Berlin, Heidelberg, 476 p.: doi:https://doi.org/10.1007/978-3-540-72318-9_3.

Horton, B. K., Saylor, J. E., Nie, J., Mora, A., Parra, M., Reyes-Harker, A., and Stockli, D. F., 2010, Linking sedimentation in the northern Andes to basement configuration, Mesozoic extension, and Cenozoic shortening: Evidence from detrital zircon U-Pb ages, Eastern Cordillera, Colombia: GSA Bulletin, v. 122, no. 9-10, p. 1423-1442. doi:http://dx.doi.org/10.1130/B30118.1.

Horton, B. K., Anderson, V. J., Caballero, V., Saylor, J. E., Nie, J., Parra, M., and Mora, A., 2015, Application of detrital zircon U-Pb geochronology to surface and subsurface correlations of provenance, paleodrainage, and tectonics of the Middle Magdalena Valley Basin of Colombia: Geosphere, v. 11, no. 6, p. 1790-1811. doi:https://doi.org/10.1130/GES01251.1.

Jaillard, E., Soler, P., Carlier, G., and Mourier, T., 1990, Geodynamic evolution of the northern and central Andes during early to middle Mesozoic times: a Tethyan model: Journal of the Geological Society, v. 147, no. 6, p. 1009-1022.

Jimenez, L., Mora, A., Casallas, W., Silva, A., Tesón, E., Tamara, J., Namson, J., Higuera-Díaz, I. C., Lasso, A., and Stockli, D., 2013, Segmentation and growth of foothill thrust-belts adjacent to inverted grabens: the case of the Colombian Llanos foothills: Geological Society, London, Special Publications, v. 377, no. 1, p. 189. doi:https://www.doi.org/10.1144/SP377.11.

Jones, P. B., 1996, Triangle zone geometry, terminology and kinematics: Bulletin of Canadian Petroleum Geology, v. 44, no. 2, p. 139-152.

Jordan, T. E., and Allmendinger, R. W., 1986, The Sierras Pampeanas of Argentina; a modern analogue of Rocky Mountain foreland deformation: American Journal of Science, v. 286, no. 10, p. 737-764. doi:https://doi.org/10.2475/ajs.286.10.737.

Julivert, M., 1970, Cover and Basement Tectonics in the Cordillera Oriental of Colombia, South America, and a Comparison with Some Other Folded Chains: GSA

Bulletin, v. 81, no. 12, p. 3623-3646. doi:https://doi.org/10.1130/0016-7606(1970)81[3623:CABTIT]2.0.CO;2.

Kellogg, J. N., and Bonini, W. E., 1982, Subduction of the Caribbean plate and basement uplifts in the overriding South American plate: Tectonics, v. 1, no. 3, p. 251-276. doi:https://doi.org/10.1029/TC001i003p00251.

Kellogg, J. N., and Vega, V., 1995, Tectonic development of Panama, Costa Rica, and the Colombian Andes: constraints from global positioning system geodetic studies and gravity: SPECIAL PAPERS-GEOLOGICAL SOCIETY OF AMERICA, p. 75-75.

Kellogg, J. N., Camelio, G. B. F., and Mora-Páez, H., 2019, Cenozoic tectonic evolution of the North Andes with constraints from volcanic ages, seismic reflection, and satellite geodesy, *in* Horton, B. K., and Folguera, A., (eds.), Chapter 4, Andean Tectonics, Elsevier, p. 69-102. doi:https://doi.org/10.1016/B978-0-12-816009-1.00006-X.

Liner, C., Li, C. F., Gersztenkorn, A., and Smythe, J., 2004, SPICE: A new general seismic attribute, SEG Technical Program Expanded Abstracts 2004, Society of Exploration Geophysicists, p. 433-436. doi:https://doi.org/10.1190/1.1845256.

Marfurt, K. J., 2018, Seismic Attributes as the Framework for Data Integration Throughout the Oilfield Life Cycle, Seismic Attributes as the Framework for Data Integration Throughout the Oilfield Life Cycle, Society of Exploration Geophysicists, p. 459-477. doi:https://library.seg.org/doi/pdf/10.1190/1.9781560803522.refs.

Martinez, J. A., 2006, Structural evolution of the Llanos foothills, Eastern Cordillera, Colombia: Journal of South American Earth Sciences, v. 21, no. 4, p. 510-520. doi:https://doi.org/10.1016/j.jsames.2006.07.010.

Matthäi, S. K., and Belayneh, M., 2004, Fluid flow partitioning between fractures and a permeable rock matrix: Geophysical Research Letters, v. 31, no. 7. doi:https://doi.org/10.1029/2003GL019027.

Maze, W. B., 1984, Jurassic La Quinta Formation in the Sierra de Perijá, northwestern Venezuela: Geology and tectonic environment of red beds and volcanic rocks: The Caribbean–South American plate boundary and regional tectonics: Geological Society of America Memoir, v. 162, p. 263-282.

Medwedeff, D., 1992, Geometry and Kinematics of an Active, Laterally Propagating Wedge Thrust, Wheeler Ridge, California, *in* Mitra, S., and Fisher, G. W., (eds.), Structural Geology of Fold and Thrust Belts, The Johns Hopkins University Press, p. 3-28.

Miller, J. F., and Mitra, S., 2011, Deformation and secondary faulting associated with basement-involved compressional and extensional structures: AAPG bulletin, v. 95, no. 4, p. 675-689. doi:https://doi.org/10.1306/09131010007.

Montoya, D., Reyes, G., Moreno, G., Fúquen, J., Torres J., E., López C., M., and Nivia G., A., 2013, Geología de la Plancha 229 Gachalá: Servicio Geológico Colombiano, scale 1:100,000. doi:https://www.doi.org/10.32685/10.143.2013.137.

Mora-Páez, H., Kellogg, J. N., Freymueller, J. T., Mencin, D., Fernandes, R. M. S., Diederix, H., LaFemina, P., Cardona-Piedrahita, L., Lizarazo, S., and Peláez-Gaviria, J.-R., 2019, Crustal deformation in the northern Andes–A new GPS velocity field: Journal of South American Earth Sciences, v. 89, p. 76-91. doi:https://doi.org/10.1016/j.jsames.2018.11.002.

Mora, A., Parra, M., Strecker, M. R., Kammer, A., Dimaté, C., and Rodríguez, F., 2006, Cenozoic contractional reactivation of Mesozoic extensional structures in the Eastern Cordillera of Colombia: Tectonics, v. 25, no. 2. doi:https://doi.org/10.1029/2005TC001854.

Mora, A., Parra, M., Strecker, M. R., Sobel, E. R., Hooghiemstra, H., Torres, V., and Jaramillo, J. V., 2008, Climatic forcing of asymmetric orogenic evolution in the Eastern Cordillera of ColombiaClimatic forcing of orogenic evolution: GSA Bulletin, v. 120, no. 7-8, p. 930-949. doi:https://www.doi.org/10.1130/B26186.1.

Mora, A., Gaona, T., Kley, J., Montoya, D., Parra, M., Quiroz, L. I., Reyes, G., and Strecker, M. R., 2009, The role of inherited extensional fault segmentation and linkage in contractional orogenesis: a reconstruction of Lower Cretaceous inverted rift basins in the Eastern Cordillera of Colombia: Basin Research, v. 21, no. 1, p. 111-137. doi:https://www.doi.org/10.1111/j.1365-2117.2008.00367.x.

Mora, A., Horton, B. K., Mesa, A. s., Rubiano, J., Ketcham, R. A., Parra, M., Blanco, V., Garcia, D., and Stockli, D. F., 2010a, Migration of Cenozoic deformation in the Eastern Cordillera of Colombia interpreted from fission track results and structural relationships: Implications for petroleum systems: AAPG Bulletin, v. 94, no. 10, p. 1543-1580. doi:https://www.doi.org/10.1306/01051009111.

Mora, A., Parra, M., Strecker, M. R., Sobel, E. R., Zeilinger, G., Jaramillo, C., Da Silva, S. F., and Blanco, M., 2010b, The eastern foothills of the Eastern Cordillera of Colombia: An example of multiple factors controlling structural styles and active tectonics: GSA Bulletin, v. 122, no. 11-12, p. 1846-1864. doi:https://www.doi.org/10.1130/B30033.1.

Mora, A., Reyes-Harker, A., Rodriguez, G., Tesón, E., Ramirez-Arias, J. C., Parra, M., Caballero, V., Mora, J. P., Quintero, I., Valencia, V., Ibañez, M., Horton, B. K., and Stockli, D. F., 2013, Inversion tectonics under increasing rates of shortening and sedimentation: Cenozoic example from the Eastern Cordillera of Colombia:

Geological Society, London, Special Publications, v. 377, p. SP377.376. doi:https://doi.org/10.1144/SP377.6.

Mora, A., Casallas, W., Ketcham, R. A., Gomez, D., Parra, M., Namson, J., Stockli, D., Almendral, A., Robles, W., and Ghorbal, B., 2015, Kinematic restoration of contractional basement structures using thermokinematic models: A key tool for petroleum system modelingKinematic Restoration of Contractional Basement Structures Using Thermokinematic Models: AAPG Bulletin, v. 99, no. 8, p. 1575-1598. doi:https://www.doi.org/10.1306/04281411108.

Mora, A., Garcia, D., Reyes-Harker, A., Parra, M., Blanco, V., Sanchez, N., de la Parra, F., Caballero, V., Rodriguez, G., and Ruiz, C., 2019a, Tectonic evolution of petroleum systems within the onshore Llanos basin: Insights on the presence of Orinoco heavy-oil analogues in Colombia and a comparison with other heavy oil provinces worldwide: AAPG Bulletin, v. 103, no. 5, p. 1179-1224. doi:https://www.doi.org/10.1306/1003181611417236.

Mora, A., Gomez, R. A., Diaz, C., Caballero, V., Parra, M., Villamizar, C., Lasso, A., Ketcham, R. A., Rico, J., and Arias-Martinez, J. P., 2019b, Water flow, oil biodegradation and hydrodynamic traps in the Llanos Basin. Colombia: AAPG Bulletin, v. 103, no. 5, p. 1225-1264. doi:https://www.doi.org/10.1306/1003181611317237.

Moreno, C. J., Horton, B. K., Caballero, V., Mora, A., Parra, M., and Sierra, J., 2011, Depositional and provenance record of the Paleogene transition from foreland to hinterland basin evolution during Andean orogenesis, northern Middle Magdalena Valley Basin, Colombia: Journal of South American Earth Sciences, v. 32, no. 3, p. 246-263. doi:https://doi.org/10.1016/j.jsames.2011.03.018.

Ojeda, G. Y., 1996, Present day and retrodeformed structure of the eastern Cordillera cretaceous basin, Colombia. M.S. thesis, University of South Carolina, pp. 57.

Ortiz, A., G. D. Mesa,, and Beltran, R. X., 2008, Fracture modeling based on lithologic controls, geometry and tectonic evolution in the Llanos Foothills, Colombia: AAPG Search and Discover 90078,AAPG Annual Convention and Exhibition, San Antonio, Texas, 20 March 2020, http://www.searchanddiscovery.com/abstracts/html/2008/annual/abstracts/410386.htm.

Parra, M., Mora, A., Jaramillo, C., Strecker, M. R., Sobel, E. R., Quiroz, L., Rueda, M., and Torres, V., 2009a, Orogenic wedge advance in the northern Andes: Evidence from the Oligocene-Miocene sedimentary record of the Medina Basin, Eastern Cordillera, ColombiaOrogenic wedge advance in the northern Andes, Colombia: GSA Bulletin, v. 121, no. 5-6, p. 780-800. doi:https://doi.org/10.1130/B26257.1.

Parra, M., Mora, A., Sobel, E. R., Strecker, M. R., and González, R., 2009b, Episodic orogenic front migration in the northern Andes: Constraints from low-temperature

thermochronology in the Eastern Cordillera, Colombia: Tectonics, v. 28, no. 4. doi:https://www.doi.org/10.1029/2008TC002423.

Parra, M., Mora, A., Jaramillo, C., Torres, V., Zeilinger, G., and Strecker, M. R., 2010, Tectonic controls on Cenozoic foreland basin development in the north-eastern Andes, Colombia: Basin Research, v. 22, no. 6, p. 874-903. doi:https://doi.org/10.1111/j.1365-2117.2009.00459.x.

Pedersen, S. I., Randen, T., Sonneland, L., and Steen, y., 2002, Automatic fault extraction using artificial ants, SEG Technical Program Expanded Abstracts 2002, Society of Exploration Geophysicists, p. 512-515. doi:https://doi.org/10.1190/1.1817297.

Price, R. A., 1986, The southeastern Canadian Cordillera: thrust faulting, tectonic wedging, and delamination of the lithosphere: Journal of structural Geology, v. 8, no. 3-4, p. 239-254. doi:https://doi.org/10.1016/0191-8141(86)90046-5.

Ramirez-Arias, J. C., Mora, A., Rubiano, J., Duddy, I., Parra, M., Moreno, N., Stockli, D., and Casallas, W., 2012, The asymmetric evolution of the Colombian Eastern Cordillera. Tectonic inheritance or climatic forcing? New evidence from thermochronology and sedimentology: Journal of South American Earth Sciences, v. 39, p. 112-137. doi:https://doi.org/10.1016/j.jsames.2012.04.008.

Ramon, J. C., and Fajardo, A., 2006, Sedimentology, sequence stratigraphy, and reservoir architecture of the Eocene Mirador Formation, Cupiagua field, Llanos Foothills, Colombia: Giant hydrocarbon reservoirs of the world: From rocks to reservoir characterization and modeling: AAPG Memoir, v. 88/SEPM Special Publication, p. 433-469. doi:https://www.doi.org/10.1306/1215884M883276.

Ramos, V. A., Cristallini, E. O., and Pérez, D. J., 2002, The Pampean flat-slab of the Central Andes: Journal of South American earth sciences, v. 15, no. 1, p. 59-78.

Randen, T., Sønneland, L., Carrillat, A., Valen, T. S., Skov, T., Pedersen, S. I., Rafaelsen, B., and Elvebakk, G., Preconditioning for optimal 3D stratigraphical and structural inversion, *in* Proceedings EAGE 65th Conference & Exhibition, Stavanger, Norway, 2003 2003, European Association of Geoscientists & Engineers. doi:https://doi.org/10.3997/2214-4609-pdb.6.B28.

Restrepo-Pace, P. A., 1989, Restauracion de la seccion geologica Caqueza-Puente Quetame: moderna interpretacion estructural del flanco este de la Cordillera Oriental. M.S. thesis, Universidad Nacional de Colombia, pp. 58.

Reyes-Harker, A., Ruiz-Valdivieso, C. F., Mora, A., Ramírez-Arias, J. C., Rodriguez, G., de la Parra, F., Caballero, V., Parra, M., Moreno, N., Horton, B. K., Saylor, J. E., Silva, A., Valencia, V., Stockli, D., and Blanco, V., 2015, Cenozoic paleogeography of the Andean foreland and retroarc hinterland of ColombiaPaleogeography of the Northern Andes: AAPG Bulletin, v. 99, no. 8, p. 1407-1453. doi:https://www.doi.org/10.1306/06181411110.

Riedel, W., 1929, Zur Mechanik Geologischer Brucherscheinungen: Zentral-blatt fur Mineralogie: Geologie und Paleontologie, p. 354-368.

Rowan, M. G., and Linares, R., 2000, Fold-Evolution Matrices and Axial-Surface Analysis of Fault-Bend Folds: Application to the Medina Anticline, Eastern Cordillera, Colombia: AAPG Bulletin, v. 84, no. 6, p. 741-764. doi:https://doi.org/10.1306/A96733E2-1738-11D7-8645000102C1865D.

Saeid, E., Bakioglu, K. B., Kellogg, J., Leier, A., Martinez, J. A., and Guerrero, E., 2017, Garzón Massif basement tectonics: Structural control on evolution of petroleum systems in upper Magdalena and Putumayo basins, Colombia: Marine and Petroleum Geology, v. 88, p. 381-401. doi:https://doi.org/10.1016/j.marpetgeo.2017.08.035.

Saeid, E., Kellogg, J., Kendall, C., Hafiz, I., and Albesher, Z., Detection of Fluvial Systems Using Spectral Decomposition (Continuous Wavelet Transformation) and Seismic Multi-Attribute Analysis–A New Potential Stratigraphic Trap in the Carbonera Formation, Llanos Foothills, Colombia, *in* Proceedings 2018 AAPG Annual Convention & Exhibition, Salt Lake City, Utah, May 20-23, 2018 2018, AAPG Search and Discovery. doi:https://doi.org/10.1306/42281Saeid2018.

Sánchez, N., Mora, A., Parra, M., Garcia, D., Cortes, M., Shanahan, T. M., Ramirez, R., Llamosa, O., and Guzman, M., 2015, Petroleum system modeling in the Eastern Cordillera of Colombia using geochemistry and timing of thrusting and deformationPetroleum Systems Modeling Colombia: AAPG Bulletin, v. 99, no. 8, p. 1537-1556. doi:https://www.doi.org/10.1306/04161511107.

Shagam, R., 1980, Fission track ages on apatite, zircon and sphene from rocks of the Andes, Perijas and Toss island: Intern. Rep, v. 9, p. 35.

Singh, S. K., Abu-Habbiel, H., Khan, B., Akbar, M., Etchecopar, A., and Montaron, B., 2008, Mapping fracture corridors in naturally fractured reservoirs: an example from Middle East carbonates: First Break, v. 26, no. 5. doi:EAGE-EXPORT-FAKE-DOI.

Smithson, S. B., Brewer, J., Kaufman, S., Oliver, J., and Hurich, C., 1978, Nature of the Wind River thrust, Wyoming, from COCORP deep-reflection data and from gravity data: Geology, v. 6, no. 11, p. 648-652. doi:https://doi.org/10.1130/0091-7613(1978)6<648:NOTWRT>2.0.CO;2.

Spikings, R., Cochrane, R., Villagomez, D., Van der Lelij, R., Vallejo, C., Winkler, W., and Beate, B., 2015, The geological history of northwestern South America: from Pangaea to the early collision of the Caribbean Large Igneous Province (290–75Ma): Gondwana Research, v. 27, no. 1, p. 95-139. doi:https://doi.org/10.1016/j.gr.2014.06.004.

Stearns, D. W., 1968, Certain aspects of fractures in naturally deformed rocks, in Rock Mechanics Seminar: Bedford, edited by RE Riecker,: Terrestrial Sciences Laboratory, p. 97-118.

Suppe, J., 1983, Geometry and kinematics of fault-bend folding: American Journal of science, v. 283, no. 7, p. 684-721. doi:https://www.doi.org/10.2475/ajs.283.7.684.

Taboada, A., Rivera, L. A., Fuenzalida, A., Cisternas, A., Philip, H., Bijwaard, H., Olaya, J., and Rivera, C., 2000, Geodynamics of the northern Andes: Subductions and intracontinental deformation (Colombia): Tectonics, v. 19, no. 5, p. 787-813. doi:https://doi.org/10.1029/2000TC900004.

Tamara, J., Mora, A., Robles, W., Kammer, A., Ortiz, A., Sanchez-Villar, N., Piraquive, A., Rueda, L. H., Casallas, W., Castellanos, J., Montana, J., Parra, L. G., Corredor, J., Ramirez, A., and Zambrano, E., 2015, Fractured reservoirs in the Eastern Foothills, Colombia, and their relationship with fold kinematics: AAPG Bulletin, v. 99, no. 8, p. 1599-1633. doi:https://www.doi.org/10.1306/09291411109.

Teixell, A., Ruiz, J.-C., Teson, E., and Mora, A., 2015, The structure of an inverted back-arc rift: Insights from a transect across the Eastern Cordillera of Colombia near Bogotá: Petroleum geology and potential of the Colombian Caribbean Margin: AAPG Special Volumes, v. 108, p. 499-516. doi:https://doi.org/10.1306/13531947M1083650.

Tesón, E., Mora, A., Silva, A., Namson, J., Teixell, A., Castellanos, J., Casallas, W., Julivert, M., Taylor, M., Ibáñez-Mejía, M., and Valencia, V. A., 2013, Relationship of Mesozoic graben development, stress, shortening magnitude, and structural style in the Eastern Cordillera of the Colombian Andes: Geological Society, London, Special Publications, v. 377, p. SP377.310. doi:https://doi.org/10.1144/SP377.10.

Toro, J., Roure, F., Bordas-Le Floch, N., Le Cornec-Lance, S., and Sassi, W., 2004, Thermal and kinematic evolution of the Eastern Cordillera fold and thrust belt, Colombia: Deformation, fluid flow, and reservoir appraisal in foreland fold and thrust belts, v. AAPG Hedberg Series, no. 1, p. 79-115. doi:https://doi.org/10.1306/1025687H13114.

Van der Hammen, T., 1958, Estratigrafía del terciario y maestrichtiano con continentales y tectogénesis de los Andes colombianos: Boletín Geológico, v. 6, no. 1-3, p. 60-116.

Velandia, F., Acosta, J., Terraza, R., and Villegas, H., 2005, The current tectonic motion of the Northern Andes along the Algeciras Fault System in SW Colombia: Tectonophysics, v. 399, no. 1, p. 313-329. doi:https://doi.org/10.1016/j.tecto.2004.12.028.

Villagómez, D., Spikings, R., Mora, A., Guzmán, G., Ojeda, G., Cortés, E., and van der Lelij, R., 2011, Vertical tectonics at a continental crust-oceanic plateau plate boundary zone: Fission track thermochronology of the Sierra Nevada de Santa Marta, Colombia: Tectonics, v. 30, no. 4. doi:https://doi.org/10.1029/2010TC002835.

Wagner, L. S., Jaramillo, J. S., Ramírez-Hoyos, L. F., Monsalve, G., Cardona, A., and Becker, T. W., 2017, Transient slab flattening beneath Colombia: Geophysical Research Letters, v. 44, no. 13, p. 6616-6623. doi:https://doi.org/10.1002/2017GL073981.

Wells, N. A., 2000, Are There Better Alternatives to Standard Rose Diagrams?: Journal of Sedimentary Research, v. 70, no. 1, p. 37-46. doi:https://doi.org/10.1306/2DC408FC-0E47-11D7-8643000102C1865D.

Wijninga, V. M., 1996, Neogene ecology of the Salto de Tequendama site (2475 m altitude, Cordillera Oriental, Colombia): the paleobotanical record of montane and lowland forests: Review of Palaeobotany and Palynology, v. 92, no. 1, p. 97-156. doi:https://doi.org/10.1016/0034-6667(94)00100-6.

APPENDIX A - PERMISSION TO REPRINT CHAPTER 3

https://www.mdpi.com/authors/rights

Copyrights

Copyright and Licensing

For all articles published in MDPI journals, copyright is retained by the authors. Articles are licensed under an open access Creative Commons CC BY 4.0 license, meaning that anyone may download and read the paper for free. In addition, the article may be reused and quoted provided that the original published version is cited. These conditions allow for maximum use and exposure of the work, while ensuring that the authors receive proper credit.

In exceptional circumstances articles may be licensed differently. If you have specific condition (such as one linked to funding) that does not allow this license, please mention this to the editorial office of the journal at submission. Exceptions will be granted at the discretion of the publisher.

Reproducing Published Material from other Publishers

It is absolutely essential that authors obtain permission to reproduce any published material (figures, schemes, tables or any extract of a text) which does not fall into the public domain, or for which they do not hold the copyright. Permission should be requested by the authors from the copyrightholder (usually the Publisher, please refer to the imprint of the individual publications to identify the copyrightholder).

Permission **is required** for:

1. Your own works published by other Publishers and for which you did not retain copyright.
2. Substantial extracts from anyones' works or a series of works.
3. Use of Tables, Graphs, Charts, Schemes and Artworks if they are unaltered or slightly modified.
4. Photographs for which you do not hold copyright.

Permission **is not required** for:

1. Reconstruction of your *own* table with data already published elsewhere. Please notice that in this case you must cite the source of the data in the form of either "Data from..." or "Adapted from...".
2. Reasonably short quotes are considered *fair use* and therefore do not require permission.
3. Graphs, Charts, Schemes and Artworks that are completely redrawn by the authors and significantly changed beyond recognition do not require permission.

Obtaining Permission

In order to avoid unnecessary delays in the publication process, you should start obtaining permissions as early as possible. If in any doubt about the copyright, apply for permission. MDPI cannot publish material from other publications without permission.

The copyright holder may give you instructions on the form of acknowledgement to be followed; otherwise follow the style: "Reproduced with permission from [author], [book/journal title]; published by [publisher], [year].' at the end of the caption of the Table, Figure or Scheme.